UCRL-10455

University of California

Ernest O. Lawrence
Radiation Laboratory

ENERGETICS IN DISLOCATION MECHANICS

Berkeley, California

DISCLAIMER

To be published in the Proceedings of the Energetic Seminar.

UCRL-10455

UNIVERSITY OF CALIFORNIA
Lawrence Radiation Laboratory
Berkeley, California

Contract No. W-7405-eng-48

ENERGETICS IN DISLOCATION MECHANICS

John E. Dorn

February 1963

ENERGETICS
IN
DISLOCATION MECHANICS

by

John E. Dorn[1]

Based on a Series of Lectures

presented at the

University of Denver

Summer 1962

as part of the National Research

Council Seminar on Energetics in Metallurgical Phenomena

[1] Professor of Materials Science of the Department of Mineral Technology and Research Metallurgist of the Lawrence Radiation Laboratory, University of California, Berkeley, California.

I. INTRODUCTION

1A. Phenomenological Approaches

Much progress has been made in understanding the molecular origins of the mechanical behavior of gases and liquids. In contrast the equivalent description of the plastic behavior of crystalline solids in terms of atomic mechanisms of deformation has only recently been initiated and progress has been slow. The reason for this fact cannot be attributed to a lack of interest, the failure to pursue the problem, a deficiency of highly qualified scientific talent, or any one of a number of similar possibilities. Rather it is intimately associated with the complexity of the problem. The relaxation times for molecular processes in gases and most liquids are usually so short that they are almost always in a well-defined state of complete equilibrium. Consequently the molecular structure of gases and liquids are not dependent on their past histories. In contrast the relaxation times for some significant atomic processes in crystals, as we shall see later, are so long that complete equilibrium is seldom if ever achieved. It is for this reason that metals exhibit the desirable feature of strain hardening, as shown in Fig. 1.1.[1] For if the relaxation times for all processes were short, the structure would recover almost immediately to its equilibrium condition and a constant stress for plastic flow would result regardless of the extent of the deformation.

If the relaxation times for all substructural modifications that are induced as a result of straining were infinitely long, however, a mechanical equation of state

$$\sigma \equiv \sigma(\varepsilon, \dot{\varepsilon}, T) \tag{1.1}$$

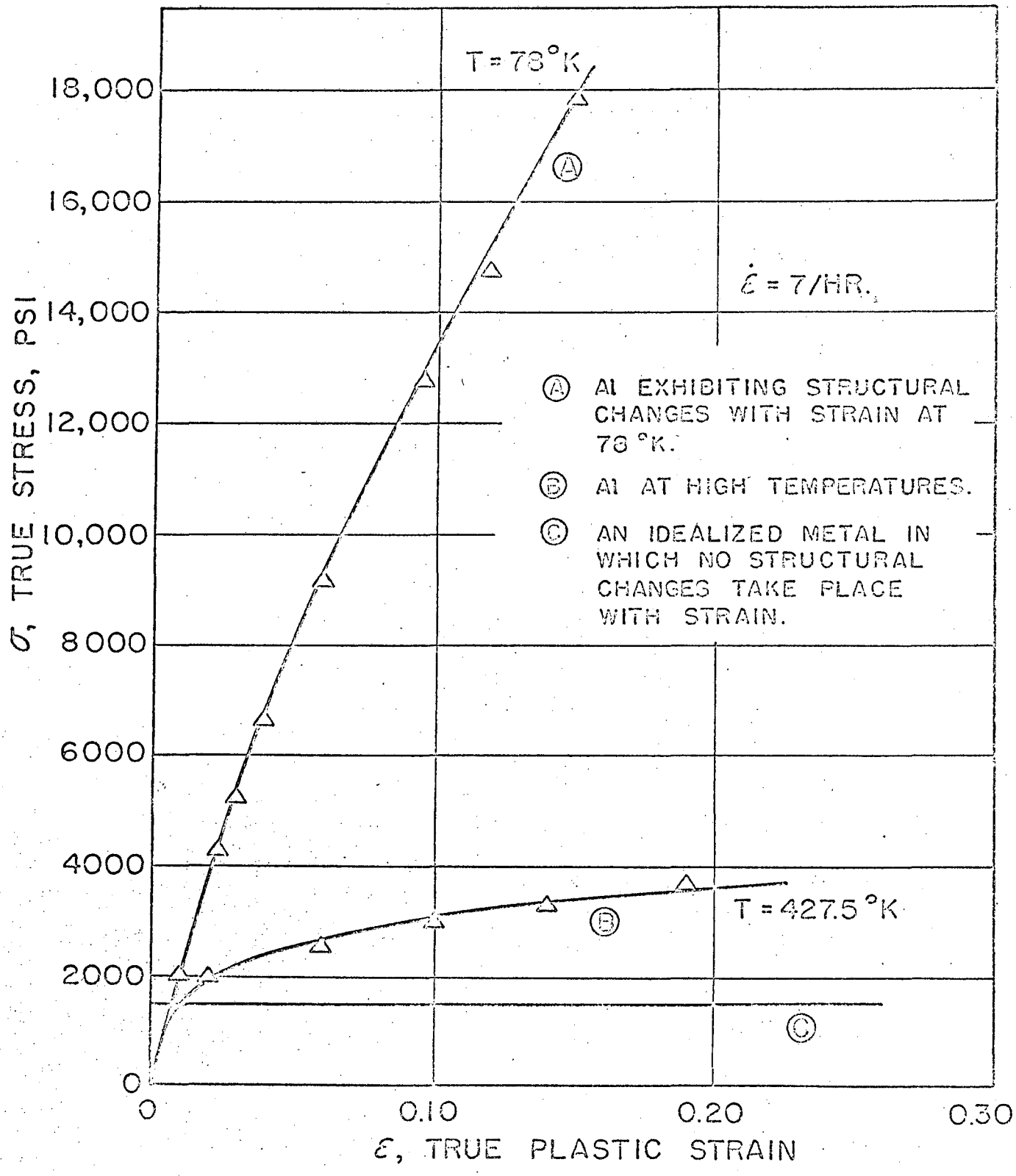

FIGURE I.1. TYPICAL STRESS-STRAIN CURVES.[1]

might be expected to be valid. Accordingly the flow stress, σ, would then be a unique function of the instantaneous values of the strain, ε, the strain rate, $\dot{\varepsilon}$, and the test temperature, T, regardless of the previous strain history. But it is well known that tension tests conducted at high temperatures, B of Fig. 1.1, begin to give stress-strain curves that approximate C of Fig. 1.1. Consequently at high temperatures, at least, the relaxation times for some substructural modifications become significantly short. Under these circumstances recovery of the substructure will continue, even during interruption of the test, so that, if the test were subsequently restarted, the substructure would no longer be a unique function of the strain alone and Eq. 1.1 would be invalid.

As shown in Fig. 1.2[2] Eq. 1.1 is also invalid for tests conducted at low temperatures. Whereas the stress-strain curve AED was obtained exclusively at 78°K, ABCF was obtained by straining to B at 292°K whereupon the test was continued at 78°K. If Eq. 1.1 were valid, point C would have coincided with D, whereas segment CF actually coincides much better with ED. Even this comparison is approximate since CF has a slightly greater slope than ED. Obviously less drastic substructural changes are introduced at the same strains for the higher temperature test. This suggests that higher rates of recovery accompany the higher temperature test. But, when a specimen prestrained from A to B is unloaded and held at 292°K, even for very long times, it will, upon reloading, again give the stress-strain curve BH showing that no recovery took place. Therefore the recovery that took place during tensile testing must have occurred as a result of the effect of stress on

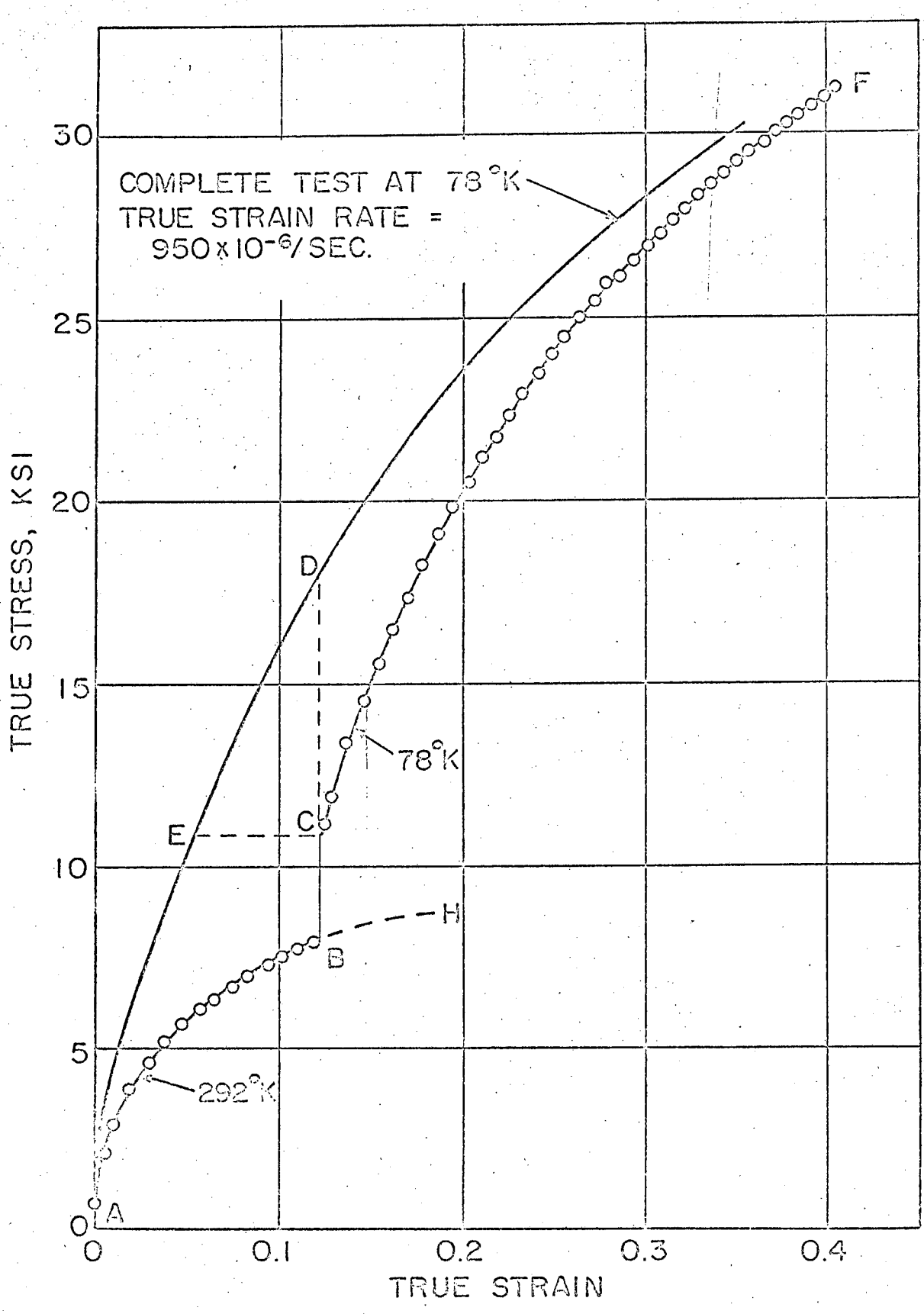

FIGURE 1.2. FAILURE OF THE MECHANICAL EQUATION OF STATE AT LOW TEMPERATURE FOR 2S-O Al.[2]

the activation energy for recovery, possibly as we shall see, [illegible] to cross slip of dislocations. Dislocation climb, usually only observed above one-half of the melting temperature, represents another dynamic recovery process.

We now see that the mechanical equation of state, as expressed by Eq. 1.1 is seldom valid. In fact there is only one known example of the validity of Eq. 1.1 and this concerns the plastic behavior of single crystals of FCC metals at very low temperatures and then only over Stages I and II of easy glide and linear hardening. In these regions the deformation mechanism has been ascribed to the thermally activated intersection of dislocations[3-9] as will be discussed in detail later. Once the stress becomes high enough to induce parabolic strain hardening, dynamic recovery due to cross slip takes place, and Eq. 1.1 is no longer applicable. Of course the Peierls[11,12] process at low temperatures, which will be discussed later, may also obey Eq. 1.1, but there is as yet no definitive experimental evidence for the operation of the Peierls mechanism.

Although Eq. 1.1 is usually invalid, each thermally activated deformation mechanism can always be described in terms of the general phenomenological expression

$$\dot{\gamma}_i = f_i e^{-\frac{U_i}{kT}} \qquad (1.2)$$

where i refers to the i^{th} kind of mechanism and

$\dot{\gamma}_i$ the shear strain rate

$f_i = f_i\{T, \tau, str\}$ = a frequency factor that equals the strain per activation per second

$U_i = U_i\{T, \tau, str\}$ = the energy of activation per unit i^{th} process

k = the Boltzmann constant

T = the absolute temperature

τ = the applied shear stress

str = the significant substructural details.

As shown by Eq. 1.2, the substructure rather than the strain is the significant variable that determines the plastic behavior of crystalline materials. Consequently, only for those processes for which str. is a unique single-valued function of the strain, does the universally valid expression for thermally activated flow, given by Eq. 1.2, reduce to Eq. 1.1. In general several different processes may be operative at one time. If they are sequential, such that C follows B which follows A, the strain rate that is observed will refer, under steady state conditions, exclusively to the slowest process. But when the mechanisms are independent the total strain rate will be given by $\dot{\gamma} = \sum \dot{\gamma}_i$. Appropriately high thermal fluctuations, needed to activate high activation energy processes, will be too infrequent to contribute much to the strain rate at low temperatures. Consequently only the more easily activated processes having low activation energies can contribute to the strain rate at low temperatures. At higher temperatures, however, the lower activation processes will occur almost instantly and further deformation will therefore depend on activation of the more difficult, higher activation energy, processes. Consequently, in general, the activation energy for deformation will increase with increasing temperature.

When only one mechanism predominates, the activation energy can be very closely estimated by the effect of an abrupt change in temperature with strain rate as given by

$$U_i \simeq \frac{\partial \ln \dot{\gamma}}{\partial -\frac{1}{kT}} \simeq \frac{\Delta \ln \dot{\epsilon}}{\Delta\left(-\frac{1}{kT}\right)} \qquad (1.3)$$

as shown by differentiating Eq. 1.2 and neglecting the truly negligible change in f_1 with T.

The application of the experimental procedure for obtaining the apparent activation energy for creep of Al is shown in Fig. 1.3.[13] Over region A to B the creep rate decreases with strain in spite of the fact that all of the external variables of stress and temperature were held constant. Consequently this reduction in the creep rate must be ascribed to the substructural changes taking place during creep. When the temperature is decreased at B the creep rate decreases as demanded for thermally activated processes, and when the original temperature is again restored creep again proceeds at the faster rate. In this example, the segment CD is merely a continuation of AB suggesting that the substructural changes taking place from B' to C' were the same as those which would have occurred from B to C had the original temperature been held constant. This observation holds quite frequently, especially at high temperatures and for small changes in temperature. The apparent activation energy obtained by applying Eq. 1.3 to these data is shown in Fig. 1.3.

When the apparent activation energy for creep is determined over the entire range of intersecting temperatures, results such as those shown in Fig. 1.4[14] for Al are obtained. The expected trend of increasing apparent activation energies with increasing temperatures is obtained. It is significant however, that these tests were conducted for creep rates of about 10^{-5} per second. As will be shown later, for such constant strain rate conditions certain processes (e.g., intersection and the thermally activated motion of jog screw dislocations) wherein

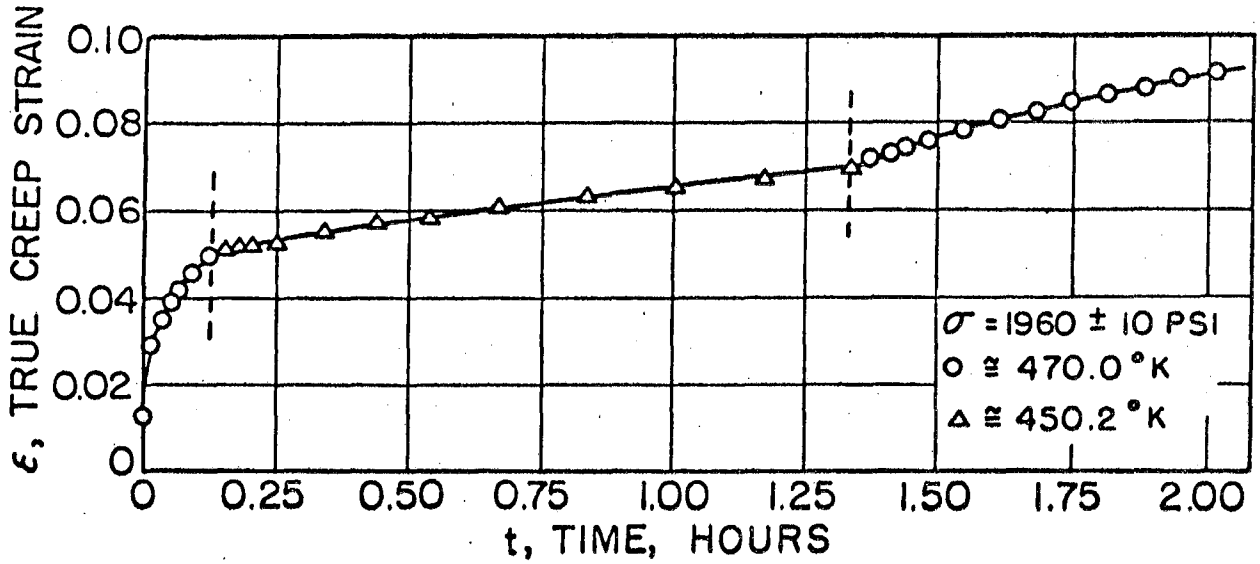

FIGURE 1.3A. CREEP CURVE AT CONSTANT STRESS.

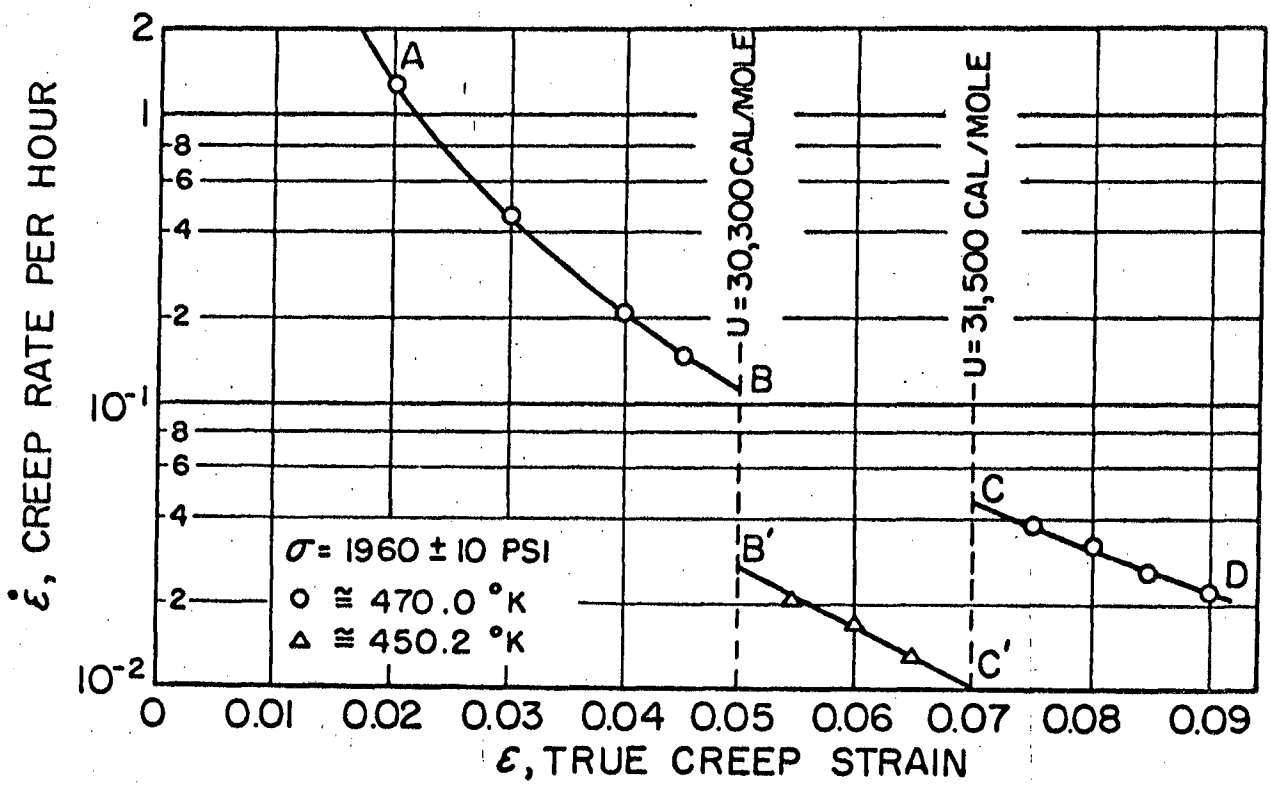

FIGURE 1.3B. EFFECT OF CHANGE IN TEMPERATURE ON THE CREEP RATE.[13]

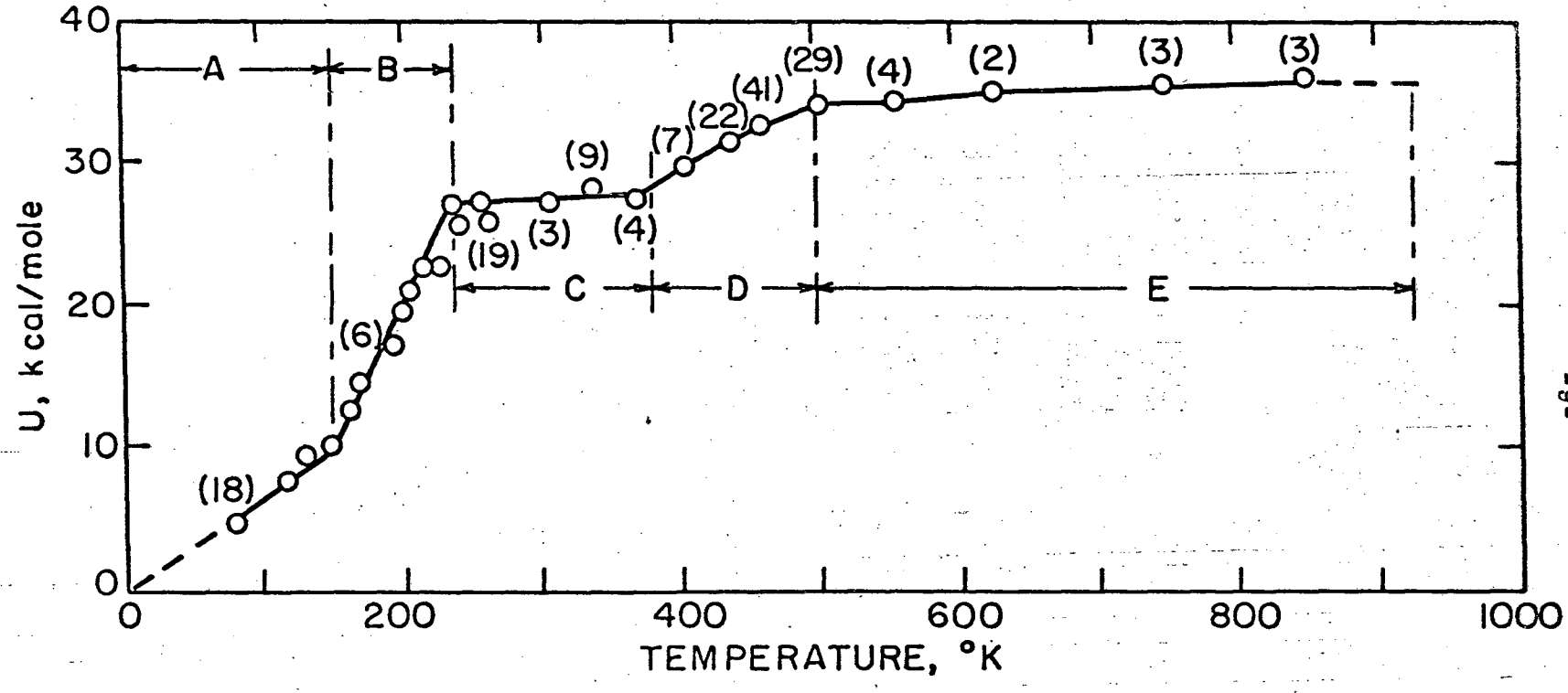

FIGURE 1.4. ACTIVATION ENERGIES FOR CREEP OF PURE ALUMINUM AS A FUNCTION OF THE ABSOLUTE TEMPERATURE.[14]

the activation energy is a function of the stress, will give activation energies that increase linearly with the absolute temperature. There can be no doubt that various mechanisms of deformation are operative over the various temperature regions. We might tentatively suggest the following:

A. Intersection of dislocations

B. Transition from intersection to cross slip

C. Cross slip

D. Principally motion of jogged screw dislocations with some cross slip and some climb

E. Climb of dislocations

Only those mechanisms for which the activation energy is less than about 50kT can occur frequently enough to contribute effectively to the strain rate. There are a number of important processes that have much greater activation energies; and such processes must be induced to operate almost exclusively mechanically by applying sufficiently high stresses. Among these are the following:

A. Generation of dislocations either at a Frank-Read source or at points of high stress concentration

B. Separation of recombined dislocations

C. Motion of dislocations through long-range stress fields induced by other dislocations

D. Motion of dislocations through short-range ordered alloys

E. Activation of Suzuki-locked dislocations

An example of the effects of long-range back stresses and possibly a small amount of effects of short-range order are illustrated,

for a dilute alpha solid solution alloy of 0.554 at. % Mg in Al, in Fig. 1.5.[15] Over region AB the flow stress decreases with increasing temperature as required by thermally activated processes, the mechanism in this case being intersection. But over region BC the flow stress is almost independent of the temperature, as required when the process is not stimulated by thermal fluctuations. In this region intersection is so facile because of its low activation energy, that it occurs without delay. And the stress must, without the aid of thermal fluctuations, force dislocations through the short-range ordered alloy and over the long-range stress fields. Over the higher temperature range, deformation again is controlled by the more difficult thermally activated mechanisms of cross slip, motion of jogged screw dislocations and, over the highest temperature range, climb of dislocations.

Another example of an athermal process is shown by the single crystal data given in Fig. 1.6.[16] The critical resolved shear stress for slip is practically independent of temperature up to about half of the melting temperature and it increases slightly with an increase in temperature as the melting temperature is approached. Furthermore the critical resolved shear stress for slip increased only slightly when the strain rate was increased about 10^8 times. This insensitivity of the yield stress to the strain rate is another characteristic of athermal mechanisms. As will be shown later, these results are ascribable to the activation of Suzuki-locked dislocations.

It is also desirable to point out at this time that there are several thermally activated mechanisms of deformation in polycrystalline aggregates that are not directly ascribable to dislocation processes.

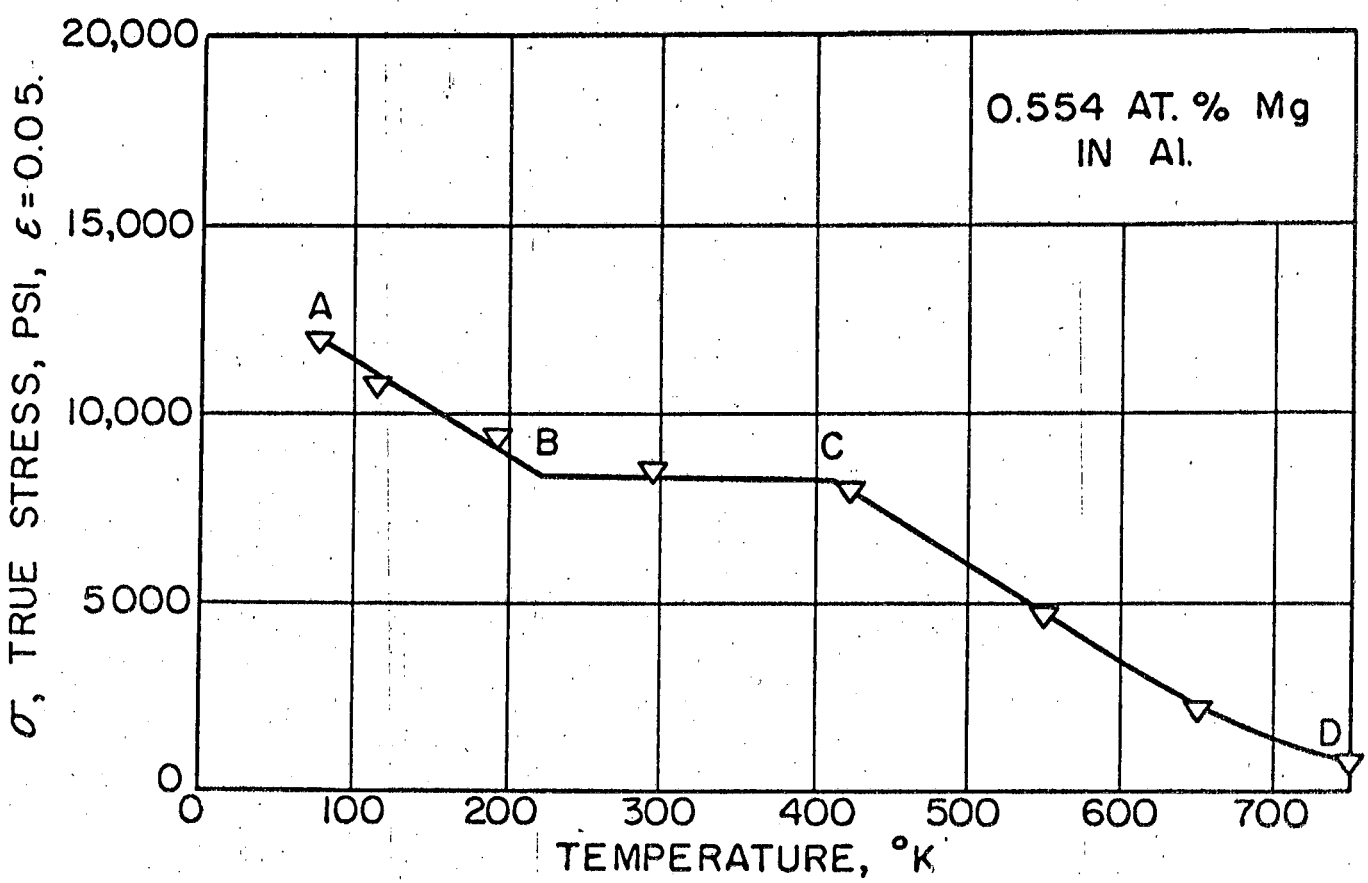

FIGURE I.5. FLOW-STRESS OF ALLOY OF 0.554 AT. % Mg IN Al AT 5% STRAIN.[15]

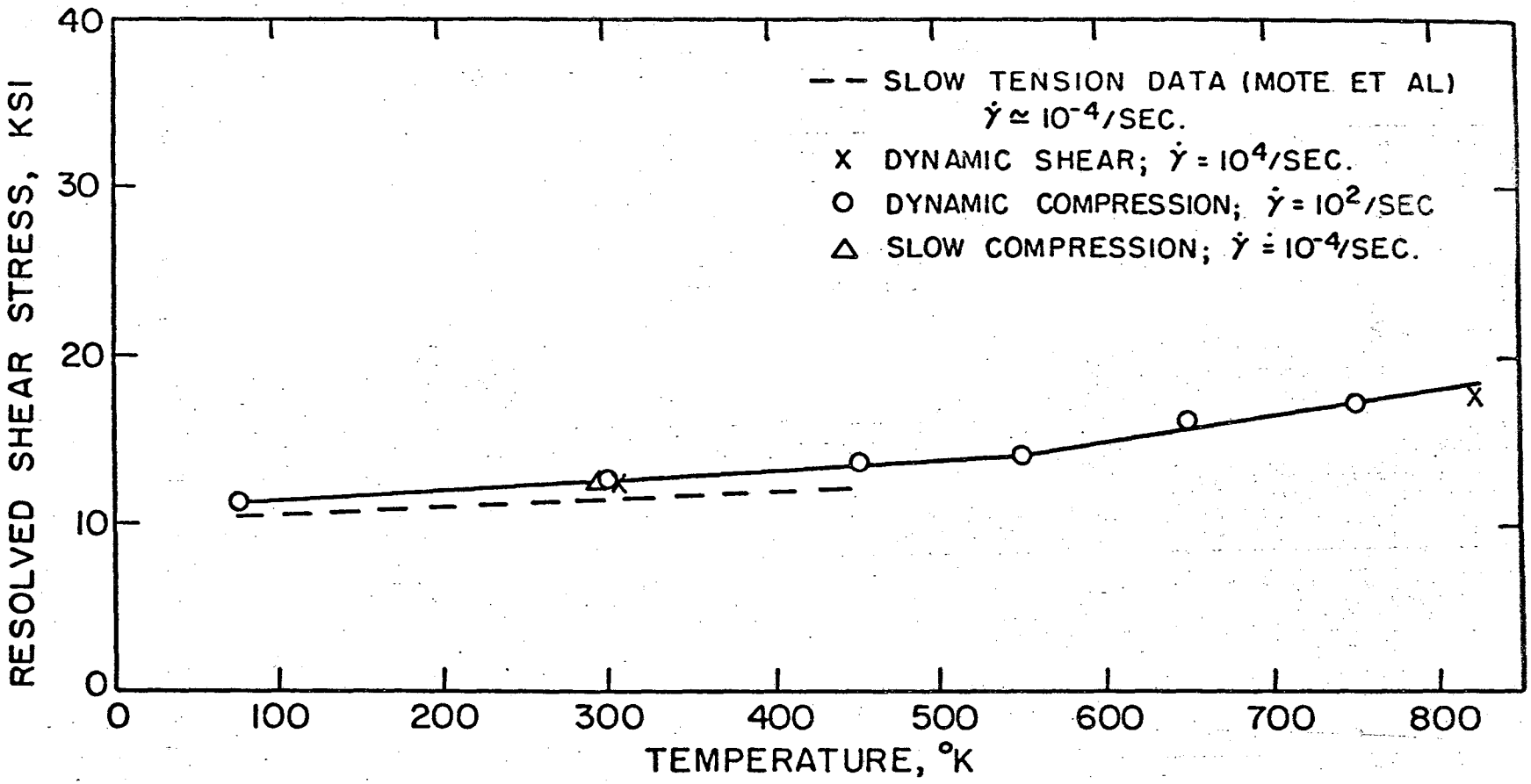

FIGURE 1.6. RESOLVED SHEAR STRESS vs. TEMPERATURE FOR BASAL SLIP IN A $66\frac{2}{3}$ AT. % Ag AND $33\frac{1}{3}$ AT. % Al PHASE.[16]

At very high temperatures and low values of the applied stress, creep can occur by the Nabarro[17] mechanism of generation of vacancies at grain boundaries normal to the applied tensile stress, followed by volume diffusion to sinks in the grain boundaries parallel to the direction of tensile stressing. Atoms, of course, migrate in the counter-current direction resulting, therefore, in creep. This process, however, only becomes significant within about 50°C or less of the melting temperature. During creep at high temperatures, high angle grain boundaries do migrate. Such migrations might be equivalent to a recovery process because the newly formed volumes of grains over which the boundaries have migrated are probably rather free of dislocations. The migration of such high angle boundaries does not require dislocation mechanisms for its operation. Grain boundary shearing also occurs during high temperature creep. But since its activation energy appears to agree with that for climb and because the amount of grain boundary shearing is linearly related to the total strain, it is now generally believed that such grain boundary shearing may be controlled by interactions with dislocation mechanisms.

Although dislocations play a significant role in many different types of solid state phenomena, the major objective of dislocation theory is the rationalization of the plastic behavior of crystalline materials in terms of atomistic mechanisms of deformation. The concept of dislocations was first announced by Prandtl[18] and Dehlinger[19] and subsequently the first detailed theoretical discussions were given by Orowan[20] and Taylor.[21] Over about the first twenty years many false ideas were promulgated, primarily because of the versatility of

the theory, and dislocation concepts were frequently discredited. But substantial progress has been made over the past fifteen years, and the theory now rests on a sound foundation. However, many phenomena dependent upon dislocations yet resist clear interpretation. And several previously held concepts concerning dislocations have had to be abandoned as a result of recent direct observations of dislocations, especially by transmission electron microscopy. It can be expected that most of the remaining general concepts of dislocation theory will be fairly completely explored and characterized within the next fifteen years.

1B. The Need for Dislocations

When metal single crystals are stressed, they deform plastically by glide on prescribed crystallographic planes and in prescribed crystallographic directions of shear as shown in Fig. 1.7. Entire blocks of the crystal shear relative to other blocks, the operative slip system being that on which the resolved shear stress, τ_s , on the slip plane in the slip direction(s) is a maximum. As deformation proceeds higher stresses must be applied and intervening slip planes begin to operate. Each slip band, which consists of a series of closely spaced slip lines, may also continue to add more lines to the band as deformation continues. A typical resolved shear stress versus resolved shear strain curve is shown in Fig. 1.8.[22] Stage I, known as easy glide, exhibits only a minor amount of strain hardening; Stage II, called linear hardening, exhibits a great linear increase in flow stress with strain; whereas in Stage III, parabolic hardening, a smaller rate of strain hardening applies. At higher test temperatures, the strain range of easy glide

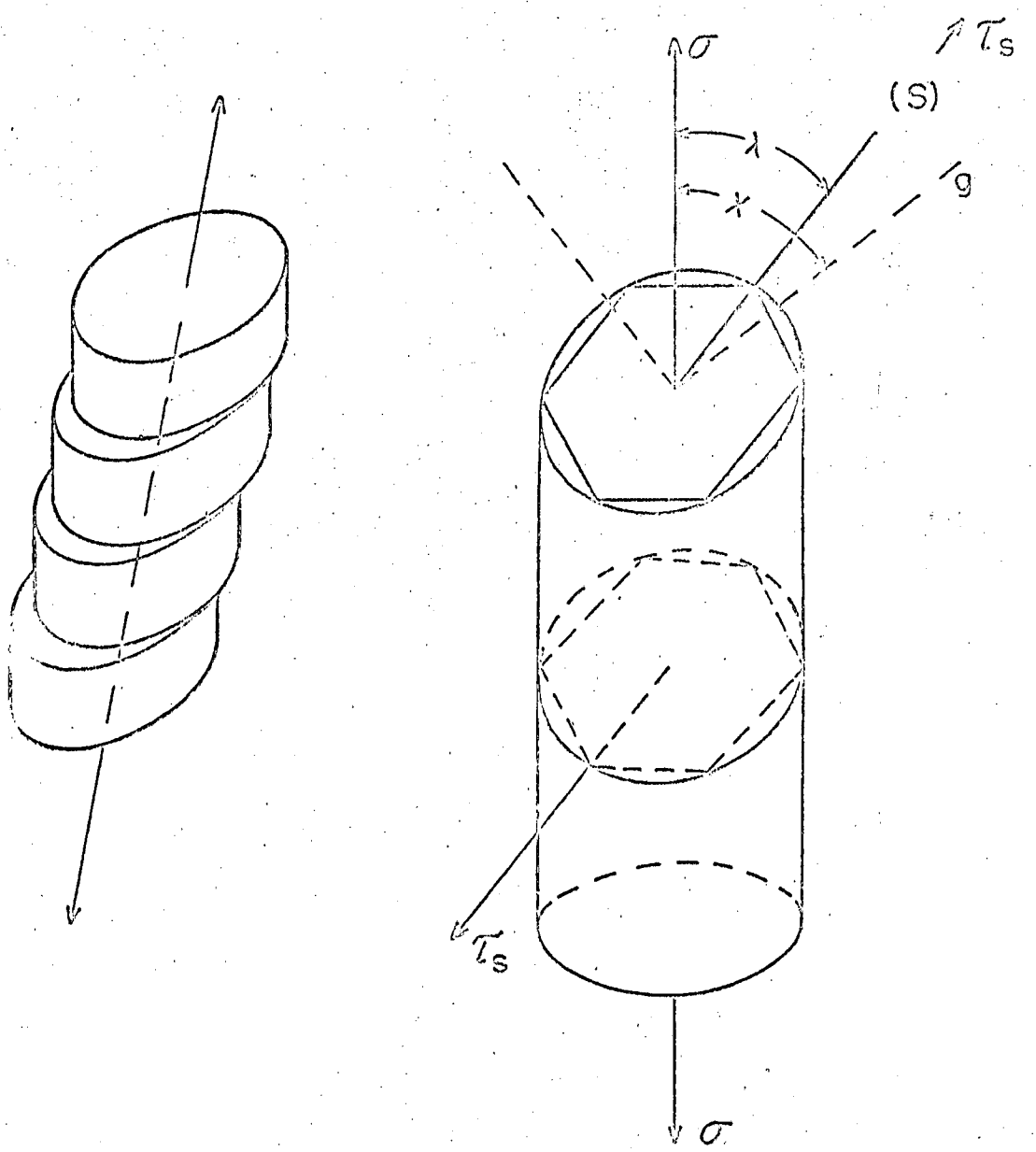

$$\tau_s = \sigma \cos \lambda \sin \chi$$

FIGURE I.7. SLIP IN SINGLE HEXAGONAL CRYSTALS.

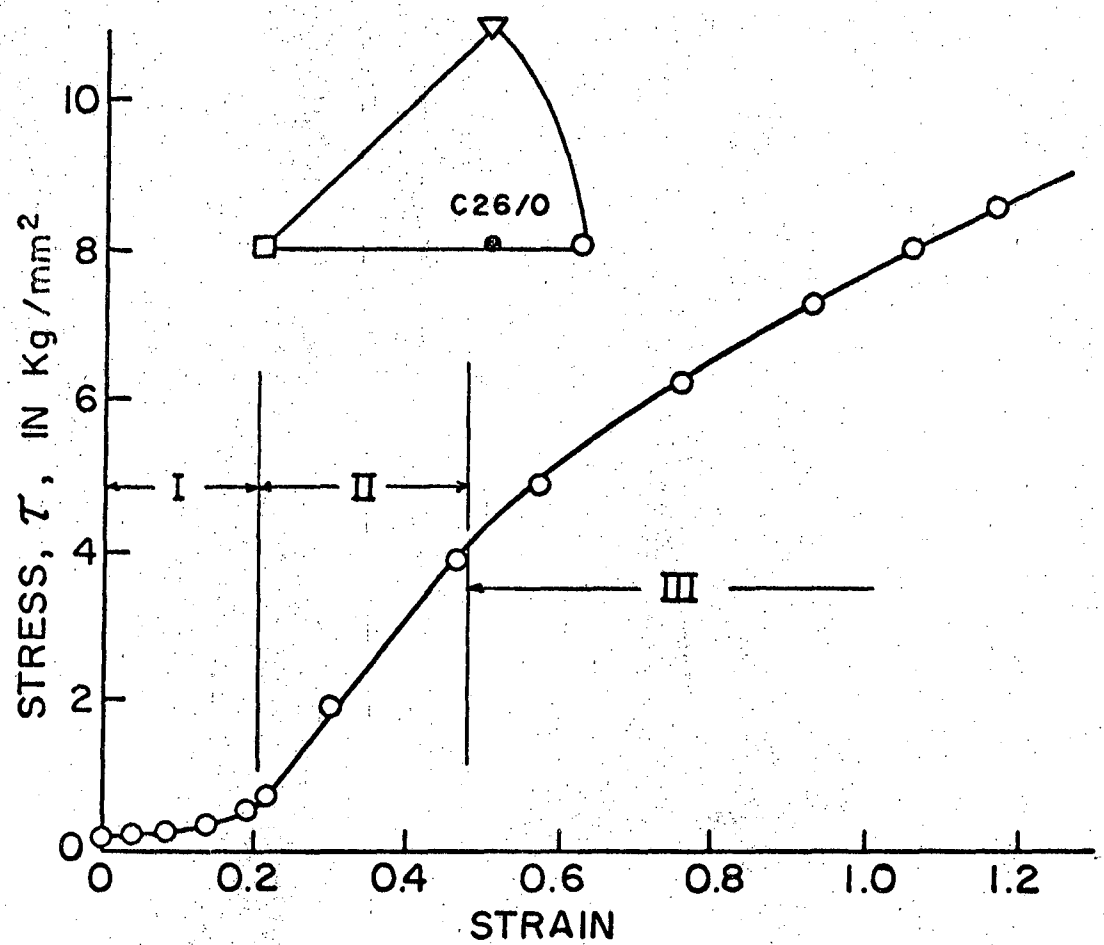

FIGURE 1.8. STRESS–STRAIN CURVE FOR SINGLE CRYSTAL OF Cu. [22]

decreases, and the flow stress also decreases as expected for a thermally activated mechanism. The slope of the linear hardening range, however, is almost independent of the temperature. But parabolic hardening begins at lower values of the flow stress in the higher temperature tests, illustrating that the mechanism operative here also depends on thermal activation. As the original crystal orientation approaches more closely those for duplex slip, the strain range of easy glide decreases, the rate of linear hardening increases, and parabolic hardening occurs at smaller strains. Face centered cubic crystals oriented so that the tension axes coincide with the [111] direction, slip simultaneously on six systems; they do not exhibit easy glide, they undergo high rates of linear hardening, and proceed almost directly to parabolic hardening giving stress-strain curves similar to those for polycrystalline metals.

The commonly observed slip systems in metals are as follows:

Crystal	Slip Direction	Slip Plane
Face Centered Cubic	$[10\bar{1}]$	(111)
Hexagonal Close Packed	$[11\bar{2}0]$	(0001)
Body Centered Cubic	[111]	(110)
	[111]	(112)
	[111]	(123)

Under special conditions, however, other slip systems become operative. Excluding rare exceptions, slip in metals always takes place in the direction of greatest atomic packing and usually, but not always, on the planes most widely separated from their nearest parallel neighbors. Any acceptable theory of plastic deformation of crystalline materials must satisfactorily account not only for all of these facts but must

equally permit Eq. 1.2 to be explicitly expressed in terms of the appropriate mechanistic details for all conditions of deformation for all crystalline materials under all possible states of aggregation.

Neglecting their thermal vibration, the atoms of an ideal crystal are arranged in a regular three-dimensional array, as shown in Fig. 1.9A. If a shear stress were applied to the single crystal, as shown in Fig. 1.9B, a shear displacement, χ , of the upper plane relative to the lower plane would occur. As a result of the periodicity of the lattice, however,

$$\tau \approx \tau_c \sin 2\pi \frac{\chi}{b} \tag{1.4}$$

where τ_c refers to the critical shear stress required to cause permanent plastic straining. For small strains the sine term reduces to its argument and Hooke's law applies, so that

$$\tau = G\frac{\chi}{a} \approx 2\pi \frac{\chi}{b}\tau_c \tag{1.5}$$

where G is the shear modulus of elasticity. Consequently the shear stress required to cause plastic deformation is about

$$\tau \approx \frac{G}{2\pi}\frac{a}{b} \tag{1.6}$$

Whereas this value is somewhat above 10^6 psi, the value observed in real crystals is only about 10^2 psi as shown in Fig. 1.8. Some improvement in the estimate given by Eq. 1.6 is possible by taking the

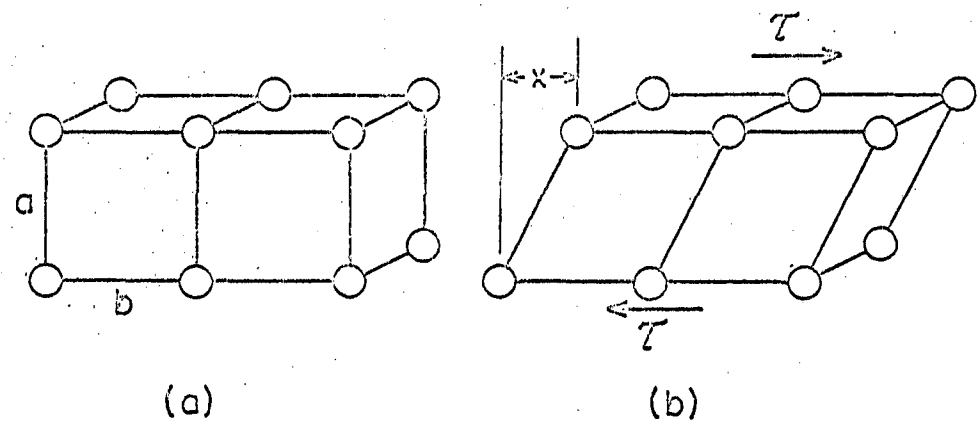

FIGURE I.9. IDEAL CRYSTAL UNDER SHEAR.

compressibility of the atoms into consideration. But even when this is done, the theoretical value of τ_c for most ideal metal crystals remains above 10^6 psi. Since the theoretical calculation, although crude, gives the correct order of magnitude of τ_c for ideal crystals, it must be evident that the single crystals, as usually prepared, are highly non-ideal. On the other hand, many metal whiskers do not deform plastically until the theoretical value of τ_c for ideal crystals is approached, illustrating that they are at least nearly ideal. Attempts to grow large crystals having the strength of whiskers are intriguing but thus far have failed. Except perhaps for special applications, the possible utility of such high strength ideal crystalline materials is questionable because they could not be machined or formed into shape without making them non-ideal and soft. We shall see, however, the versatility of dislocation theory which will show that those imperfections which in modest concentration, permit a metal to be easily deformed, will, in sufficiently high concentration, lead to strengthening which in special cases and under special conditions begins to approach within about one-half of the theoretical strength.

Since imperfections are responsible for the observed plastic behavior of most real crystalline materials, we need to determine what kind of imperfections could possibly be responsible for the observations. And since crystals are geometric objects, the possible types of imperfections are limited to point imperfections, line imperfections, and surface imperfections. Point imperfections appear either at lattice sites which are supposedly occupied by the atoms of the crystal or at interstitial sites that are supposedly unoccupied. Random mixing of

various atomic species in solid solution alloys does not constitute point imperfections. Typical examples of point imperfections, vacancies, and interstitials are shown in Fig. 1.10. There are two major reasons why such imperfections cannot be responsible for the plastic shear deformation of crystals. First, they cannot undertake extensive mass migration as a result of a shear stress. Secondly, even if they did move large distances, they could not account for slip on a slip plane in a slip direction. Furthermore, as we shall see later, the various surface imperfections that arise in real crystals can all be ascribed to line imperfections. And therefore line imperfections must be thought to be the primary factors responsible for the plastic deformation of crystals. Such line imperfections are called dislocations.

II. THE STRUCTURE AND NATURE OF DISLOCATIONS

2A. The Viewpoint to be Adopted

From a detailed analytical viewpoint, dislocation theory appears to be a rather formidable subject, having many complex facets and presenting many complicated mathematical problems. It is not the objective here to elaborate on such features of the subject. Rather, I propose to discuss dislocation theory, not in the full rigor of high sophistication, but with vigor and clarity to provide the neophyte with a lucid picture of some of the major issues. Several factors permit such an elementary approach. First, dislocations are simple geometric imperfections and second, the major phenomena can often be described in terms of a few interacting dislocations without requiring a complete statistical formulation of the problem.

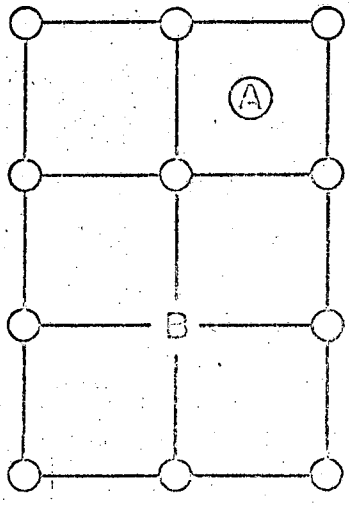

FIGURE I.10. POINT IMPERFECTIONS.
A. INTERSTITIAL ATOM
B. VACANCY

2B. The Edge or Taylor Dislocation

Consider the ideal single crystal shown in Fig. 2.1A and let a dislocation be produced by shearing the upper left-hand section of the crystal one atomic spacing, i.e., one Burgers vector, $\vec{b}$, along a slip plane. Since slip will not, in this visualization, be permitted to proceed over the entire slip plane, the atomic configuration that is obtained for a simple cubic lattice is as shown in Fig. 2.1B. The plane ABCD represents the extra half plane of atoms (associated with the edge dislocation) that was crowded into the lattice. The edge dislocation itself is given by the line AB. To determine the Burgers vector, $\vec{b}$, we look along the dislocation from A to B and formulate the circuit cdefg in the clockwise direction making equal numbers of lattice spacing steps downward (c to d), to the left (d to e), upward (e to f), and to the right (f to g). Where the crystal is ideal, or contains only interstitials and vacancies, this Burgers circuit will close. But when the circuit is made around a dislocation, such as AB, it fails to close by g to c. The Burgers vector, $\vec{b}$, of the dislocation gives the failure to close in terms of the lattice spacing in the ideal crystal. The same failure to close, $\vec{b}$, is obtained for circuits anywhere along the length of AB. When the Burgers circuit does not include the dislocation line but does extend across the extra half plane, it nevertheless closes. Consequently, excepting for elastic lattice distortions, the crystal is ideal in this region and no special significance, excepting that of geometric convenience, can be ascribed to the extra half plane. The only imperfection present is the dislocation line AB.

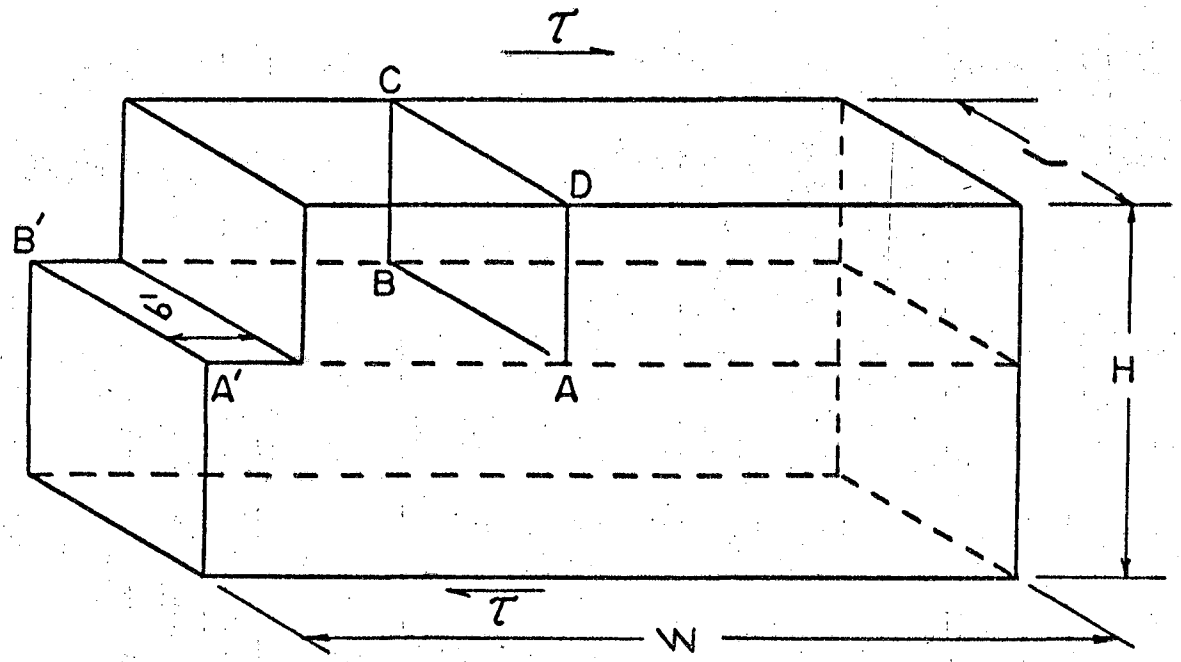

(a)

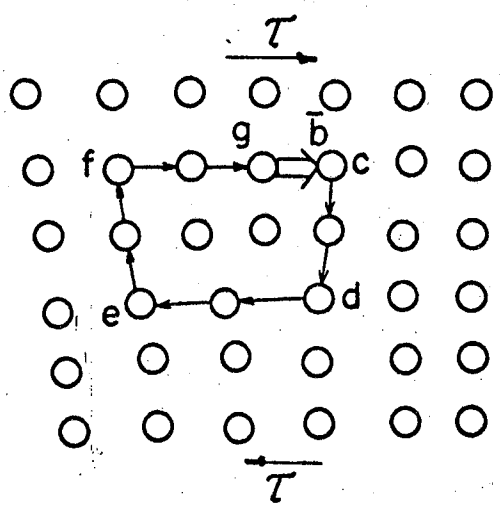

(b)

FIGURE 2.1. AN EDGE OR TAYLOR DISLOCATION.

As we can readily see, the characteristic of an edge dislocation line resides in the fact that it is perpendicular to its Burgers vector. Since the edge dislocation and its Burgers vector are perpendicular to each other, they define a plane. The plane so defined is the slip plane on which the edge dislocation is constrained to move when diffusion is prohibited. Since slip has taken place over the area A'AB'B of the slip plane, the dislocation is the line separating the slipped from the unslipped portion of the slip plane. Since this is generally true for all dislocations, a dislocation line cannot end in the center of a crystal; it must either end on the surface, as shown at points A and B, or it must form a closed loop in the crystal.

When an appropriate shear stress is applied to the crystal, the dislocation will move as shown in Fig. 2.2. As the dislocation moves forward one Burgers vector only a small atomic adjustment is required in the vicinity of the dislocation core. Along the entire dislocation line atoms "C" which are shown below "B" in Fig. 2.2A move one Burgers vector so that they are below "A" as shown in Fig. 2.2B. Proceeding step by step, the dislocation can leave the crystal as shown in Fig. 2.2C resulting in a shear displacement of the upper section of the dislocation one Burgers vector relative to the lower section.

The motion of a dislocation through the lattice, as shown in Fig. 2.2, is quite different from the uniform shear displacement required to cause plastic deformation of an ideal crystal, shown in Fig. 1.9. In the ideal crystal high stresses were required to cause a shear displacement because the entire slip plane was sheared as a unit. But in the dislocation process only small atomic adjustments are required near

FIG. 2.2 MOTION OF AN EDGE DISLOCATION.

the core of the moving dislocation and consequently the stress required to induce flow is small.

When the dislocation moves forward one Burgers vector the bond angles of the atoms in the vicinity of the core must change. The bond energy of covalently bonded atoms changes appreciably with the bond angle. Consequently high stresses are required to move dislocations in such crystals as diamond. In contrast ionic crystals are bonded principally by radial forces and therefore dislocations are somewhat more readily moved in these materials. But metals, being bonded by the Fermi energy of the electron gas, have bond strengths that are practically independent of the bond angle. Consequently dislocations begin to move at extremely low stresses in metals. Dislocations not only account for the low shear stresses for slip but also for the fact that slip occurs on a slip plane and in a slip direction.

2C. The Screw or Burgers Dislocation

If a stress is applied to induce the deformation shown in Fig. 2.3A a screw dislocation is produced. Slip was permitted to take place by a shear deformation of $\vec{b}$, one Burgers vector, over only a part of the slip plane, namely A'B'AB. The line AB that demarks the slipped from the unslipped region is, in this case, a screw dislocation.

The characteristics of a screw dislocation are revealed by making a Burgers circuit about the dislocation line. Using Fig. 2.3B as a guide we proceed as follows in a clockwise direction: starting above the slip plane at atom "a" we go down two atoms, to the left from "a" to "b" to "c" and up two atoms at "c" to "d" and then to "e". The circuit does not close by "e" to "a" which is the Burgers vector $\vec{b}$. Whereas in the

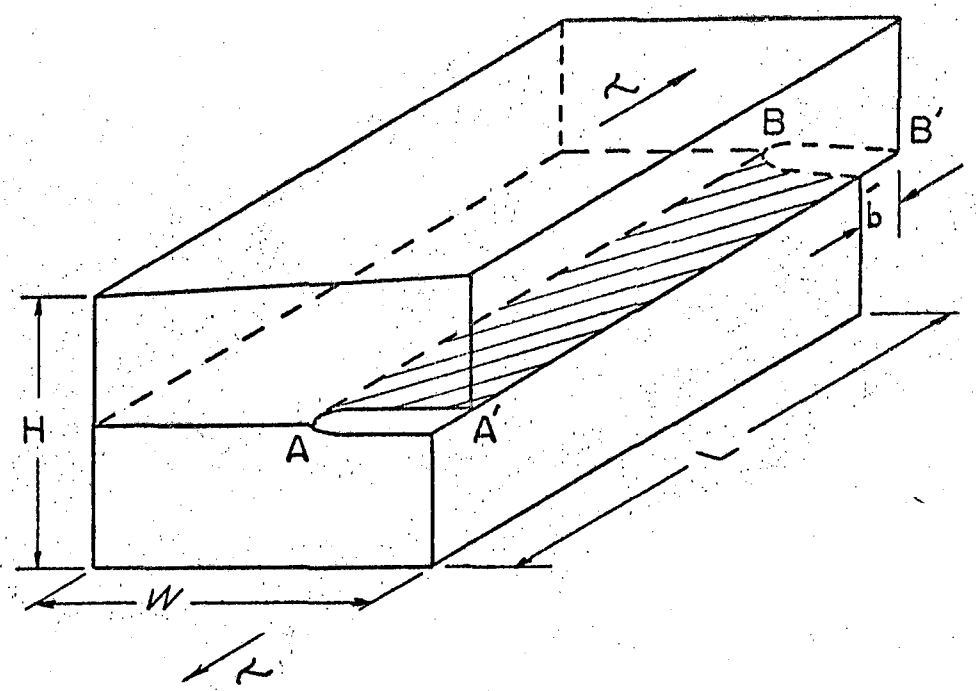

(a)

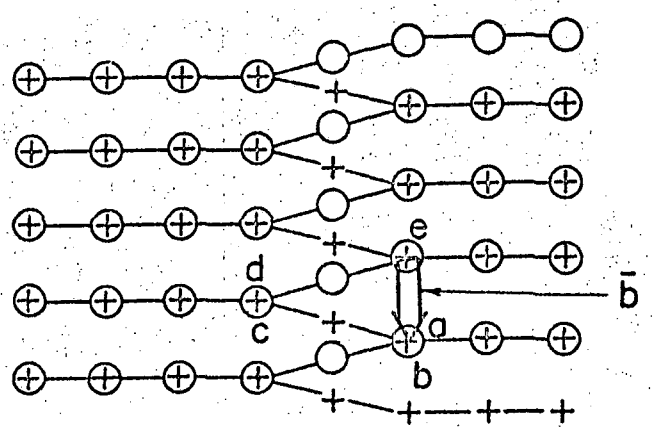

(b) PLAN VIEW OF SLIP PLANE

○ ATOMS ABOVE SLIP PLANE
\+ ATOMS BELOW SLIP PLANE

FIGURE 2.3. A SCREW OR BURGERS DISLOCATION.

edge dislocation, the dislocation line was perpendicular to the Burgers vector, in the screw dislocation the dislocation line is parallel to the Burgers vector. And whereas the edge dislocation, being perpendicular to its Burgers vector, defines a unique slip plane, no such unique slip plane is defined by a screw dislocation since the line and Burgers vector of the dislocation are parallel. Thus, edge dislocations are confined to slip on their unique slip planes, whereas screw dislocations may cross-slip on any facile slip plane in which the Burgers vector, or dislocation line, lies.

2D. Dislocations in General

A general dislocation is shown in Fig. 2.4. Slip was induced to take place on a slip plane over the crosshatched region only up to line ABCD. This line, which demarks the slipped from the unslipped region is a single dislocation line. To reveal this we may take a Burgers circuit around the line, looking along the line from A to B to C to D. No matter where the circuit is taken the Burgers vector, $\vec{b}$, is always the same, as identified in the figure. The dislocation line segment AB is perpendicular to the Burgers vector, $\vec{b}$, and it is therefore an edge segment of the dislocation line. The segment CD, however, is parallel to the Burgers vector and it is, therefore, a screw segment. Between B and C, the dislocation line has both screw and edge components, as shown by the broken lines in Fig. 2.4B.

As shown in Fig. 2.5 there are two kinds of dislocations, called positive and negative dislocations. Under the applied stress shown, the positive dislocation moves to the right whereas the negative dislocation moves to the left. If the dislocations of opposite sign were on the same

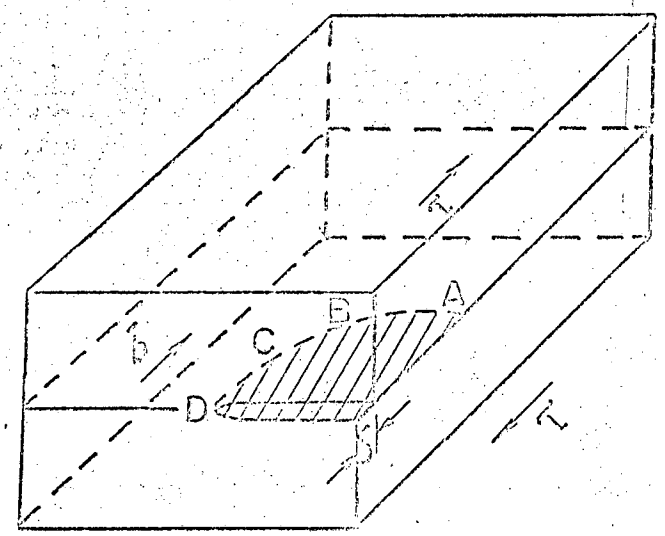

(a)

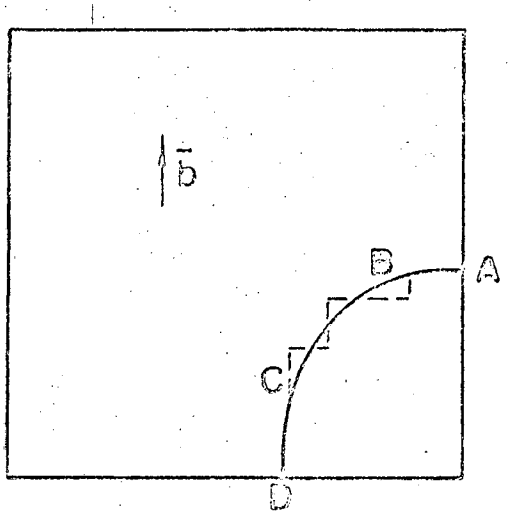

(b)

FIG. 2.4 A GENERAL DISLOCATION.

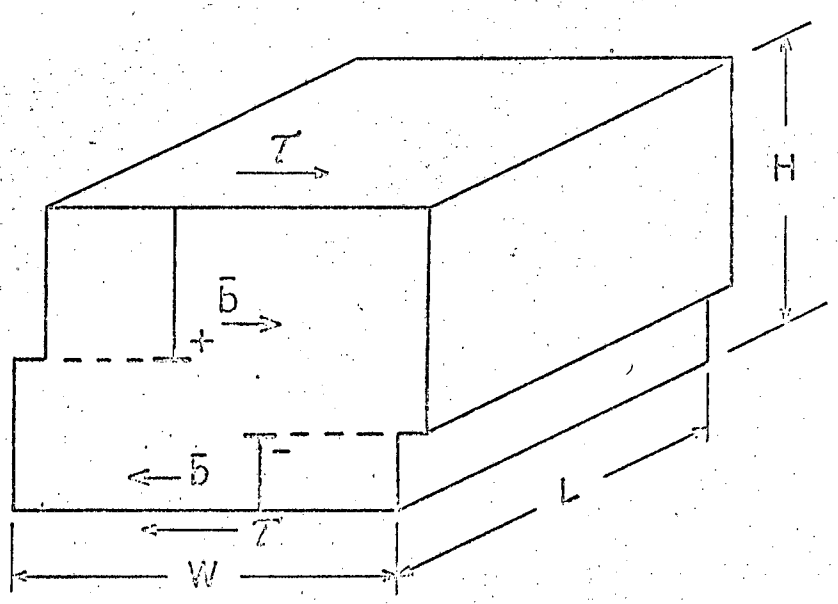

(a) POSITIVE AND NEGATIVE EDGE DISLOCATIONS.

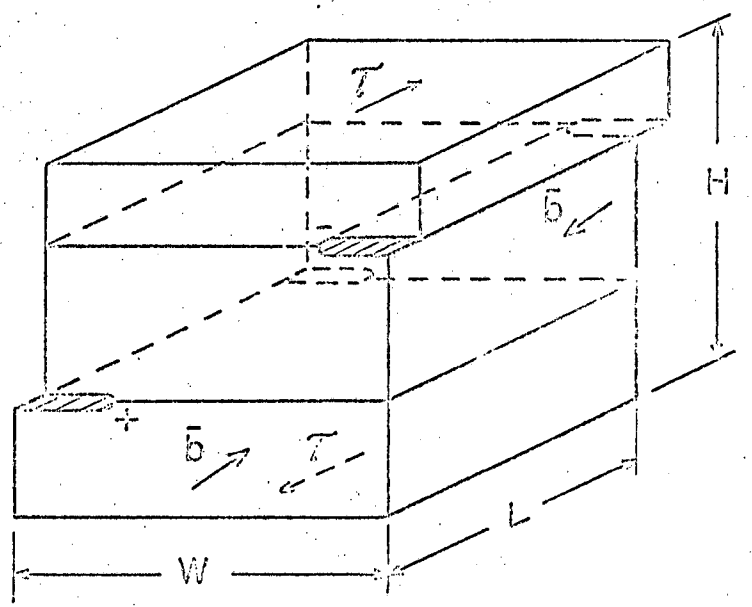

(b) POSITIVE AND NEGATIVE SCREW DISLOCATIONS.

FIGURE 2.5. POSITIVE AND NEGATIVE DISLOCATIONS.

slip plane the elastic strain energy of the crystal would be lowered if they combined and annihilated each other. Therefore dislocations having unlike signs attract each other. As two dislocations having the same signs are brought together, the elastic strain energy increases. Thus dislocations of the same sign repel each other.

If Fig. 2.5 is turned upside down the signs of the dislocations will change. Thus dislocation signs have unique values only relative to fixed orientations. Suppose we introduce the square dislocation loop shown in Fig. 2.6 by shearing the prism above the loop one Burgers vector in the slip direction. The positive direction of the dislocation line will be taken from A to B to C to D to A. The entire line has the single Burgers vector, $\bar{b}$. But the signs of the line must then be taken as shown in Fig. 2.6. By this convention the Burgers vector of a dislocation is constant all along the dislocation line.

In general dislocations in real crystals form a three-dimensional network. On occasions they form two-dimensional arrays of tilt or twist boundaries. There are many reported examples of networks in the literature. The point of junction of dislocation segments of the networks as shown in Fig. 2.7 are known as nodes. The Burgers vectors were obtained by looking along AN, NC, and NB. The vector, $\bar{b}_1$, refers to the difference in slip between regions "a" and "c". But $\bar{b}_2 + \bar{b}_3$ also refers to this difference. Therefore $\bar{b}_1 = \bar{b}_2 + \bar{b}_3$. If, however, Frank's[22] convention is adopted, all Burgers vectors are determined by looking toward the node. Here the signs of $\bar{b}_2$ and $\bar{b}_3$ will be negative. Then looking into the node $\sum \bar{b}_i = 0$.

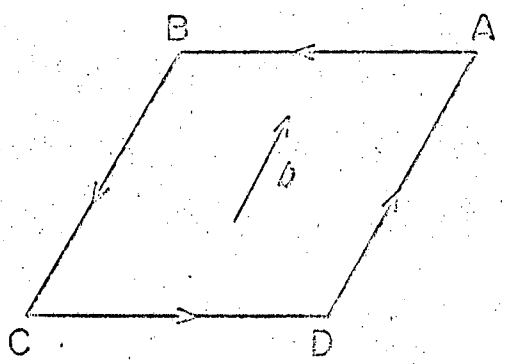

A B - POSITIVE EDGE

B C - NEGATIVE SCREW

C D - NEGATIVE EDGE

D A - POSITIVE SCREW

FIGURE 2.6 POSITIVE AND NEGATIVE DISLOCATIONS IN A SQUARE LOOP.

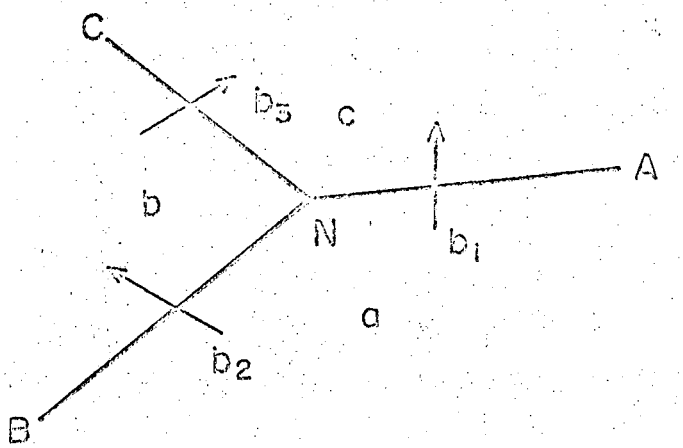

FIGURE 2.7. DISLOCATIONS AT A NODE.

2E. Force on a Dislocation

The principle of virtual work will be invoked to calculate the force, F, per unit length of a dislocation as a result of a shear stress, τ, acting in the direction of the Burgers vector. As shown in Fig. 2.1 the dislocation moves in the direction of W under the action of the stress. Although it moves in the direction of the stress and the Burgers vector, it is more significant to note that it moves on the slip plane in a direction normal to its length. Since the force per unit length is F, the length L and the distance moved to traverse the crystal W, the work done is FLW. This work is done by the stress, τ, acting over area, LW, and the force, τ LW, acts through a distance, b, as the dislocation traverses the crystal. Therefore, FLW = τ WLb or

$$F = \tau b \qquad (2.1)$$

acting normal to the dislocation line.

The force acting on a screw dislocation can be determined by the same procedure. Again only the component of the shear stress, τ, in the direction of the Burgers vector causes deformation as shown in Fig. 2.3. The screw dislocation, however, moves at right angles to the Burgers vector, that is normal to itself. Again Eq. 2.1 is obtained. Consequently Eq. 2.1 gives, in general, the force acting normal to a dislocation and forcing it to move in its slip plane. And therefore, in general, dislocation segments that are acted upon by shear stresses on the slip plane in the direction of the Burgers vector, move in their slip planes in a direction that is normal to the dislocation line.

2F. Stress Fields Around Dislocations

Dislocations are lines representing the cores of internal strain discontinuities in crystals. These strain fields and their associated stress fields move with the dislocations. In this sense dislocation theory describes the plastic behavior of crystalline materials in terms of the theory of elasticity as applied to static and moving internal strain and stress fields. Although the full treatment of this subject can become very mathematical, it is possible to obtain a lucid physical insight into the salient features from very simple approaches.

As illustrated in Fig. 2.3 a screw dislocation consists of a spiral ramp of atoms that advances one Burgers vector per circuit about the dislocation. This is also shown in Fig. 2.8 for a screw dislocation lying along the Z axis. Using cylindrical coordinates, it is immediately seen that all strains are zero excepting $\varepsilon_{\theta z}$ which is

$$\varepsilon_{\theta z} = \frac{b}{2\pi r} \tag{2.2}$$

For $r \geq b$, Hooke's law applies and

$$\sigma_{\theta z} = \frac{Gb}{2\pi r} \tag{2.3}$$

where G is the shear modulus of elasticity, and for the sake of simplicity, elastic isotropy is assumed. Thus the shear stresses around a screw dislocation are inversely proportional to the distance from the core of the dislocation. For $r \leq b$, however, Hooke's law no longer applies and special difficult analyses are required in order to define the details

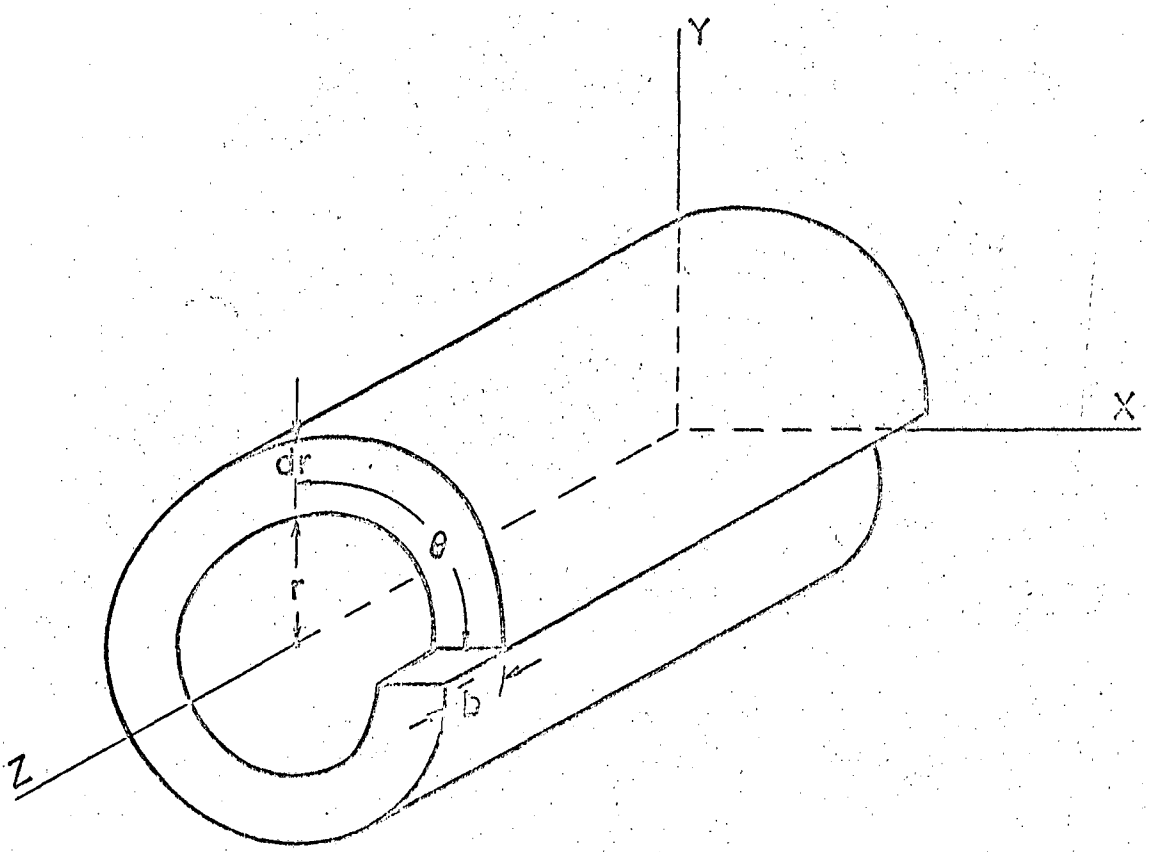

FIGURE 2.8. SCREW DISLOCATION LYING ALONG Z AXIS.

at the core. Such detailed knowledge, however, is only required for certain special problems and need not be considered here. For future reference we will refer the stress field around a screw dislocation to the Cartesian coordinate system. Using the Mohr circle analysis, or applying the tensor transformation

$$\sigma_{ij} = \ell_{ik}\,\ell_{jl}\,\sigma_{kl}$$

where the ℓ's are direction cosines, we find that

$$\sigma_{xx} = \sigma_{yy} = \sigma_{zz} = \sigma_{xy} = 0$$

$$\text{and } \sigma_{zx} = \ell_{z\theta}\,\ell_{xz}\,\sigma_{\theta z} + \ell_{zz}\,\ell_{x\theta}\,\sigma_{z\theta} = -\frac{Gb}{2\pi r}\sin\theta$$

$$\sigma_{zy} = \ell_{z\theta}\,\ell_{yz}\,\sigma_{\theta z} + \ell_{zz}\,\ell_{y\theta}\,\sigma_{z\theta} = \frac{Gb}{2\pi r}\cos\theta$$

Therefore, the stresses for a screw dislocation lying along the Z axis are:

$$\sigma_{zx} = -\frac{Gby}{2\pi(x^2+y^2)} \tag{2.4}$$

$$\sigma_{zy} = \frac{Gbx}{2\pi(x^2+y^2)} \tag{2.5}$$

The stress field around an edge dislocation is slightly more difficult to determine. For an edge dislocation lying along the Z axis the stresses are given in polar coordinates by

$$\sigma_{rr} = \sigma_{\theta\theta} = -\frac{Gb\sin\theta}{2\pi(1-\mu)r} \tag{2.6}$$

$$\sigma_{r\theta} = \frac{Gb\cos\theta}{2\pi(1-\mu)r} \tag{2.7}$$

where μ is Poisson's ratio, and by

$$\sigma_{xx} = -\frac{Gb}{2\pi(1-\mu)} \frac{y(3x^2+y^2)}{(x^2+y^2)^2} \tag{2.8}$$

$$\sigma_{yy} = \frac{Gb}{2\pi(1-\mu)} \frac{y(x^2-y^2)}{(x^2+y^2)^2} \tag{2.9}$$

$$\sigma_{zz} = \mu(\sigma_{xx} + \sigma_{yy}) \tag{2.10}$$

$$\sigma_{xy} = \frac{Gb}{2\pi(1-\mu)} \frac{x(x^2-y^2)}{(x^2+y^2)^2} \tag{2.11}$$

in Cartesian coordinates. Eqs. 2.6 and 2.7 reveal that the stress field around an edge dislocation also varies with the reciprocal of the distance from the dislocation core. But as shown by Eqs. 2.8 to 2.10, dilatational stresses are present around an edge dislocation. Therefore edge dislocations will interact with centers of volumetric straining as well as shear straining whereas screw dislocations react only with centers of shear straining.

2G. Energy of Dislocations

The strain energy of the lattice due to the presence of a dislocation is known as the energy of the dislocation. We will consider the geometry in Fig. 2.8 to calculate the energy of a screw dislocation that is 1 cm long. Since the shear strain and shear stress are given by Eqs. 2.2 and 2.3, the strain energy per unit volume at a distance r from the

dislocation core is:

$$\frac{d\Gamma_s}{dV} = \frac{1}{2}\sigma_{\theta z}\varepsilon_{\theta z} = \frac{1}{2}\,\frac{Gb^2}{4\pi^2 r^2} \tag{2.12}$$

where Γ_s is the total energy per unit length of the screw dislocation. As seen by Fig. 2.8, the element of volume is $dV = 2\pi r dr$, and therefore

$$d\Gamma_s = \frac{1}{2}\,\frac{Gb^2}{4\pi r^2}\,2\pi r\,dr = \frac{Gb^2}{4\pi}\,\frac{dr}{r} \tag{2.13}$$

Since Eq. 2.13 is based on Hooke's law which is invalid for $r < b$, the integral is written as

$$\Gamma_s = \frac{Gb^2}{4\pi}\int_b^{r_c}\frac{dr}{r} + \Gamma_{sc} = \frac{Gb^2}{4\pi}\ln\frac{r_c}{b} + \Gamma_{sc} \tag{2.14}$$

where r_c is the radius of the crystal, and Γ_{sc} is the energy per unit length of the core from $r = 0$ to $r = b$. Consequently the line energy does not have a unique value since it depends on the radius of the crystal, r_c. But since the radius of the crystal enters the energy expression in a logarithmic term, large increases in r_c produce only modest changes in Γ_s. Furthermore in a real crystal, dislocations of opposite sign result in cancellation of stress fields at large distances from the dislocation cores. In this event r_c can be approximated by about the mean spacing between dislocations, say $r_c \simeq 10^5 b$.

No accurate calculation of the core energy, Γ_{sc}, of a dislocation in metals has yet been made. Since the core represents a region of

severe disordering of the atoms, Bragg suggested that the core energy might be estimated by the product of the number of atoms per unit length in the core and the latent heat of fusion. Slightly more sophisticated estimates based on extensions of elastic behavior to large strains suggest that $\Gamma_{sc} \approx \frac{G b^2}{4\pi} \cdot 2$. Consequently,

$$\Gamma_s \approx \frac{G b^2}{4\pi}\left\{\ln \frac{r_c}{b} + 2\right\} \approx \frac{G b^2}{2} \tag{2.15}$$

and therefore

$$\Gamma_{sc} \approx \frac{\Gamma_s}{\pi} \tag{2.16}$$

By an analogous technique involving a slightly more complicated analysis, the energy of an edge dislocation can be shown to be slightly greater than that for a screw dislocation, namely,

$$\Gamma_E = \frac{\Gamma_s}{(1-\mu)} \tag{2.17}$$

The contributions of a dislocation line to the configurational and thermal entropy are small, as shown by Friedel. Consequently the free energy of a dislocation line differs rather insensibly from the energy of the line. The probability of forming a dislocation line of length ℓ as a result of thermal fluctuations is given by $e^{-\frac{\Gamma \ell}{kT}}$, where $\Gamma \ell \approx \frac{G b^2}{2} \ell$. Taking the values of $G \approx 4\times10^{11}$ dynes/cm^2, $b \approx 2\times10^{-8}$ cm and $\ell = 1$, the probability of forming a centimeter long dislocation is $e^{-\frac{6\times10^{11}}{T}}$, where k, the Boltzmann constant, is 1.4×10^{-16} ergs/deg. Thus

dislocations cannot be produced as a result of thermal fluctuations. They are formed either in the crystal during its preparation, or they are produced as a result of shear stressing. Since the shear stress necessary to produce a dislocation begins to approximate the theoretical shear stress for slip in an ideal crystal, as given by Eq. 1.6, dislocations can only be formed at points of high stress concentrations, at surfaces, grain boundaries, precipitates or various other discontinuities.

Although the energy of a long, not too rapidly curving dislocation line can usually be approximated by the value given in Eq. 2.15, the dislocation can occasionally have energies less than this value dependent on its surroundings, its length and radius of curvature. As a dislocation approaches the surface of a crystal, its energy obviously decreases, and therefore dislocations near a surface are attracted to it. A continuous dislocation loop of radius, r, has a stress field that becomes negligible at distances greater than about 2r from the line due to the mutual cancellation of the stresses arising from the positive and negative dislocation segments. Consequently its energy is about

$$2\pi r \Gamma_r \approx 2\pi r \frac{Gb^2}{4\pi}\left\{\ln \frac{2r}{b} + 2\right\} \qquad (2.18)$$

which is appreciably less than that given by Eq. 2.15 for a straight dislocation line when $r \ll r_c$. Sharp kinks and jogs shown in Fig. 2.9 have only about the core energy, since their stress fields extend only to $r_c = b$.

Although the energy of a dislocation line is not uniquely defined, and the currently used energies are approximations, good progress has

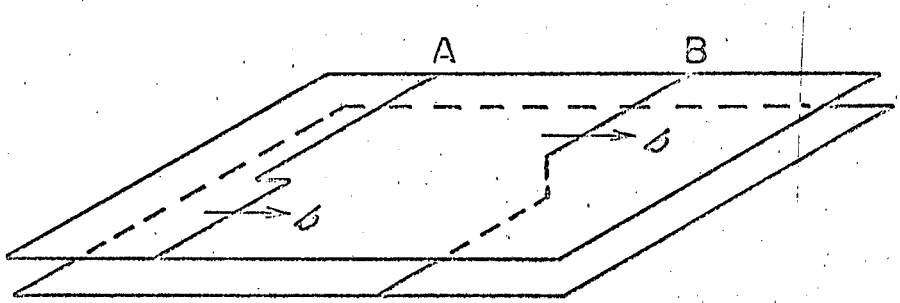

A. BURGERS VECTOR LONG KINK:
THE KINK SHOWN HERE AS A SHARP KINK WILL STRAIGHTEN OUT UNDER THE LINE TENSION. WHEREAS THE LINE IS AN EDGE DISLOCATION, THE KINK IS IN SCREW ORIENTATION.

B. A UNIT JOG WHICH EXTENDS FROM ONE SLIP PLANE TO THE NEXT PARALLEL SLIP PLANE:
THE JOG IN THIS CASE IS AN EDGE JOG.

FIGURE 2.9. KINKS AND JOGS.

nevertheless been made in characterizing, in fair quantitative detail, various interesting dislocation reactions.

2H. Dislocation Line Tension

The energy of a dislocation of length ℓ is given by

$$U = \Gamma \ell \tag{2.19}$$

where Γ is the energy per unit length. Therefore, there is a line tension equal to

$$-\frac{dU}{d\ell} = -\Gamma \tag{2.20}$$

acting along the dislocation line and attempting to shorten it. Consequently, a dislocation line is like a stretched string having a constant internal force acting so as to shorten the string. Therefore, dislocations that are free to move always have straight segments between pinned points when under zero stress.

If r is not too small, a dislocation loop, as shown in Fig. 2.10, has the energy

$$U = 2\pi r \Gamma \tag{2.21}$$

when we neglect the small differences in energies of edge and screw dislocations. In the absence of a stress the energy, U, would decrease to zero and the dislocation would vanish. This is the result of the mutual attractions of the positive and negative edge (E) and screw (S) dislocations comprising the loop. In order to maintain the loop, a stress must be applied. We let the local shear stress on the slip plane in the direction of the Burgers vector be $\tau - \tau^*$ where τ is the externally applied stress

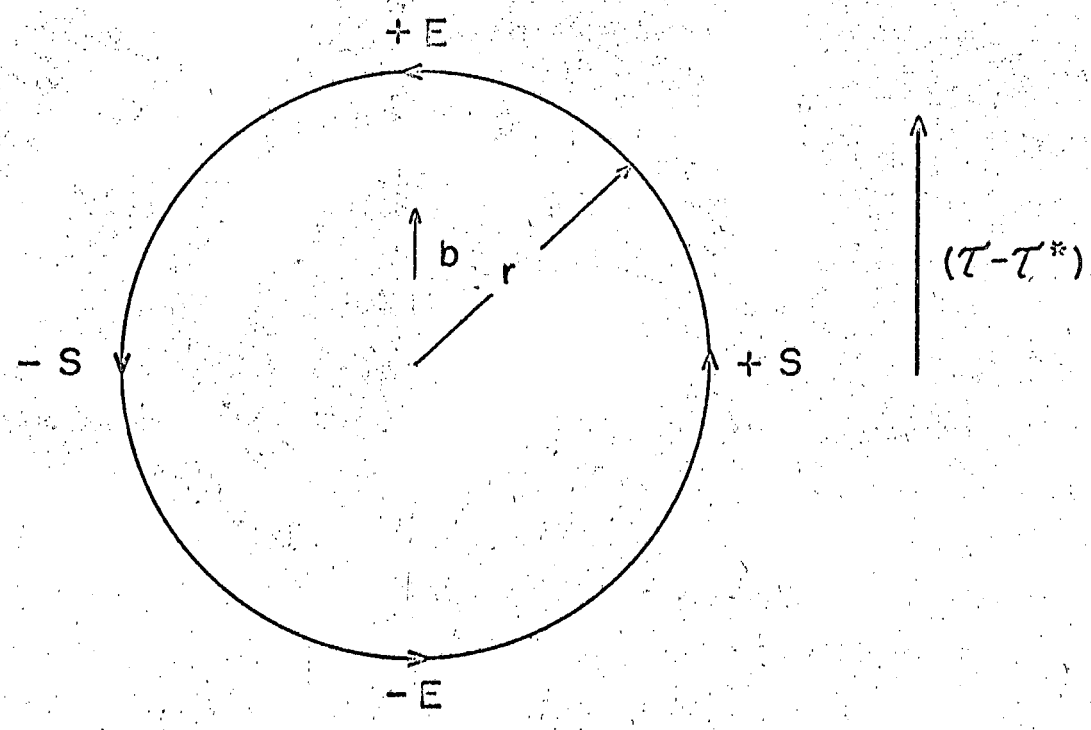

FIGURE 2.10. DISLOCATION LOOP UNDER STRESS.

and τ^* is a local back stress, to be described in more detail later, due to stress fields arising from other nearby dislocations. To determine the equilibrium radius of curvature of the loop under the local stress we will invoke the principle of virtual work. The change in the line energy obtained by increasing the radius of curvature from its equilibrium value of r to a value r + dr is

$$dU = 2\pi\Gamma dr \tag{2.22}$$

The work done by the local stress, as shown in Section 2E, on increasing the radius dr is $(\tau - \tau^*)$b times the area swept out by the dislocation or

$$dW = (\tau - \tau^*)b2\pi r dr \tag{2.23}$$

Since all of this work is converted into line energy dW = dU, and, therefore, at equilibrium,

$$(\tau - \tau^*) = \frac{\Gamma}{br} \tag{2.24}$$

Therefore, under zero local stress, the dislocations will have infinite radii of curvature and will, therefore, be straight lines. The higher the local stress, the smaller will be the radius of curvature.

2I. Dislocations Impeded at Points

A free dislocation moves normal to itself under the action of a local stress $(\tau - \tau^*)$ acting on the slip plane in the direction of the Burgers vector. If the motion of the dislocation is arrested at points along its length, it will bow out, as shown in Fig. 2.11, between the points at which it is arrested. These points might be nodal points, jogs in screw dislocations, points where forest dislocations thread the slip

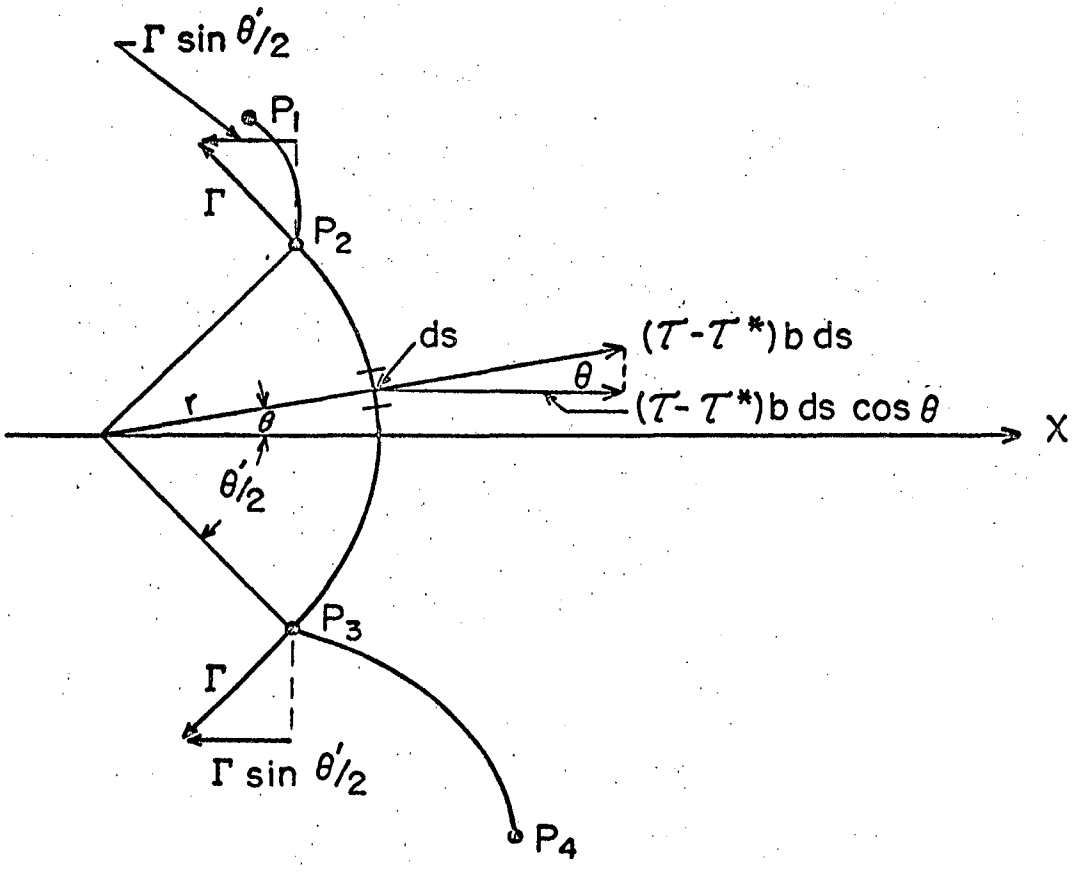

FIGURE 2.11. DISLOCATION UNDER A LOCAL STRESS HELD UP AT POINTS.

plane, fine precipitates, etc. It is easy to reaffirm that the radius of curvature of each arc is the same as that given by Eq. 2.24 regardless of the distance between points.

The two sources of forces acting on the arc segment extending from $-\theta'/2$ to $+\theta'/2$ are the line tensions, Γ, and the forces acting on the dislocation segment. The component in the X direction from the line tension is:

$$F_{1x} = -2\Gamma \sin \theta'/2$$

And the component of the force due to the local stress acting on segment ds in the X direction is $(\tau - \tau^*)b \cos \theta \, ds$. Therefore, the total force in the X direction arising from the local stress is:

$$F_{2x} = \int_{-\theta'/2}^{\theta'/2} (\tau - \tau^*) b \cos \theta \, ds = (\tau - \tau^*) br \int_{-\theta'/2}^{\theta'/2} \cos \theta \, d\theta$$

$$= (\tau - \tau^*) br 2 \sin \theta'/2$$

the radius of curvature being constant over the small range $-\theta'/2 \leq \theta \leq \theta'/2$. Therefore, under equilibrium conditions ($F_{1x} + F_{2x} = 0$) Eq. 2.24 is again obtained.

The formation of a large number of dislocations over a narrow range of slip planes may be achieved by successive generation of dislocations at points of stress concentration, the multiplication of dislocations by cross-slip or by the operation of a Frank-Read source. The Frank-Read[24] source mechanism, depicted in Fig. 2.12, will operate only if the dislocation segments are not locked by precipitates or otherwise immobilized.

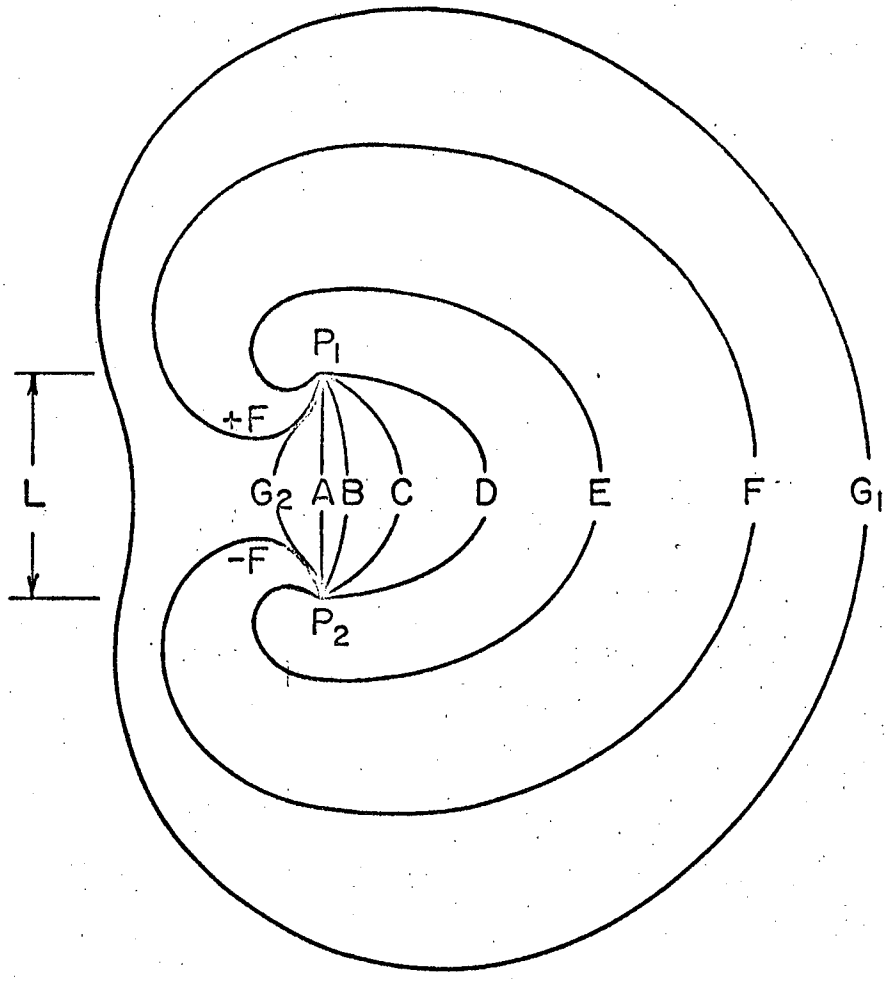

FIG. 2.12 A FRANK - READ SOURCE.

The dislocation segment A between the nodal points P_1 and P_2 of a dislocation network is a straight line under zero local stress. As the stress is increased the radius of curvature decreases as shown by Eq. 2.24. At stage D the radius of curvature is L/2 and

$$(\tau - \tau^*)_c = \frac{\Gamma}{b\,L/2} \qquad (2.25)$$

Any infinitesimal increase in stress will induce a further displacement of the dislocation arc. But as a result of the geometry induced by having the dislocation pinned at the nodal points P_1 and P_2, the arc now acquires successively greater radii of curvature. The maximum stress required to operate the Frank-Read source is, therefore, given by Eq. 2.25. The dislocation, therefore, continues to move normal to itself giving stage F. As motion continues the +F and -F dislocation segments of opposite sign annihilate each other by pinching together. If the dislocation segments are on different slip planes due to the presence of jogs, however, they will not be able to annihilate each other, unless they are in screw orientation and can cross slip. Thus, dislocations G_1 and G_2 are formed. Whereas G_1 is now free to sweep through the crystal, G_2 can repeat the process. Therefore, a single active source can produce innumerable dislocations, at least until the back stress τ^* becomes so large as to prevent further operation of the source. Those sources for which $(\tau - \tau^*)L$ is the greatest will operate first. Thus, the number of sources operating at a given stress level will depend on the distribution of source sizes (L) and the local back stresses (τ^*).

Orowan[25] applied the concepts of the Frank-Read source, with appropriate modification, to the theory of dispersion strengthening of

alloys. The solid points of Fig. 2.13 represent hard incoherent precipitates, through which, of course, the dislocations cannot pass. If, as is the usual case in a dispersion hardened alloy, the moduli of elasticity of the precipitate is higher than that of the matrix, the dislocation energy will increase as the dislocation approaches each particle. Therefore, it will not enter the surface of the precipitate. As the local stress $(\tau - \tau^*)$ is increased, the first dislocation will bow out between the particles as shown in (b). And when

$$(\tau - \tau^*)_c = \frac{\Gamma}{b L_m/2} \qquad (2.26)$$

the positive and negative segments of adjacent loops will coalesce permitting the dislocation to move forward. Eq. 2.26, therefore, reveals that the yield strength of a dispersion hardened alloy increases with decreasing distances between the dispersed particles, that is for finer dispersions. The closed dislocation loops left behind provide higher back stresses, τ^*, for the next dislocation and were thus assumed to be responsible for the higher rates of strain hardening observed in the initial stages of cold working dispersion hardened alloys. Recent investigations[26] have shown, however, that the greater rates of strain hardening are probably attributable to the very high density of the dislocations in entanglements that occur about the particles, the theory being more complicated than so naively depicted in Fig. 2.13. Furthermore, the slower rates of strain hardening of dispersion strengthened alloys in the high strain range is not due to fracturing of the dispersed particles, as suggested by Fisher, Hart and Pry.[27] Electron microscopic observations have revealed that the leveling off of the flow stress

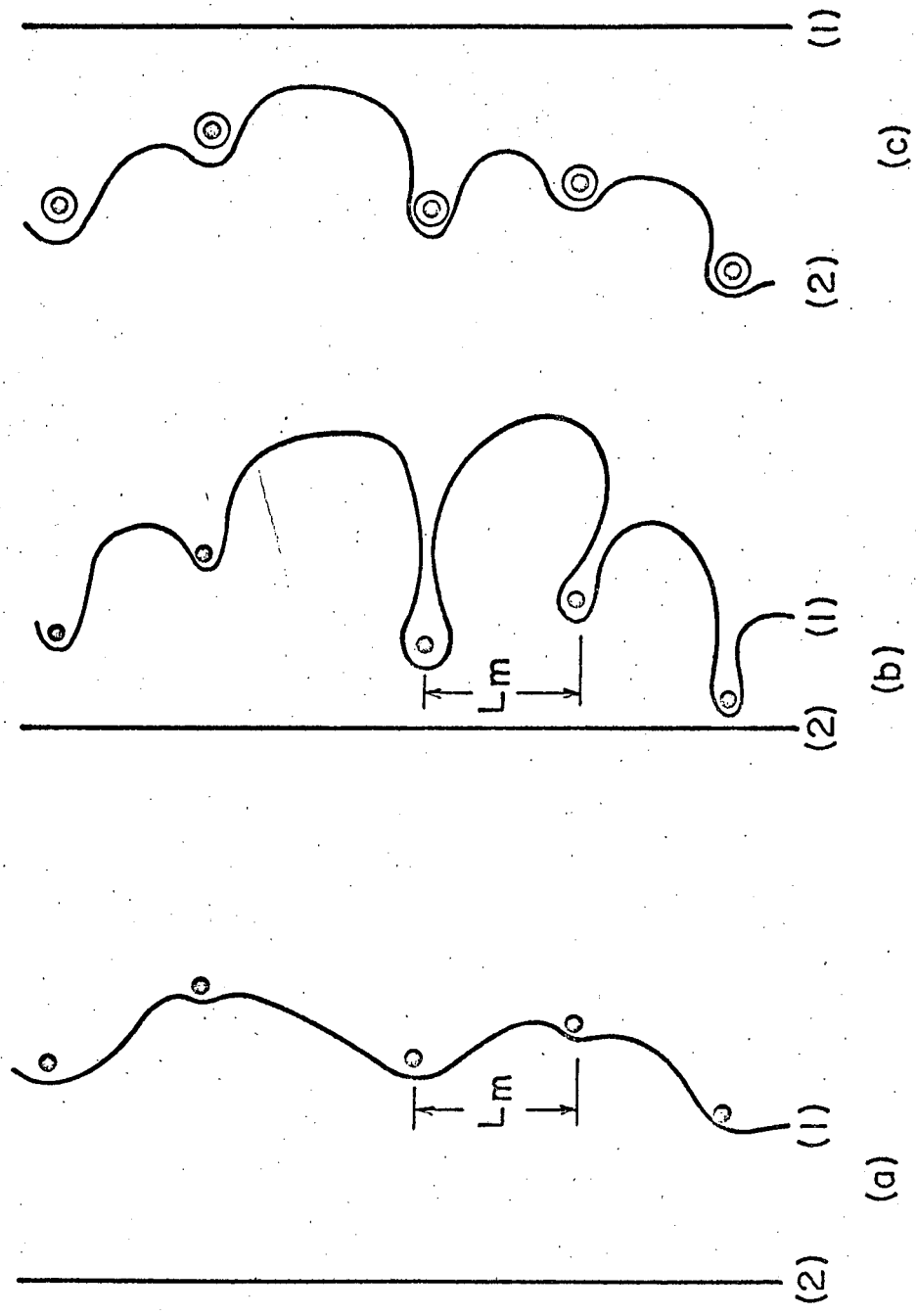

FIG. 2.13 OROWAN'S THEORY FOR DISPERSION STRENGTHENING.

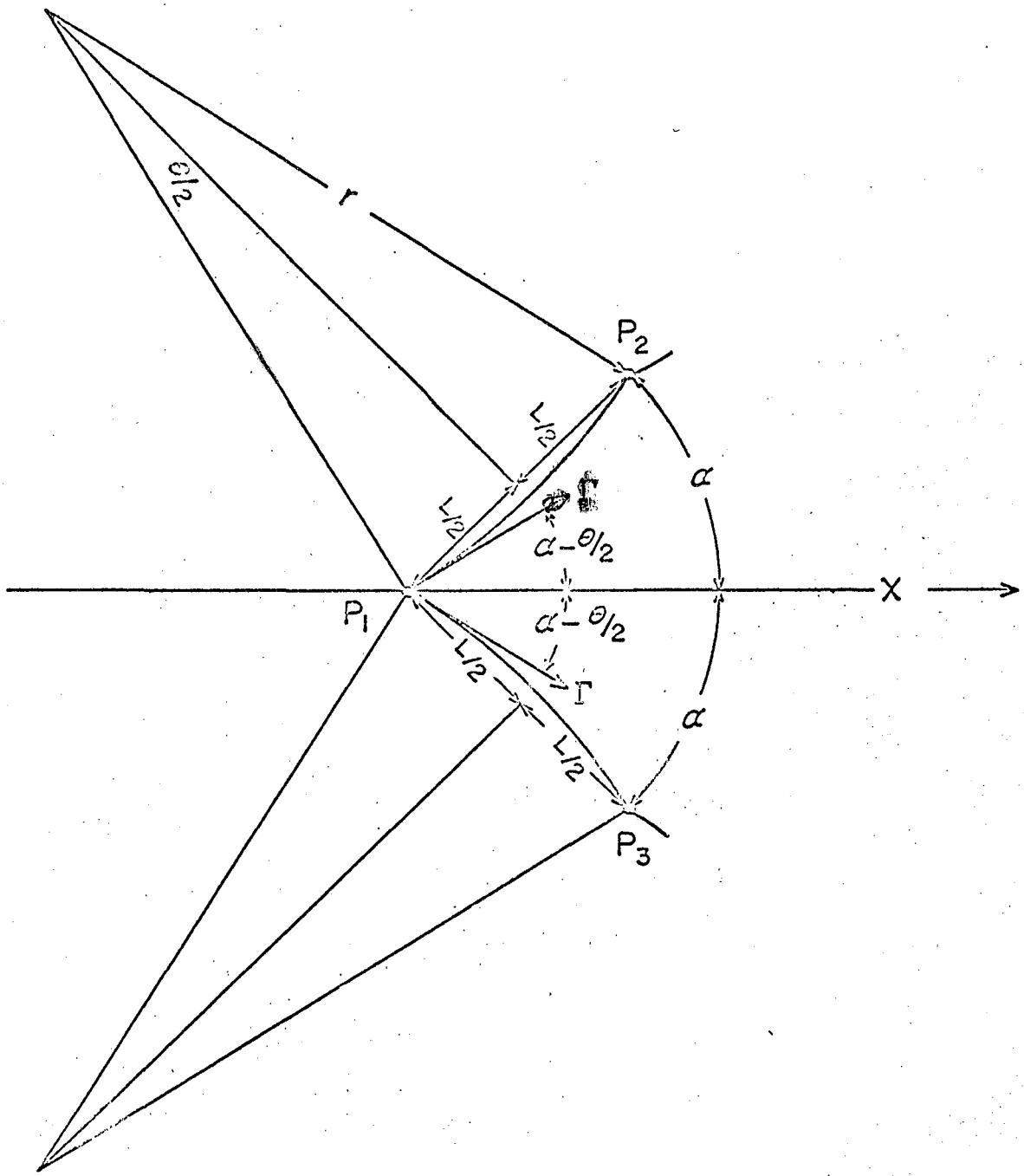

FIG. 2.13A. FORCE AT A POINT DUE TO A STRESS.

frequently occurs before any fracturing can be detected. Most likely this leveling off of the flow stress can be attributed to relief of the back stresses by cross slip.

When the local stress is less than the critical value, $(\tau=\tau^*)_c$, the dislocation segments will bow out between any arresting points as shown for a symmetrical case in Fig. 2.13. The force in the X direction at P_1 due to the line tensions is

$$F_x = 2\Gamma \cos(\alpha - \theta/2) = 2\Gamma\{\cos\alpha \cos\theta/2 + \sin\alpha \sin\theta/2\}$$

Therefore, the maximum force is 2Γ, whereas the minimum force is zero. By application of Eq. 2.24

$$\sin\frac{\theta}{2} = \frac{L}{2r} = \frac{(\tau-\tau^*)Lb}{2\Gamma} \quad \text{and}$$

$$\cos\frac{\theta}{2} = \frac{\{r^2-(L/2)^2\}^{1/2}}{r} = \left\{1-\left(\frac{L}{2r}\right)^2\right\}^{1/2} = \left\{1-\left[\frac{(\tau-\tau^*)Lb}{2\Gamma}\right]^2\right\}^{1/2}$$

Therefore,

$$F_x = \left\{(2\Gamma)^2-(\tau-\tau^*)Lb^2\right\}^{1/2}\cos\alpha + (\tau-\tau^*)Lb\sin\alpha \qquad (2.27)$$

Actually the force will be somewhat higher than this value, since the near segments have opposite signs and will attract each other. As $\alpha \to 0$ the force increases. In general for random positioning of the points and assuming L to be the average distance between points, the average value of F_x is usually estimated to be about

$$F_x = (\tau-\tau^*)Lb \qquad (2.28)$$

This force aids the thermally activated process of intersection and motion of jogged screw dislocations to be discussed later. If the thermally activated processes at P_2 or P_3 are easier than at P_1, the dislocation will move forward at these points causing α to decrease, thus introducing higher forces to activate the slip process at P_1. This somewhat justifies the use of Eq. 2.23 as the average value of the force.

If the process at P_1 cannot be activated, even at the highest stresses one of two possible mechanisms can occur. If the two bowed segments of the dislocation are on the same slip plane, they will join, as previously described in the Orowan theory for dispersion hardening, leaving a dislocation ring at P_1. But if the two bowed dislocation segments lie on different parallel slip planes, as is obtained when P_1 is the point of a jog in a screw dislocation, branches of the two bowed segments will attract each other and form a dipole, as shown in Fig. 2.14. Such dipoles, usually initiated at superjogs, are often observed in electron micrographs of cold worked metals.

If the superjogs at P_1 and P_1' are very far apart, they may play a very small role in strain hardening, since the stress fields from superjogs only a few slip planes in height are quite small and local and since the two arms are composed of dislocations of opposite sign.

2J. Elastic Interactions Between Dislocation Pairs

As described in Section 2E, when they are long distances apart, dislocations of the same sign repel and dislocations of opposite sign attract each other with forces that depend on the reciprocal of the distance between the dislocations. When the two dislocations are nearby, however, the result is slightly more complicated, especially for edge dislocations.

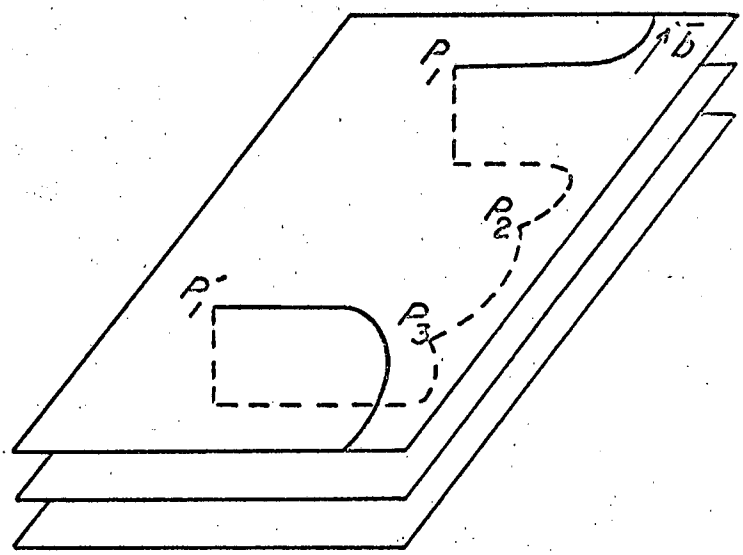

FIGURE 2.14. SUPERJOGS P_1 AND P_2 FORMING DIPOLES.

We will consider the two dislocations of the same sign lying on two slip planes separated by a distance Y_o, as shown in Fig. 2.15, and we will calculate the force due to the dislocation at the origin on a unit length of the other dislocation. Since the dislocations have edge components, they are confined to move on their slip planes.

The stresses due to the screw component of the dislocation lying at the origin are given by Eqs. 2.4 and 2.5, and those due to the edge component are given by Eqs. 2.8 to 2.11. Since the force per unit length of the dislocation is given by the resolved shear stress on the slip plane in the direction of the Burgers vector times the Burgers vector,

$$F_x = \sigma_{zy} b_s + \sigma_{xy} b_E \qquad (2.29)$$

where the stresses refer to those due to the stress field of the dislocation at the origin acting on the second dislocation. Since the Burgers vectors of the two dislocations are identical, in this case, there is no interaction between the screw and edge components of the two dislocations. Consequently, the effects of the screw and edge components can be treated separately.

The force acting in the x direction of the second dislocation due to the screw components is, therefore,

$$F_{xs} = \frac{G b_s^2}{2\pi} \frac{x}{(x^2+y_o^2)} \qquad (2.30)$$

and is shown by the solid curve of Fig. 2.16 in terms of units of $\frac{G b_s^2}{2\pi} \frac{1}{y_o}$. It has extreme values at $\frac{dF_{xs}}{dx} = 0$ giving a maximum and a minimum value at $x = y_o$ and $x = -y_o$, respectively. The maximum force, given by introducing $x = y_o$ into Eq. 2.30, is

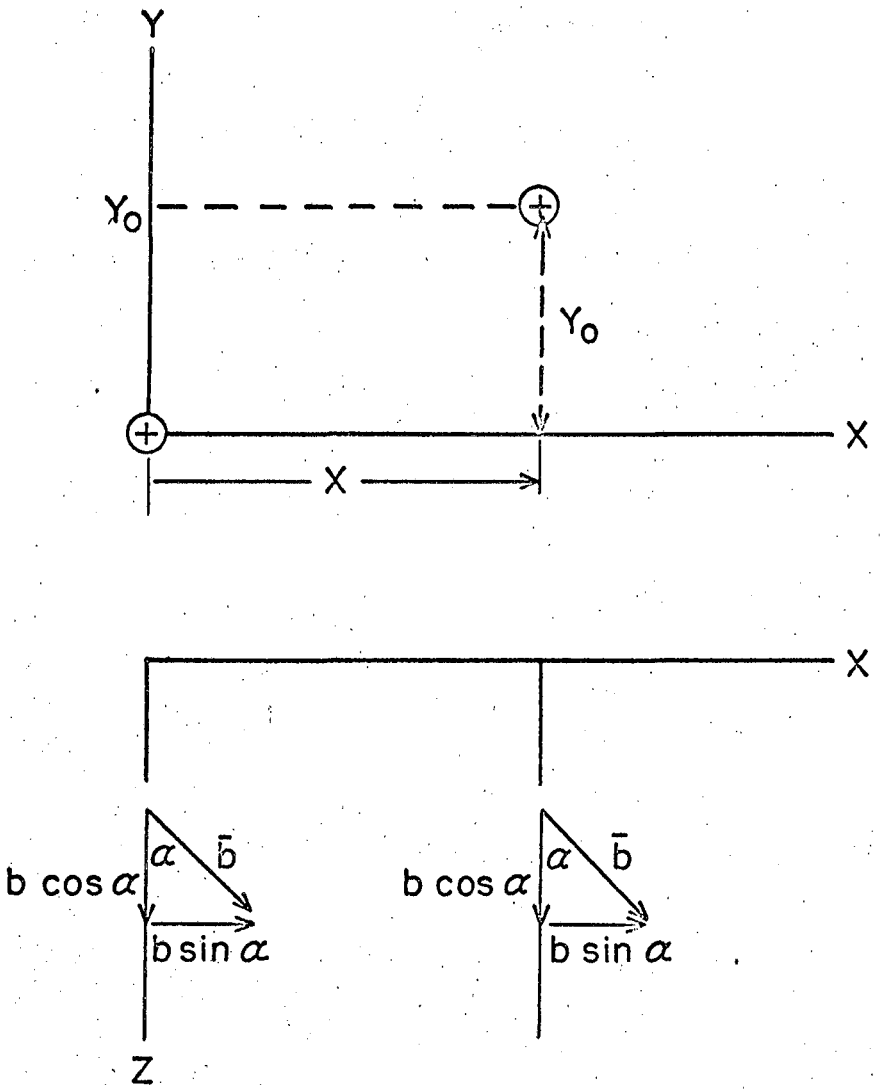

FIG. 2.15 INTERACTION BETWEEN TWO DISLOCATIONS.

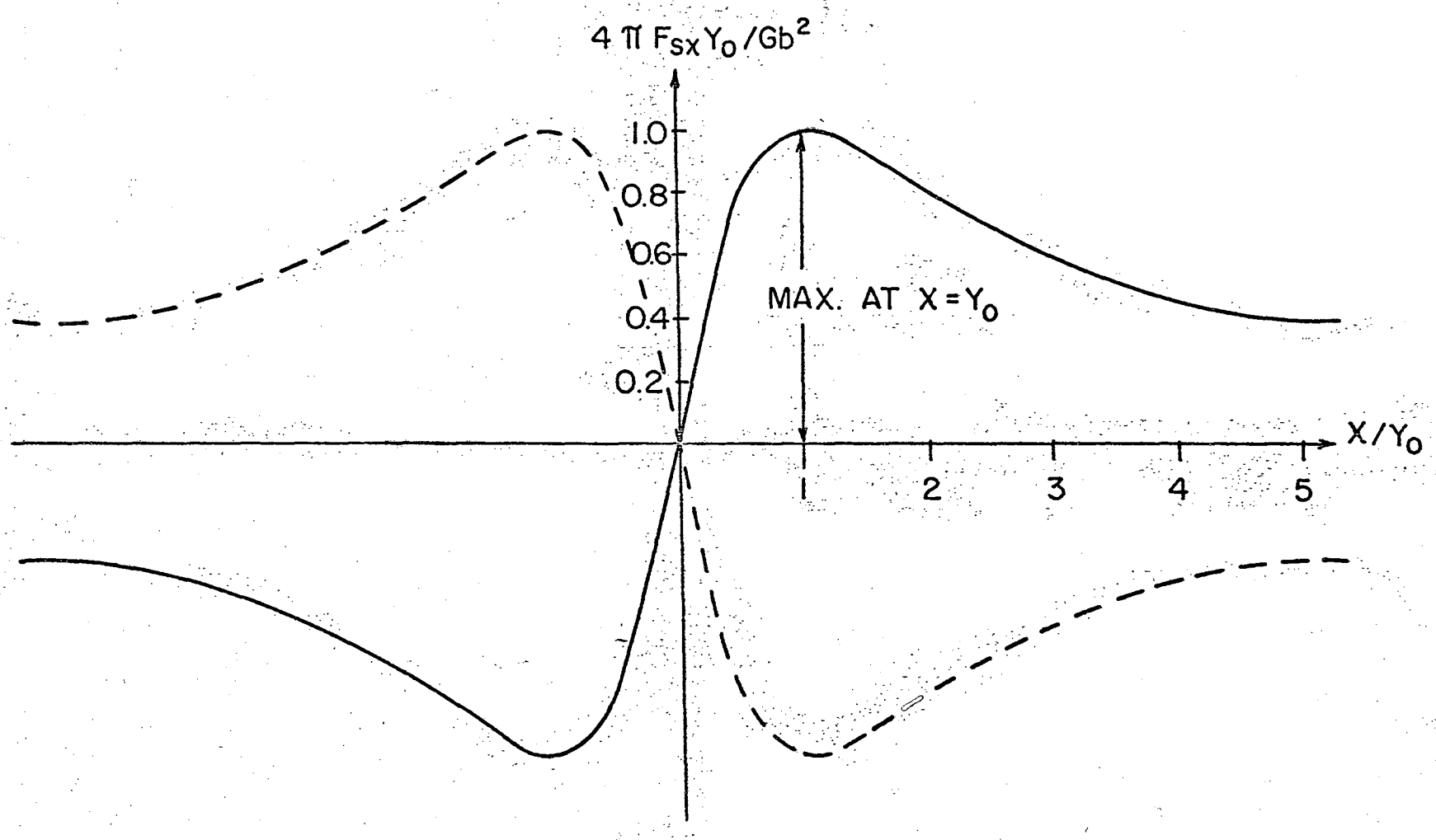

FIGURE 2.16. FORCE OF INTERACTION BETWEEN TWO SCREW DISLOCATIONS.

$$F_{sx\,max} = \frac{Gb_s^2}{4\pi y_o} \tag{2.31}$$

If the second dislocation had a negative sign, the signs of Eqs. 2.30 and 2.31 would have been negative and the result shown by the broken curve in Fig. 2.16 would have been obtained. Thus, for dislocations of the same sign, the second dislocation will be acted upon by a positive force when x is positive and a negative force when x is negative, whereas if the second dislocation has a negative sign it will be attracted so as to come to rest directly above the first dislocation.

When a shear stress S_{yz} is applied to a crystal containing two screw dislocations, as depicted in Fig. 2.5B, the positive dislocation will move to the right and the negative dislocation will move to the left under the force $S_{yz}b_s$. As shown by the broken curve in Fig. 2.16, they will not pass each other until

$$S_{yz}\, b_s \geq \frac{Gb_s^2}{4\pi y_o} \tag{2.32}$$

This requirement leads to strain hardening as Y_o decreases with strain. On the other hand, other screw dislocations, as we shall see later, can pile up against the leading one to introduce a sufficiently high stress concentration to force the passage. Furthermore, pure screw dislocations, if undissociated might cross slip and annihilate each other.

As shown by Eq. 2.29, the force due to one edge dislocation on a parallel dislocation on a parallel slip plane, Y_o above the first is given by

$$F_{xE} = \frac{Gb_E^2}{2\pi(1-\mu)} \frac{x(x^2+y_o^2)}{(x^2+y_o^2)^2} \qquad (2.33)$$

The force, therefore, is zero at $x = -\infty\ ;\ -Y_o;\ 0;\ Y_o;\ \infty$ and since it is a continuous function of x, it must have four extreme values. The extreme values found by the usual procedure of placing $\partial F_{xE}/\partial x = 0$ are given by $x^2 = y_o^2\,(3 \pm 2\sqrt{2})$. And F_{xE} has its maximum value, using the positive sign, of

$$F_{xE\,max} \simeq \frac{Gb_E^2}{8\pi(1-\mu)y_o} \qquad (2.34)$$

which is just slightly less than the value given in Eq. 2.31 for screw dislocations. The force, given by Eq. 2.33, is shown in Fig. 2.17. When the second dislocation lies in the range $-Y_o < x < Y_o$ it is attracted to the first and, in the absence of any other local stress, will come to rest at $x = 0$. This is the basis for the formation of tilt boundaries. But if the second dislocation is in the range $-\infty < x < -Y_o$ or $Y_o < x < \infty$ two edge dislocations of the same sign will repel each other. One edge dislocation will pass another only if an auxiliary shear stress S_{xy} is imposed on the pair when

$$S_{xy} b_E \geq \frac{Gb_E^2}{8\pi(1-\mu)y_o} \qquad (2.35)$$

The force between edge dislocations having opposite signs is shown by the broken curve of Fig. 2.17. Such dislocations will come to rest at $x = \pm Y_o$ in the absence of an applied stress. If an applied stress S_{xy} less than that given by the condition of Eq. 2.35 is applied, the equilibrium

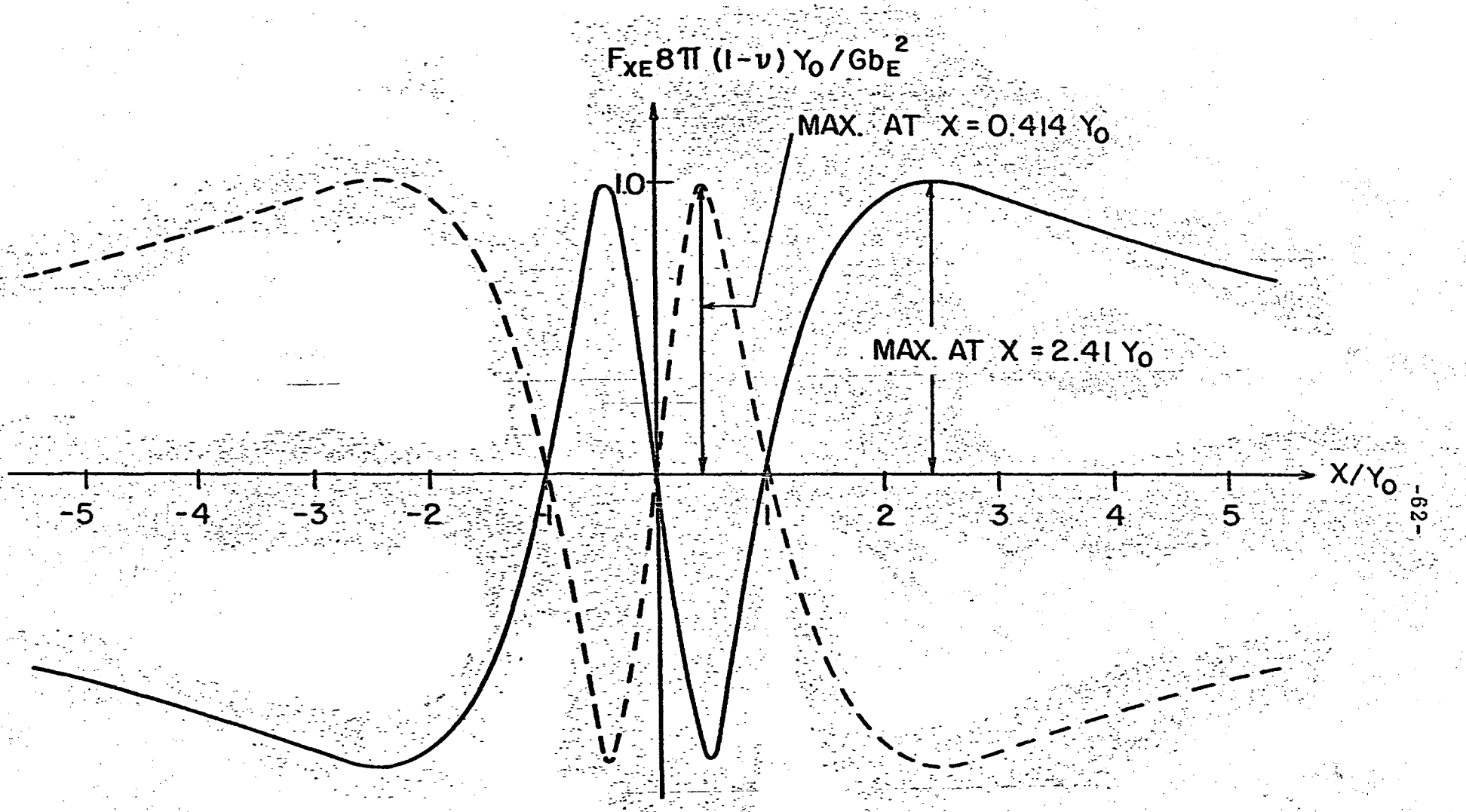

FIGURE 2.17. THE FORCE ACTING BETWEEN TWO EDGE DISLOCATIONS.

value of x will be given by

$$S_{xy} b_E = \frac{G b_E^2}{2\pi(1-\mu)} \frac{x(x^2+y_o^2)}{(x^2+y_o^2)^2} \qquad (2.36)$$

where x is positive.

2K. Dislocation Arrays on Slip Planes

When dislocations from a common source are subjected to an applied shear stress, they may pile up against barriers. Such pile ups are frequently observed in crystals with low stacking fault energies. The barriers may be precipitates, grain boundaries, low angle boundaries, sessile dislocations, locked dislocations, or Lomer-Cottrell[28] dislocations. A typical example of a piled-up array is illustrated in Fig. 2.18 where the X-Z plane is the slip plane and the barrier is parallel to the Z axis. Under the applied shear stress in the direction of the Burgers vector

$$(\tau - \tau^*) = S_{yz} \cos\theta + S_{yx} \sin\theta \qquad (2.37)$$

the dislocations pile up over a distance L, as shown, parallel to the barrier. The forces acting on each dislocation of the array, excepting the last, arise from three factors, (1) the applied stress, (2) the interaction of the screw components, and (3) the interaction of the edge components. The n^{th} dislocation is acted upon by the forces due to the applied stress and the sums of the effects of all other dislocations in the array, its motion being arrested by the barrier which is here assumed to have a short-range stress field interaction only with the leading dislocation of the array.

The total force, therefore, acting on a unit length of the η^{th} dislocation ($1 \leq n$) is as follows:

(a) From the applied stress, and long-range stress fields

$$(\tau - \tau^*)\, b$$

(b) From the screw components of the remaining dislocations of the array

$$\sum_{\substack{j=1 \\ j\neq i}}^{n} \frac{G b_s \cdot b_s}{2\pi (x_i - x_j)}$$

(c) From the edge components of the dislocations in the array

$$\sum_{\substack{j=1 \\ j\neq i}}^{n} \frac{G b_e \cdot b_e}{2\pi (1-\mu)(x_i - x_j)}$$

Under equilibrium conditions, the sum of the forces acting on each dislocation is zero; hence

$$(\tau - \tau^*) b + \frac{G b^2}{2\pi}\left\{\cos^2\theta + \frac{\sin^2\theta}{(1-\mu)}\right\} \sum_{\substack{j=1 \\ j\neq i}}^{n} \frac{1}{(x_i - x_j)} = 0 \qquad (2.38)$$

For convenience we let

$$X_i = x_i / L \qquad (2.39)$$

and rewrite the equilibrium equation for each dislocation of the array as

$$T = \frac{2\pi (\tau - \tau^*) b L}{G b^2 \left\{\cos^2\theta + \frac{\sin^2\theta}{(1-\mu)}\right\}} = \sum_{\substack{j=1 \\ j\neq i}}^{n} \frac{1}{(x_j - x_i)} \qquad (2.40)$$

An exact solution of Eqs. 2.40 has been given by Eschelby, Frank, and Nabarro.[29] Inasmuch as this solution is lengthy and involves rather sophisticated mathematics, we will be content here to undertake an approximate solution that reveals the physical content of the problem.

Equations 2.40 apply to each dislocation. For the first dislocation, i = 1, and

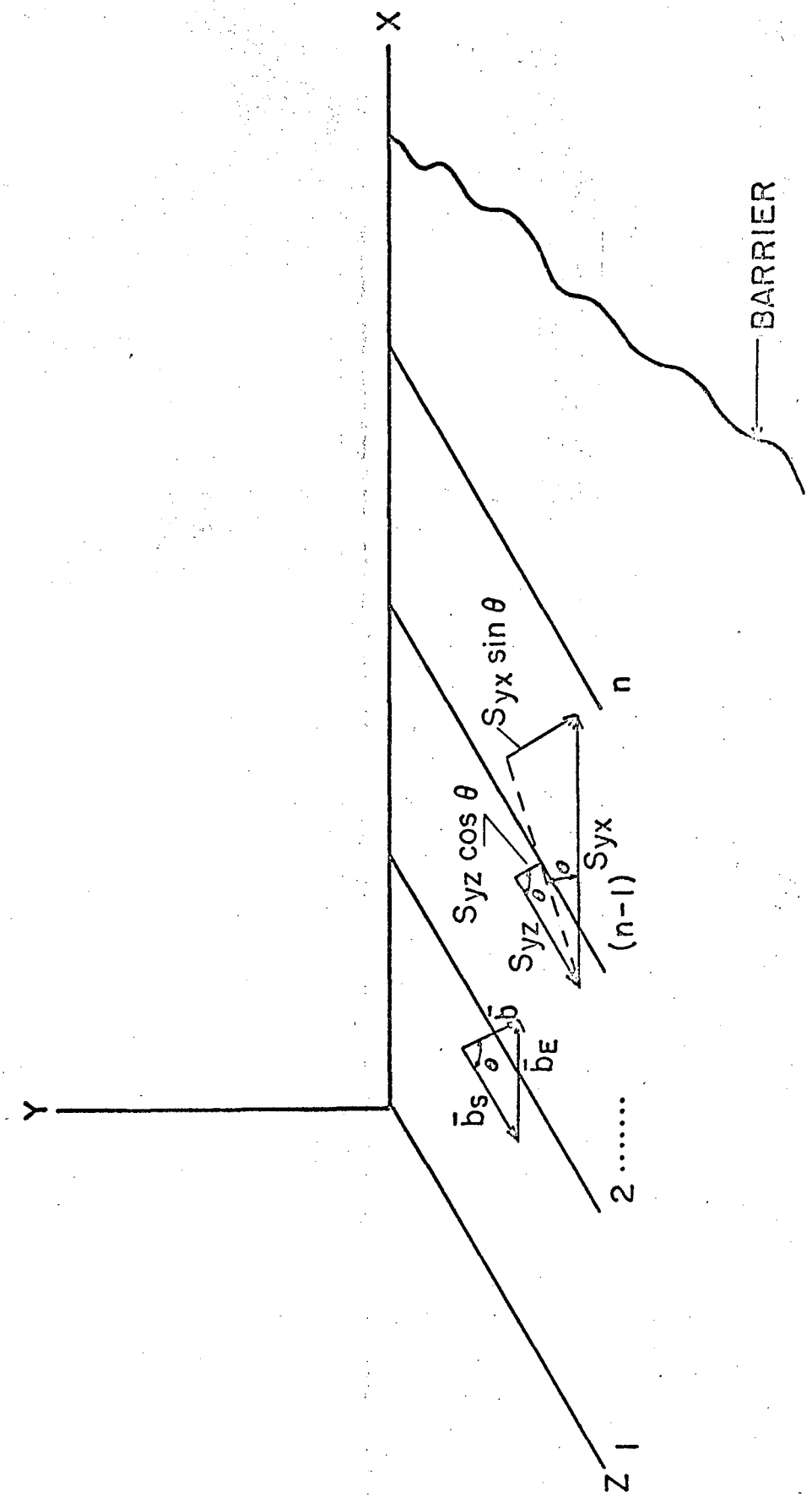

FIGURE 2.18. A PILED-UP ARRAY OF DISLOCATIONS.

$$T = \frac{1}{X_2} + \frac{1}{X_3} + \cdots\cdots + \frac{1}{X_{n-1}} + \frac{1}{X_n} \qquad (2.41a)$$

Since the X_js are fractions, as given by the definition of Eq. 2.39, T is equal to a sum of reciprocals of fractions, and, therefore,

$$T = (n-1)\left(\frac{1}{X}\right)_{avg} = \frac{n-1}{\alpha}$$

or

$$(n-1) = \alpha T = \frac{2\pi\alpha L\,(\tau - \tau^*)}{Gb\left\{\cos^2\theta + \frac{\sin 2\theta}{(1-\mu)}\right\}} \qquad (2.42)$$

which demands that the number of dislocations in the array increases linearly with the length of the array, L, and the average applied shear stress, $\tau - \tau^*$. A little reflection will reveal that $1/2 < \alpha < 1$. The more sophisticated analysis shows that α depends on the number of dislocations in the array where $\alpha \simeq 3/4$ is, generally, a good approximation.

To complete the analysis we now write Eqs. 2.40 for all excepting the last dislocation as follows:

$$(i=1);\ T = \frac{1}{X_2} + \frac{1}{X_3} + \cdots\cdots + \frac{1}{X_{n-1}} + \frac{1}{X_n} \qquad (2.41a)$$

$$(i=2);\ T = -\frac{1}{X_2} + \frac{1}{X_3 - X_2} + \cdots\cdots + \frac{1}{X_{n-1} - X_2} + \frac{1}{X_n - X_2} \qquad (2.41b)$$

$$(i=3);\ T=-\frac{1}{X_3}-\frac{1}{X_3-X_2}+\frac{1}{X_4-X_3}+\cdots+\frac{1}{X_{n-1}-X_3}+\frac{1}{X_n-X_3} \quad (2.41c)$$

$$(i=n-2);\ T=-\frac{1}{X_{n-2}}-\frac{1}{X_{n-2}-X_2}+\cdots+\frac{1}{X_{n-1}-X_{n-2}}+\frac{1}{X_n-X_{n-2}} \quad (2.41p)$$

$$(i=n-1);\ T=-\frac{1}{X_{n-1}}-\frac{1}{X_{n-1}-X_2}\cdots-\frac{1}{X_{n-1}-X_{n-2}}+\frac{1}{X_n-X_{n-1}} \quad (2.41q)$$

It is an easy matter to see that when the n - 1 Eqs. 2.41 are added, terms cancel so that

$$(n-1)T=\frac{1}{X_n}+\frac{1}{X_n-X_2}+\cdots\cdots\frac{1}{X_n-X_{n-1}} \quad (2.43)$$

The total local stress acting on the n^{th} dislocation is, of course, zero. Thus, the barrier reaction stress equals the applied stress plus the sums of the stresses due to all the remaining dislocations in the array. The local stress on the n^{th} dislocation, due exclusively to the remaining dislocation of the array, is

$$\tau_\ell'=\frac{Gb}{2\pi}\left\{\cos^2\theta+\frac{\sin^2\theta}{(1-\mu)}\right\}\left\{\frac{1}{X_n}+\frac{1}{X_n-X_2}+\cdots\frac{1}{X_n-X_{n-1}}\right\} \quad (2.44)$$

as suggested previously, or

$$\tau_\ell'=\left\{\frac{Gb}{2\pi L}\left\{\cos^2\theta+\frac{\sin^2\theta}{(1-\mu)}\right\}\right\}\left\{\frac{1}{X_n}+\frac{1}{X_n-X_2}+\cdots\frac{1}{X_n-X_{n-1}}\right\}$$

Introducing Eq. 2.40 for the first bracketed term and Eq. 2.43 for the second bracketed term, reveals that

$$\tau_\ell' = \left(\frac{\tau - \tau^*}{\tau - \tau^*}\right)(n-1)\,l = (n-1)(\tau - \tau^*) \qquad (2.45)$$

Adding the applied shear stress $(\tau - \tau^*)$, to τ_ℓ' reveals that the local shear stress, due to the array and the applied shear stress, acting on the n^{th} dislocation of the array is

$$\tau_\ell = n(\tau - \tau^*) \qquad (2.46)$$

Consequently, piled-up arrays generate a stress concentration factor proportional to the number of dislocations in the array. On occasions this factor might exceed 100 or so, producing very great local stresses.

When Eq. 2.42 is introduced into Eq. 2.45, the local stress is given by

$$\tau_\ell' = \frac{2\pi\alpha L\,(\tau - \tau^*)^2}{Gb\left\{\cos^2\theta + \frac{\sin^2\theta}{(1-\mu)}\right\}} \qquad (2.47)$$

Thus, for a given length of array, the local stress increases as a function of the square of the applied stress.

When the grain boundary constitutes the principal barrier, L can be associated with the grain diameter, D. Then, the applied stress becomes[30]

$$\tau = \tau^* + \sqrt{\frac{k\tau_\ell'}{D}} \qquad (2.48)$$

where

$$k = \frac{Gb}{2\pi\alpha}\left\{\cos^2\theta + \frac{\sin^2\theta}{(1-\mu)}\right\} \qquad (2.49)$$

If τ_ℓ' is associated with the local stress necessary to induce slip on five slip systems in the adjacent grain, a requirement suggested by von Mises[31] in order to preserve continuity at the grain boundary, the applied shear stress for deformation should increase linearly with $D^{-1/2}$. There is extensive correlation with this suggestion, a typical example of which is given in Fig. 2.19.[30]

The preceding analysis describes the state of stress at the n^{th} dislocation of the array. For distances greater than L away from the array, the stress field is equal to that of a single dislocation at $x \simeq 3/4$ having a Burgers vector nb. Over intervening ranges, as shown by Stroh[32] the stress field is approximately given by

$$S = \sqrt{4/r}\, S_1 f(\theta) \qquad (2.50)$$

where r is the distance from the n^{th} dislocation, and S_1 is the applied shear stress.

2L. Superdislocations

For the superlattice AB shown in Fig. 2.20A the Burgers vector is $2\bar{b}$, that is twice the usual Burgers vector appropriate for a random solid solution of the alloy AB for the same crystal structure. But the superdislocation will dissociate into two unit dislocations as shown in Fig. 2.20B. This dissociation must occur because the energy decreases as it takes place. Considering only the interaction energy between the dislocations, the change in energy when the superdislocation dissociates completely (i.e., when the two dislocations are separated an infinite distance) is

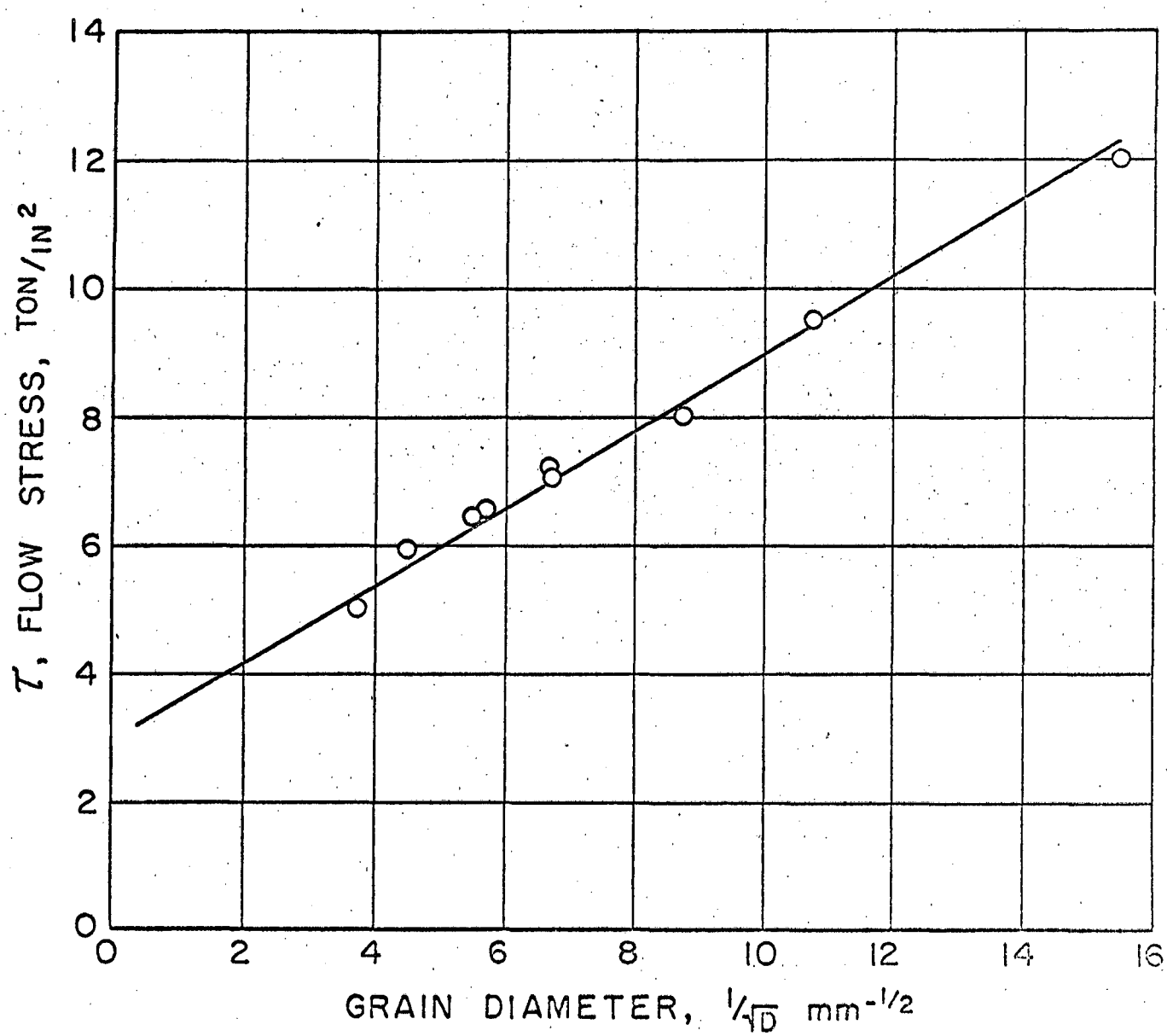

FIGURE 2.19. EFFECT OF GRAIN SIZE ON THE FLOW STRENGTH OF METALS.

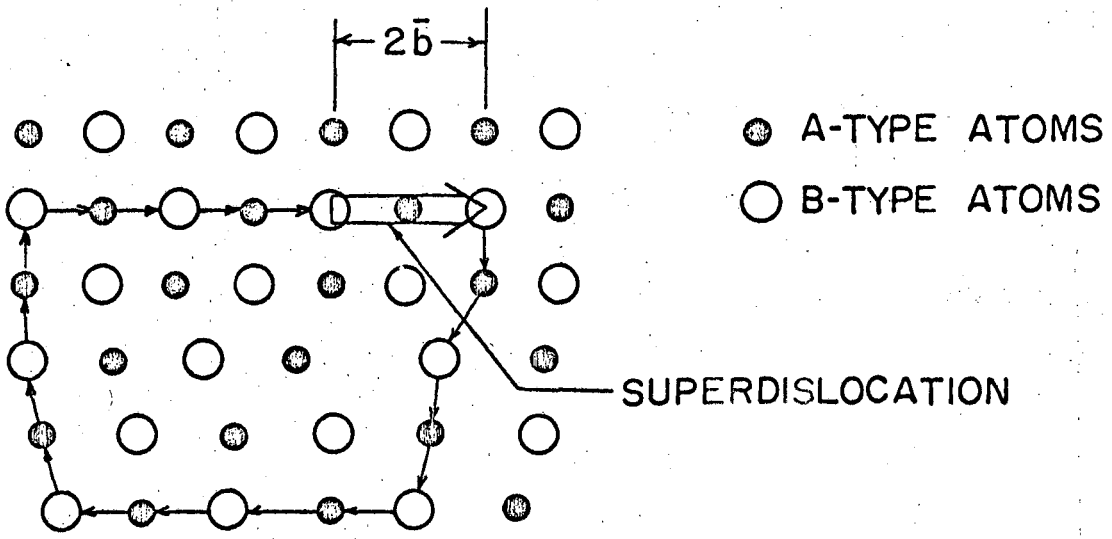

(a) ARROWS INDICATE A BURGERS CIRCUIT WHICH FAILS TO CLOSE BY $2\bar{b}$.

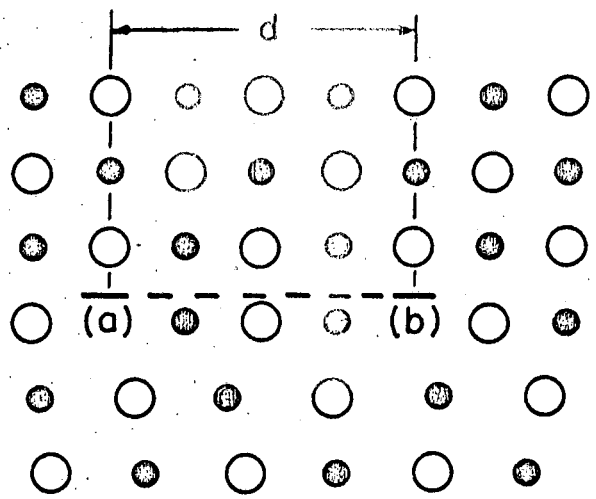

(b) DISSOCIATION OF A SUPERDISLOCATION AND FORMATION OF AN ANTIPHASE BOUNDARY.

FIGURE 2.20. A SUPERDISLOCATION.

$$\Delta U = 2\left(\frac{Gb^2}{2}\right) - \frac{G(2b)^2}{2} = -Gb^2 \qquad (2.51)$$

since the energy of a dislocation is about one-half of the shear modulus times the square of its Burgers vector. Because the energy decreases, the reaction will take place; but it cannot go to completion yielding infinitely separated dislocations, because as the dislocations move apart they increase the antiphase boundary, shown in Fig. 2.20B. Therefore, the two dislocations will remain somewhat associated at an equilibrium distance of separation equal to d.

In order to determine the separation distance, d, consider the unit-long dislocations shown in Fig. 2.21 where the dislocation line makes an angle θ with the Burgers vector. The force due to the first dislocation on the second will be

$$F_x = \sigma_{yz} b_s + \sigma_{xy} b_E \qquad (2.52)$$

where σ_{yz} and σ_{xy} are the stresses at the second dislocation due to the first dislocation. Introducing Eqs. 2.5 and 2.11 (for y = 0) reveals that

$$F_{1x} = \frac{Gb_s^2}{2\pi x} + \frac{Gb_E^2}{2\pi(1-\mu)x} = \frac{Gb^2}{2\pi}\left\{\cos^2\theta + \frac{\sin^2\theta}{(1-\mu)}\right\}\frac{1}{x} \qquad (2.53)$$

If γ_a^ℓ is the surface energy per cm^2 of antiphase boundary, the total surface energy is $U_s = \gamma_a^\ell x$. Therefore, the force due to the

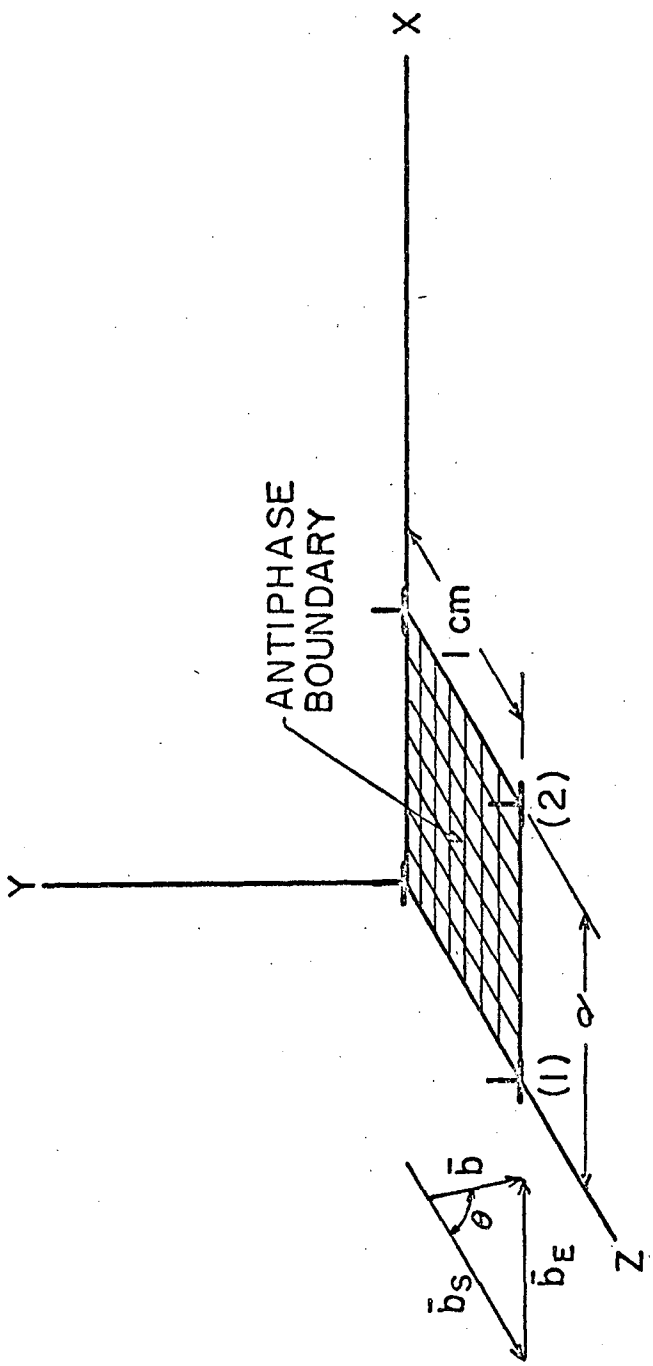

FIGURE 2.21. A PARTIALLY DISSOCIATED SUPERDISLOCATION.

antiphase boundary acting on the second dislocation is

$$F_{2x} = -\frac{dU_s}{dx} = -\gamma_a \qquad (2.54)$$

Consequently, equilibrium is obtained when $F_{1x} + F_{2x} = 0$ at $x = d$ or

$$d = \frac{Gb^2}{2\pi\gamma_a}\left\{\cos^2\theta + \frac{\sin^2\theta}{(1-\mu)}\right\} \qquad (2.55)$$

2M. Partial Dislocations and Stacking Faults

The normal stacking of atoms in the hexagonal close-packed system is shown in Fig. 2.22A where the atoms in the third basal plane are directly above those in the first and those in the fourth directly above those in the second, etc. The stacking sequence is described as ABAB - - - -. The stacking sequence for the (111) planes of the face-centered cubic system as shown in Fig. 2.22B, however, is ABCABC - - - - . These two stacking sequences differ in only a minor way from each other: The basal (0001) plane of the close-packed hexagonal (HCP) crystal is made up of an hexagonal array of atoms, which can be represented as spheres that touch each other like cued-up billiard balls. Precisely the same geometry applies to the atomic arrangement on the (111) plane of the face-centered cubic (FCC) crystal. Whereas the B layers of atoms are over the same alternate depressions in the first layer in both the HCP and FCC crystals, the third layer of atoms in the HCP is over the A layer but the third layer of atoms in the FCC system is over the alternate positions known as C; and the fourth layer in the FCC is directly above the first or A layering. True HCP crystals, namely those having the ideal axial

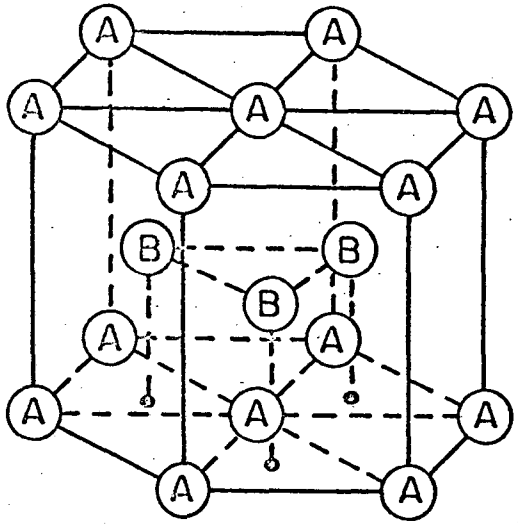

A. STACKING OF (0001) PLANES ALONG THE [0001] AXIS OF HCP CRYSTALS.

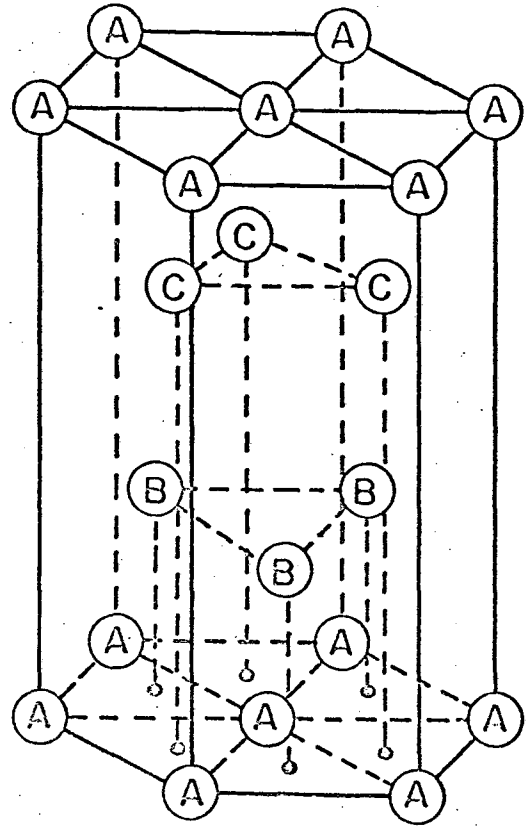

B. STACKING OF (111) PLANES ALONG THE [111] AXIS IN FCC CRYSTALS.

FIGURE 2.22. ATOM LAYER STACKING IN HCP AND FCC CRYSTALS

UCRL-18155

ratio of c/a = 1.633, differ relative to second nearest neighbors from FCC crystals. Consequently, the free energies for HCP and FCC crystals cannot be greatly different since most of the bonding energy arises from nearest-neighbor effects and these are identical for the two types of crystals.

Slip occurs between the B and A layers of atoms on the (111) plane of the FCC lattice in the direction of the Burgers vector $\bar{b} = a/2\,[\bar{1}10]$ as shown in Fig. 2.23. But when such a slip is propagated, the B atoms must pass near the A atoms, the resulting distortion being severe. It appears that slip would be easier by the path $\bar{b}_1 + \bar{b}_2 = \bar{b}$ because by this path the atoms would pass over the saddle points between the A atoms. In order to ascertain whether this conjecture is correct, we will determine whether the dislocation having the Burgers vector $\bar{b}$ can dissociate into the two partials, often called Shockley dislocations, $\bar{b}_1$ and $\bar{b}_2$.

In Fig. 2.24, the various significant vectors are identified. The vector equation for the proposed dissociation is, therefore,

$$a/2\,[\bar{1}10] \longrightarrow a/6\,[\bar{2}11] + a/6\,[\bar{1}2\bar{1}] \qquad (2.57)$$

Since the vector components of the products equal the vector components of the reactant, the dislocation equation is balanced vectorially. The change in energy for the reaction of Eq. 2.57 per unit length of dislocations is

$$\Delta U = \frac{G}{2}\,\bar{b}_1 \cdot \bar{b}_1 + \bar{b}_2 \cdot \bar{b}_2 - \bar{b} \cdot \bar{b} \qquad (2.58)$$

Executing the dot vector products gives

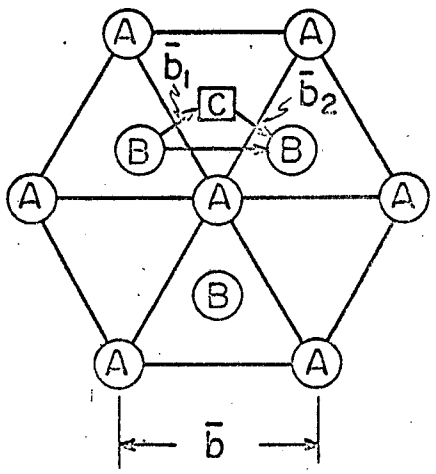

FIGURE 2.23. PLAN VIEW OF THE (111) PLANE IN THE FCC LATTICE.

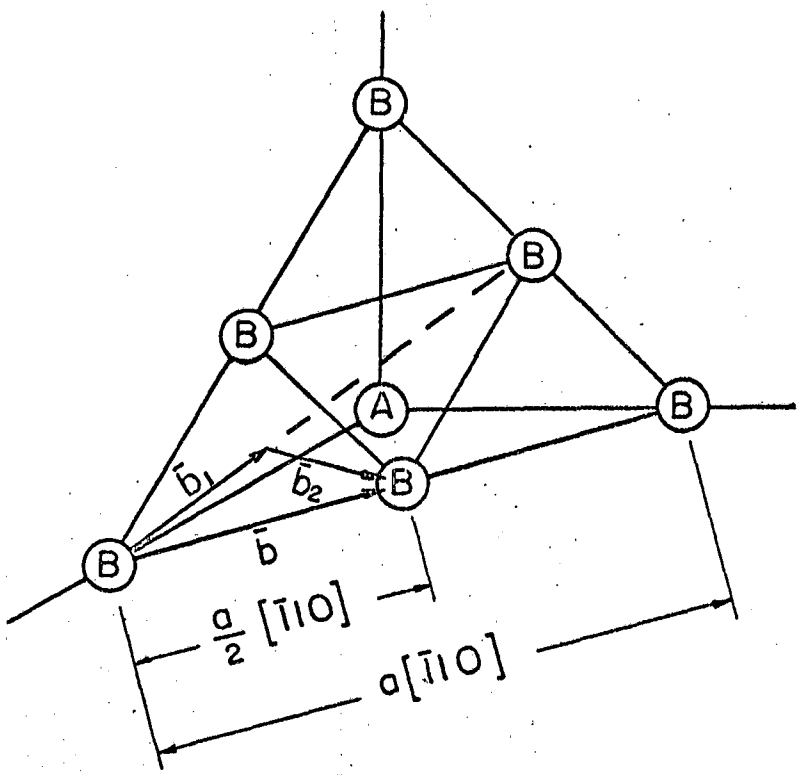

$$\bar{b} = a/2\ [\bar{1}10]$$

$$b_1 = a/3\ [\bar{1}\ 1/2\ 1/2] = a/6\ [\bar{2}11]$$

$$b_2 = a/3\ [\bar{1}/2\ 1\ \bar{1}/2] = a/6\ [\bar{1}2\bar{1}]$$

FIGURE 2.24. BURGERS VECTOR FOR SHOCKLY PARTIALS.

$$\Delta U = G/2\left\{\frac{a^2x6}{36} + \frac{a^2x6}{36} - \frac{a^2x2}{4}\right\}$$

$$= \frac{Ga^2}{2}\left\{-\frac{1}{6}\right\} \qquad (2.59)$$

Since the dislocation energy decreases when dissociation into partials takes place, the suggested reaction will occur.

If no other factor were involved the partials would separate completely. But as in the case of the dissociation of a superdislocation, a surface energy again intrudes into the analysis for the dissociation reaction of Eq. 2.57. A plan view of the (111) slip plane showing the two partial dislocations $\bar{b}_1$ and $\bar{b}_2$ is illustrated in Fig. 2.25. To the left of the first, and to the right of the second partial, the stacking of atoms is that appropriate to an ideal FCC structure. But between the two partials a different sequence is obtained. Whereas the first layering is A, the second layering of atoms is in the C position. In the third layer, not shown in Fig. 2.25, the displacement of the atoms is the same as in the second layer. Therefore, as a result of the Burgers vector $\bar{b}_1$, the atoms of the third layer have moved from C to A positions. And the atoms of the fourth layer which were originally in A positions have moved to B positions. Therefore, as a result of the splitting of a total dislocation into the two partials, the stacking sequence between the partials has changed as follows:

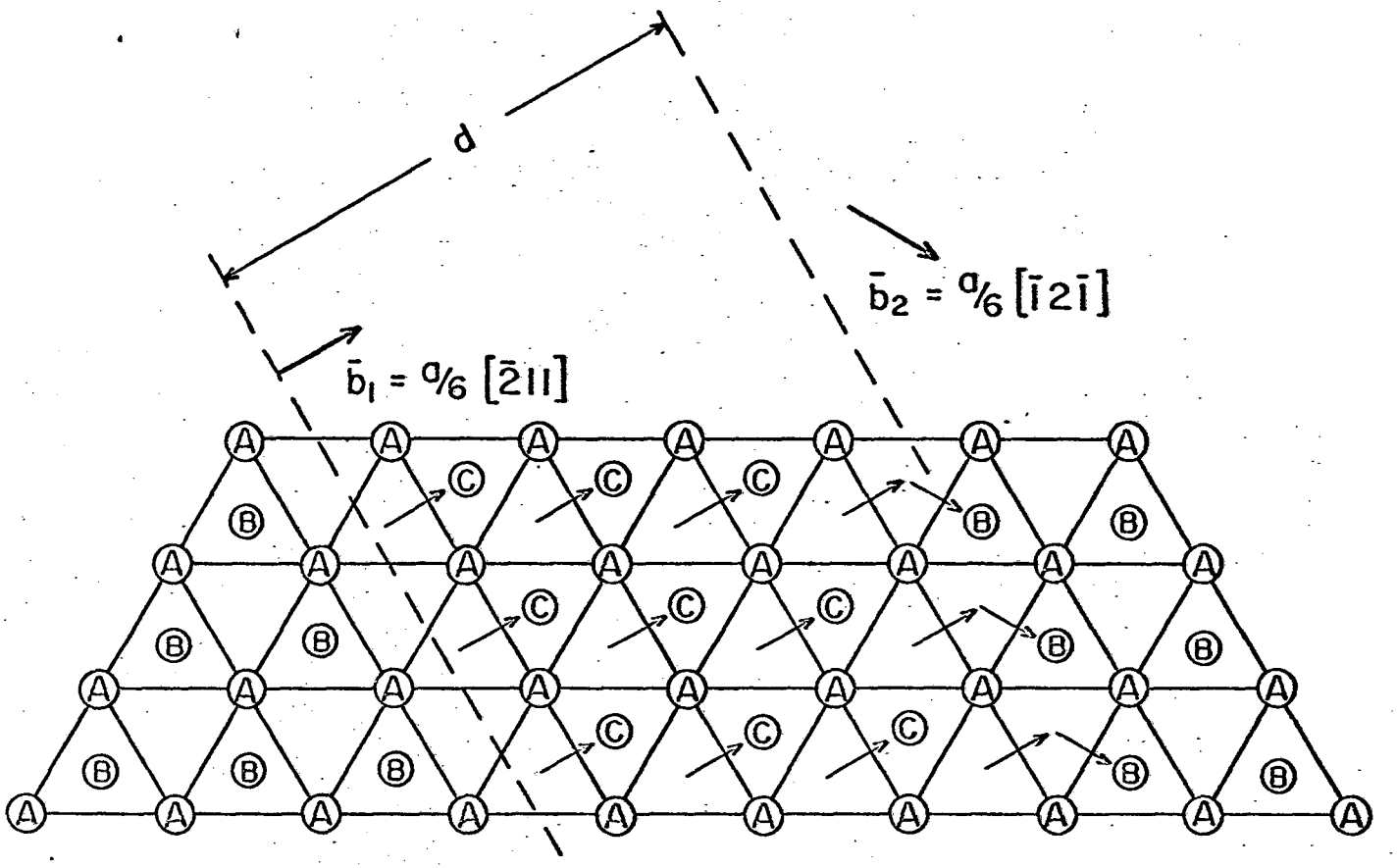

FIGURE 2.25. SEPARATION OF PARTIALS BY SLIP BETWEEN A AND B LAYERS.

Layer	Former Stacking	New Stacking	Frank's Index	Structure
below the First	no change	no change	no change	FCC
F 0	C	C	▽	
1	A	A	△	HCP
2	B	C	▽	
3	C	A	▽	
4	A	B	▽	FCC
5	B	C		

above the Fifth similarly no change

Frank's index can be used to designate the stacking order. If the order is the usual ABCA, the symbol ▽ will be used. But if the stacking is AC or another inverted order, the symbol △ applies. As shown above, there are two investions of stacking order between the partials. Each investion represents a stacking fault. And the stacking fault between the partials consists of a planar region that is two atomic layers high, which has the stacking appropriate to the HCP phase. Since the FCC phase is stable, it has the lower free energy. Therefore, the free energy of the system increases as the partial dislocations move apart. When the increase in stacking fault energy equals the decrease in the interaction energy of the two partials, equilibrium in established and the two partials remain, if otherwise undistrubed, the equilibrium distance, d, apart. A similar analysis applies to the basal plane stacking for the HCP system. In this event the stacking fault consists of two layers that have the sequence of stacking appropriate for the FCC structure. Dislocations lying on other planes than the basal plane cannot dissociate.

In FCC metals the stacking fault energy is about twice the twin boundary energy. This arises from the fact that, in FCC metals, twinning takes place by the twin displacement vector of $\eta = a/6\,[\bar{1}\bar{1}2]$ on

the (111) plane, the shear displacement being proportional to the distance of the atomic plane from the twin plane. The twin vector and the twin plane are shown in Fig. 2.26. Assuming that the first layer and all below it remain unchanged, the second layer shifts an amount η_1 from B to C. The third atom layer shifts $2\eta_1$ from C to B and the fourth atom layer shifts $3\eta_1$ from A to A. Therefore, the stacking sequence for a $\eta_1 = a/6\,[\bar{1}\bar{1}2]$ twin on the (111) plane is as follows:

Layer	Former Stacking	New Stacking	Frank's Index	Structure
below the First	no change	no change	no change	FCC
0	C	C		
1	A	A		HCP
2	B	C		
3	C	B		FCC
4	A	A		

above the fourth similarly no change

Consequently a twin boundary exhibits a single inversion in Frank's index and it is represented by a single layer of atoms having the hexagonal stacking. Therefore, the stacking fault energy is approximately twice the twin boundary energy. Alloys that twin readily, such as Co-Ni compositions near the transition from FCC to HCP structures, have extremely low twin boundary energies. As the electron/atom ratio of Cu alloys decreases, the twin boundary energy increases and twinning is less prevalent. Al and its alloys have high twin boundary energies and rarely exhibit twins. Stacking fault energies follow the same sequence.

2N. Separation of Partials and Recombination Energies

The problem of determining the equilibrium separation distance between two partial dislocations is analogous to that, which has already

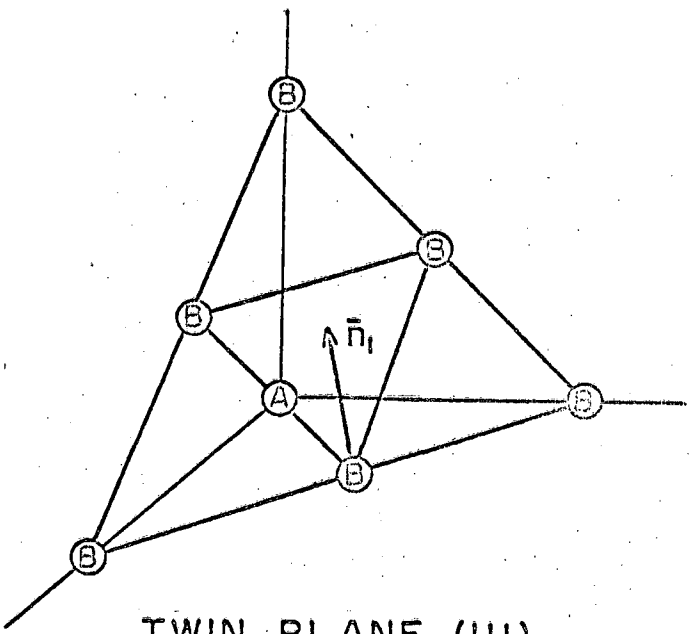

TWIN PLANE (111)
$\bar{n}_1 = {}^{0}/_{6}\,[\bar{1}\bar{1}2]$

FIGURE 2.26. TWIN PLANE AND VECTOR.

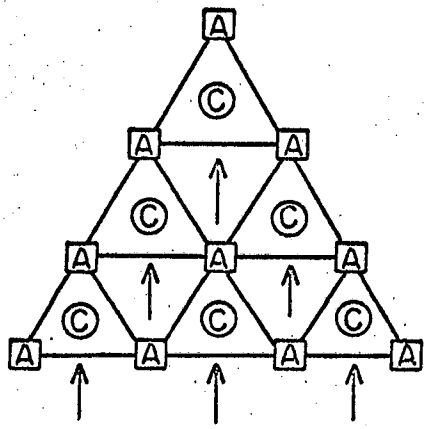

A. MOVEMENTS OF THE FIRST TWIN LAYER FROM B TO C.
$n_1 = a/6\,[\bar{1}\bar{1}2]$

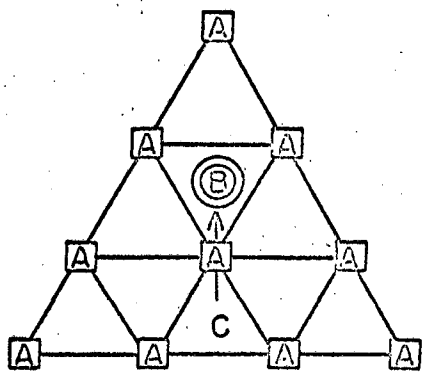

B. MOVEMENT OF THE SECOND TWIN LAYER FROM C TO B.
$n_2 = 2n_1$

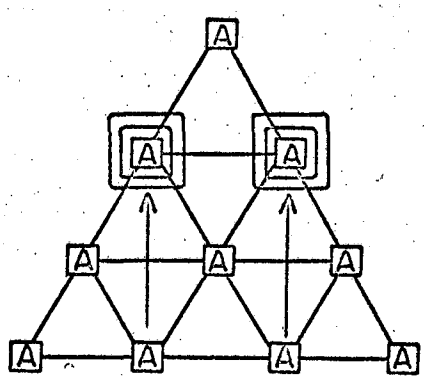

C. MOVEMENT OF THE THIRD TWIN LAYER FROM A TO A.
$n_3 = 3n_1$

FIGURE 2.27. LAYERING SHIFTS DUE TO TWINNING.

been reviewed, of calculating the equilibrium distance between the two halves of a dissociated superdislocation. Consider unit lengths of the two partial dislocations shown in Fig. 2.28 separated a distance x. The stacking fault energy between the two dislocations is γ_s^e per cm^2 and the stacking fault energy is therefore $U_s = \gamma_s^e \chi$, assuming that the first partial is fixed, a force

$$F_s = -\frac{dU}{d\chi} = -\gamma_s^e \tag{2.60}$$

acts on the second partial due to the stacking fault. The force acting on a unit length of the second partial is given by

$$F_\chi = \frac{G b_{1s} \cdot b_{2s}}{2\pi\chi} + \frac{G b_{1E} \cdot b_{1E}}{2\pi(1-\mu)\chi} \tag{2.61}$$

It is readily evident from Fig. 2.28 that

$$b_{1s} = \sqrt{\bar{b}_1 \cdot \bar{b}_1}\cos(\theta+30) = \frac{a}{6}\sqrt{6}\cos(\theta+30)$$

$$b_{1E} = \sqrt{\bar{b}_1 \cdot \bar{b}_1}\sin(\theta+30) = \frac{a}{6}\sqrt{6}\sin(\theta+30)$$

$$b_{2s} = \sqrt{\bar{b}_2 \bar{b}_2}\cos(\theta-30) = \frac{a}{6}\sqrt{6}\cos(\theta-30)$$

$$b_{2E} = \sqrt{\bar{b}_2 \bar{b}_2}\sin(\theta-30) = \frac{a}{6}\sqrt{6}\sin(\theta-30)$$

where θ is the angle the total Burgers vector $\bar{b}$ makes with the dislocation line. Therefore the force due to the interaction of the first dislocation on a unit length of the second dislocation is

$$F_\chi = \frac{G a^2}{12\pi\chi}\left\{\cos(\theta+30)\cos(\theta-30) + \frac{\sin(\theta+30)\sin(\theta-30)}{1-\mu}\right\}$$

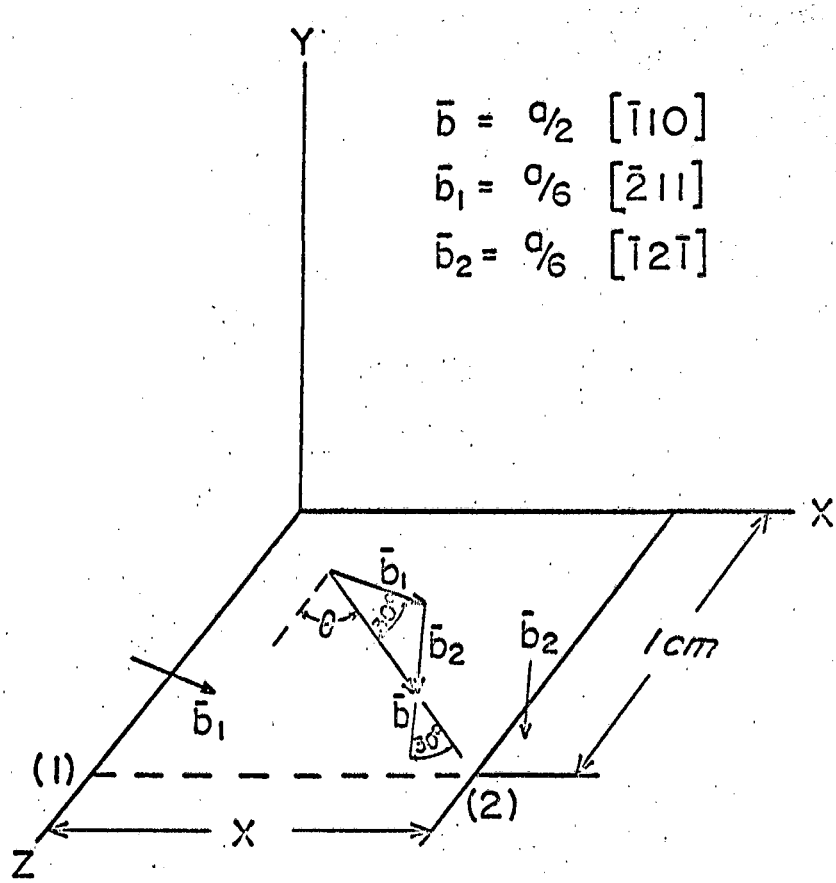

FIGURE 2.28. SEPARATION OF TWO PARTIAL DISLOCATIONS.

which reduces to

$$F_x = \frac{Ga^2}{48\pi x}\left\{\left(3-\frac{1}{1-\mu}\right)\cos^2\theta+\left(\frac{3}{1-\mu}-1\right)\sin^2\theta\right\} \quad (2.62)$$

At equilibrium $F_x + F_s = 0$ and therefore, letting $d = x$ at equilibrium,

$$\gamma_s^e = \frac{Ga^2}{48\pi d}\left\{\left(3-\frac{1}{1-\mu}\right)\cos^2\theta+\left(\frac{3}{1-\mu}-1\right)\sin^2\theta\right\} \quad (2.63)$$

Consequently the separation of the partials is somewhat dependent on the orientation, θ, of the total dislocation. For the interesting case, where the total dislocation is in screw orientation, $\theta = 0$, and

$$d = \frac{Ga^2}{24\pi\gamma_s^e}\left\{\frac{1-3\mu/2}{1-\mu}\right\} \simeq \frac{Ga^2}{24\pi\gamma_s^e}\left(\frac{3}{4}\right) \quad (2.64)$$

taking $\mu \simeq 1/3$. Therefore the partial dislocations will be more widely separated as γ_s^e decreases.

If dislocation 2 of Fig. 2.28 encounters a barrier so that it can no longer move in the positive x direction, and if a local stress, τ_{b1}, is applied parallel to the Burgers vector of the first dislocation, the resulting force $\tau_{b1} b_1$, will force the first dislocation to approach the second, thereby reducing the separation of the partials. The net force acting in the positive direction on the first partial is

$$F_{x1} = \tau_{b1} b_1 + \gamma_s^e$$

whereas the repulsion force on the first partial due to the second is

$$F_p = -\frac{Ga^2}{24\pi(d-x)}\left(\frac{3}{4}\right)$$

as seen from Eq. 2.62 for $\theta = 0$. Letting the new equilibrium spacing between the partials be $d - x = d_\ell$ for a stress τ_{b1}, gives

$$\tau_{b1} b_1 + \gamma_s^\ell = \frac{Ga^2}{24\pi d_\ell}\left(\frac{3}{4}\right) \tag{2.65a}$$

or

$$d_\ell = \frac{3/4\, Ga^2}{24\pi(\tau_{b1} b_1 + \gamma_s^\ell)} \tag{2.65b}$$

The recombination energy is the work that must be done to coalesce the two partials into the total dislocation. We will consider here, that a local stress, τ_{b1} has been applied to the first dislocation and ascertain what additional work need be done to bring the partials together. This work is

$$R = \int_{d_\ell}^{b} \frac{3/4\, Ga^2}{24\pi x}(-dx) - (\tau_{b1} b_1 + \gamma_c^\ell)(d_\ell - b)$$
$$+ (\Gamma_c - 2\Gamma_{cp}) - (\tau_{b1} b_1 + \gamma_c^\ell) b \tag{2.66}$$

The first two terms refer to the work done to bring the two partials from d_ℓ to a distance b apart, and the last two terms refer to the work that need be done to coalesce the cores. Γ_c refers to the core energy of the total dislocation and Γ_{cp} to the core energy of each partial dislocation per unit length. Integrating Eq. 2.66 and introducing Eq. 2.65b gives

$$R = \frac{(3/4)Ga^2}{24\pi} \ln \frac{3/4\, Ga^2}{24\pi b e(\tau_{b1} b_1 + \gamma_s^\ell)} \tag{2.67}$$
$$+ \{\Gamma_c - 2\Gamma_{cp}\}$$

R then is the energy that must be supplied by a thermal fluctuation in order to effect the recombination per unit length of two partial dislocations, when the recombination is stress aided. But since the stress enters the energy expression as part of a logarithmic term, the recombination energy is insensitive to the applied stress. An alternate equivalent expression for the recombination energy is

$$R = \frac{3/4\, Ga^2}{2\pi} \ln \frac{d_\tau}{eb} + \left\{\Gamma_c - 2\Gamma_{cp}\right\} \qquad (2.67b)$$

Therefore when $d = eb$, the recombination energy involves only the bracketed term of Eq. 2.67. But the recombination energy increases as the distance d_τ between the partials increases or as the stacking fault energy decreases.

When two partial dislocations are forced together at a point, as shown in Fig. 2.29, a constriction is formed. By a detailed calculation, Stroh[34] has shown that the constriction energy is

$$U_c \simeq \frac{Gb^2 d_\tau}{30}\left(\ln \frac{d_\tau}{b}\right)^{1/2} \qquad (2.68)$$

where d_τ depends on the applied stress as shown by Eq. 2.65b.

3. SOME THERMALLY ACTIVATED DISLOCATION MECHANISMS

3A. Introduction

Whereas the emphasis in Section 2 was on dislocation statics, we will concentrate in this section on the dynamic behavior of dislocations with special emphasis on thermally activated dislocation motion. Those dislocation mechanisms that have activation energies above about 50kT are activated so infrequently that they contribute in only a minor way to

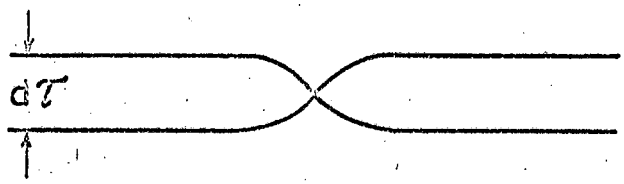

FIG. 2.29 CONSTRICTION.

the strain rate. But mechanisms having activation energies less than about 50kT have appreciable probabilities of occurrence and contribute effectively to the strain rate. Since the probability for activation is exp. $\{-\text{free energy of activation} \div kT\}$ only those processes that have low activation energies can be activated at low temperatures. At higher temperatures these processes, such as those which occur in the initial straining when a creep specimen is first stressed, take place so rapidly that they are almost instantaneous. During such initial straining, dislocations move up to barriers that demand operation of higher activation energy processes. Consequently, the activation energy for the strain rate will, in general, be expected to increase with an increase in temperature. For most dislocation processes, the free energy of activation decreases as the stress is increased. It is possible on occasions to isolate, experimentally, regions of temperature and stress where the measured strain rate is predominantly the result of a single mechanism. But dislocation theory has not yet matured to that stage of completeness where the ranges of operation of specified mechanisms can be prescribed theoretically. Therefore, the experimental data must still always be compared with theoretical deductions in an attempt to identify operative mechanisms. Only a few examples are currently available where the correlations between experimental evidence and theoretical predictions are sufficiently close to permit confidence in the identity of the mechanism. Some experimental data are difficult to rationalize, at present, because of the simultaneous operation of several mechanisms. And there are several rather well documented pieces of experimental evidence that suggest the operation of only one mechanism but yet cannot be appropriately

correlated with existing theory. Obviously dislocation theory does not yet embrace all possible mechanisms. In spite of the versatility and complexity of dislocation theory, substantial progress has nevertheless been made in formulating the basic tenets of the problem. And additional progress can be expected in the near future that will amplify existing theories and formulate new possible mechanisms of deformation. The future theoretical developments can be expected to rely more heavily on more precise mechanical data, better planned experiments, and more detailed correlations with pertinent transmission electron microscopical observations.

A complete survey of all of the known thermally activated dislocation mechanisms will not be attempted here. Rather only a few representative examples of the known mechanisms will be discussed to provide a background for approaching other thermally activated dislocation motion processes. The selection of only the intersection, cross slip, motion of jogged screw dislocation and climb of edge dislocation mechanisms for inclusion in this report was based primarily on the fact that in each of these cases there is at least a modest amount of correlative evidence to confirm the possible operation of these mechanisms.

3B. The Geometry of Intersection

Simple examples of a glide dislocation AA' on a glide plane, intersecting a forest dislocation BB', are shown in Fig. 3.1. The following rules can be seen to apply:

1. Since dislocations cannot terminate in the center of a crystal, they must remain continuous following intersection.
2. The forest dislocation always increases in length by the Burgers vector of the glide dislocation.

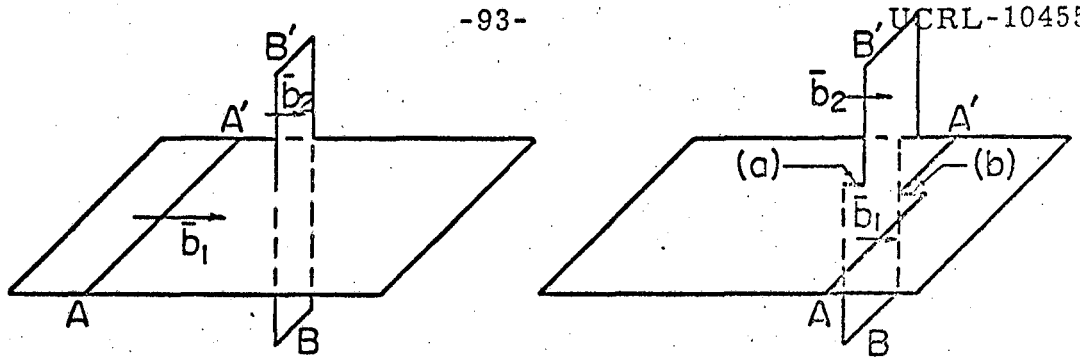

(a) INTERSECTION OF TWO EDGE DISLOCATIONS PRODUCING SCREW KINKS AT (a) AND (b).

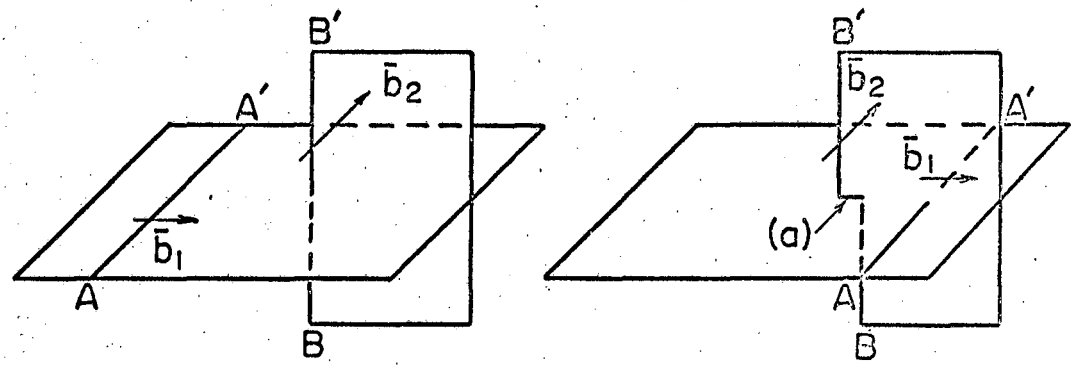

(b) INTERSECTION OF TWO EDGE DISLOCATIONS PRODUCING (a) AN EDGE JOG.

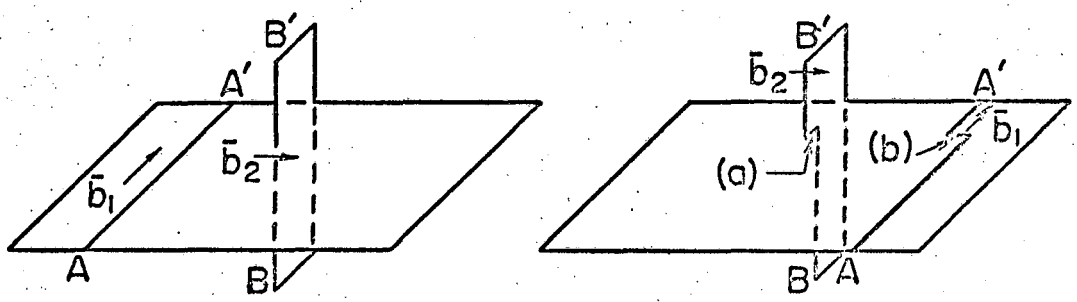

(c) INTERSECTION OF AN EDGE DISLOCATION BY A SCREW DISLOCATION PRODUCING (a) AN EDGE JOG, AND (b) AN EDGE KINK.

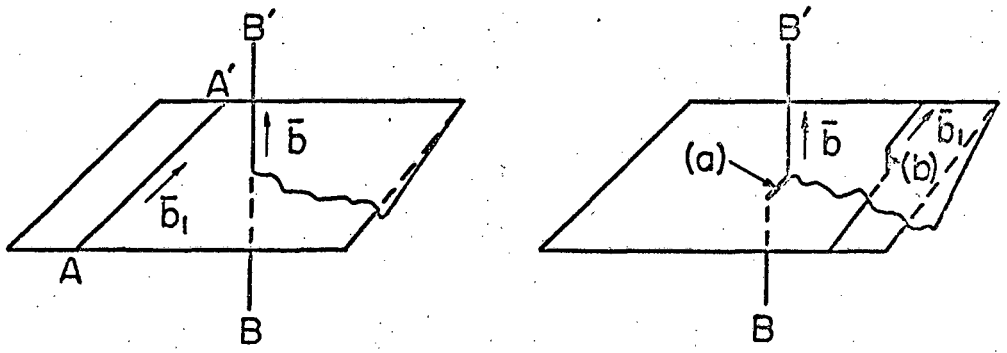

(d) INTERSECTION OF TWO SCREW DISLOCATIONS PRODUCING (a) AN EDGE KINK, AND (b) AN EDGE JOG.

FIG. 3.1 SIMPLE CASES OF INTERSECTION IN SIMPLE CUBIC LATTICE.

3. The glide dislocation always increases in length by the Burgers vector of the forest dislocation.
4. If the increased length lies in the slip plane of the dislocation, it is called a kink. Kinks will soon straighten out due to the line tension.
5. If the increased length extends from one slip plane to an adjacent parallel slip plane it is called a jog. In the case of edge dislocations, jogs are always clearly distinguishable from kinks. But in the case of undissociated screw dislocations, jogs and kinks are only distinguishable from each other when the slip plane is arbitrarily defined. This ambiguity does not exist in the case of dissociated screw dislocations because here the edge components of the partials define the slip plane.
6. Because dislocations get longer as a result of intersection, work equal to the increased energy of the dislocation must be done in order to cause intersection. As described in Section 2G, the energy of a jog is approximately $\frac{Gb^3}{12}$, the core energy. Although a sharp kink has the same energy as a jog, kinks straighten out due to the line tension. Therefore, somewhat less work is expended in producing a kink than in producing a jog during intersection. Consequently, the energy required to effect intersection depends on the detailed geometric conditions that apply. On the average it is approximately

$$U_j \simeq \frac{Gb^3}{12} \qquad (3.1)$$

where U_j is the jog energy.

The geometric details of intersection of dislocations in FCC metals are incomparably more complicated than that depicted in Fig. 3.1. Dependent upon their orientations in their slip planes and on their Burgers vector, intersecting dislocations in FCC metals may either attract or repel each other. These details have been described by Saada[35] and cannot be reviewed here. In general the repulsion interaction is

$$\tau_i^* \simeq \alpha G b / L \qquad (3.2)$$

where α is a constant, and L is the mean distance between points at which the dislocations intersect or are otherwise held up.

Additional complications also arise because dislocations in FCC metals are dissociated into their partials. The Burgers vector of a partial dislocation does not correspond with a translational vector between near atoms in the crystal. Therefore, the energy to form a jog equal to the Burgers vector of a partial would result in extreme crowding of atoms and would have correspondingly high energy. Consequently the saddle of the reaction path for intersection is obtained when the two partials of both the glide and forest dislocations are first constricted, as discussed in Section 2N, following which the jogs are easily produced. Therefore the total energy for intersection, U_i, is of the order of magnitude of

$$U_i' = U_j' + 2U_c = \frac{Gb^3}{12} + \frac{Gb^2 d}{15}\left(\ln \frac{d}{b}\right)^{1/2} \qquad (3.3)$$

as given by Eqs. 3.1 and 2.68. Consequently the intersection energy increases as the stacking fault energy decreases.

3C. Thermally Activated Intersection

The intersection mechanism has been discussed by Mott,[3] Cottrell,[36] Friedel,[5] Seeger,[6] Basinski,[37] Thornton and Hirsch,[38] and other investigators. In all of the approaches that have been used thus far, smeared average values have been adopted for the activation energy, distances between dislocations, back stress fields, area swept out and number of intersecting dislocations per unit volume. Since the detailed statistics cannot at present be extracted from the experimental data for verification, this method of averaging will also be adopted here.

An idealized plan view of a slip plane is shown in Fig. 3.2. The dislocation AA' is acted upon by the stress $\tau-\tau^*$ where τ is the applied stress and τ^* are internal back stresses acting in the direction of the Burgers vector. Under the action of the stress, all glissile dislocations move so as to contact, at least elastically, the forest dislocations threading the slip plane, as shown at the open circles in the figure. Let N be the number of such contacts per unit volume of the crystal. The force acting at the point of intersection, as given by Eq. 2.28 is

$$F=(\tau-\tau^*)Lb \qquad (3.4)$$

We will be concerned only with the instances where this force is not great enough to effect intersection per se. Consequently intersection will take place only when a thermal fluctuation of sufficient magnitude aids the local force. During this process of thermal activation, the dislocation sweeps through the doubly crosshatched area. After this it continues to move under the action of the local stress until it impinges on the next set of forest dislocations. Thus, it sweeps out the total crosshatched area,

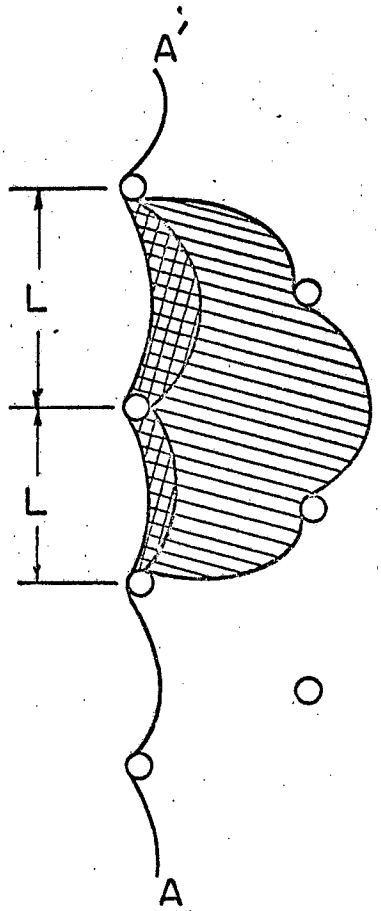

FIG. 3.2 PLAN VIEW OF A SLIP PLANE SHOWING A GLIDE DISLOCATION AA' UNDER A STRESS HELD UP AT FOREST DISLOCATIONS.

A, per activation. This takes place at each point of contact between the glide and forest dislocations. Consequently the strain rate, $\dot{\gamma}$, is given by

$$\dot{\gamma} = NAb\nu' \tag{3.5}$$

where ν' is the frequency of activation.

Let F_o vs. x be the force displacement diagram for completion of intersection at the absolute zero of temperature as shown schematically in Fig. 3.3. The diagram is to be interpreted as follows: As the glide dislocation approaches the forest dislocation, x decreases. When contact is made between the leading partial of the glide dislocation and the first partial of the forest dislocation, constriction begins and F_o increases. When x decreases to b the partials have been completely constricted. In order to complete intersection, the jog must now be produced. The force necessary to produce the jog is taken to be F_{oj} over the region $0 < x < b$. The total area under the F_o - x curve is therefore the energy for intersection U'_{jo} at the absolute zero as approximated by Eq. 3.3. The curve shown is appropriate to high stacking fault energy crystals. The processes of constricting and jogging are linearly related to the shear modulus of elasticity. Therefore the force F at a temperature where the shear modulus of elasticity is G, as shown by the broken curve in Fig. 3.3 is given by

$$F = \frac{F_o G}{G_o} \tag{3.6}$$

where G_o is the shear modulus at the absolute zero.

When a force $F = (\tau - \tau^*)Lb$ is applied at the point of imminent intersection, the energy equal to the crosshatched area under the F - x

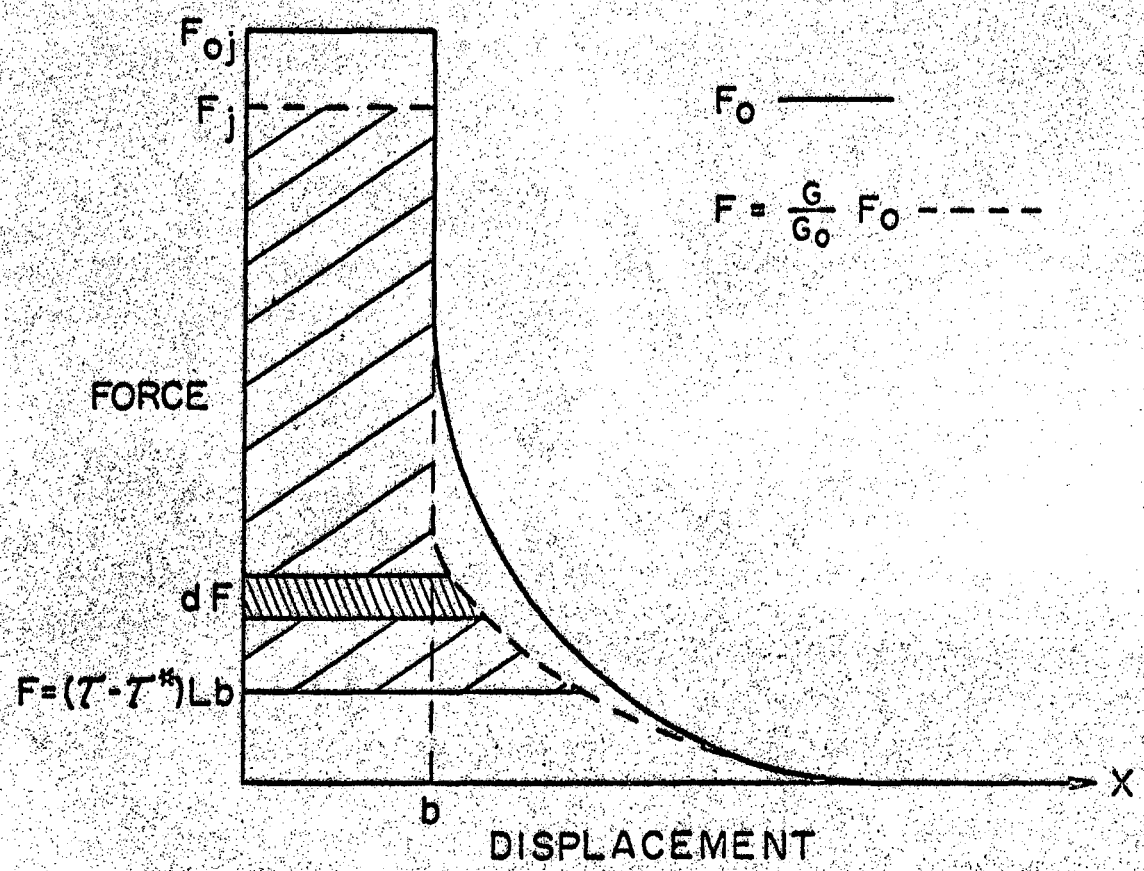

FIG. 3.3 FORCE DISPLACEMENT DIAGRAM FOR INTERSECTION.

curve from $(\tau-\tau^*)Lb$ to F_j must be supplied by a thermal fluctuation to complete intersection. This energy is given by

$$u_i = \int_{(\tau-\tau^*)Lb}^{F_j} x\,dF \tag{3.7}$$

Since the natural frequency of vibration at the point of intersection is about the Debye frequency, ν, the frequency for a single successful thermal fluctuation is

$$\nu' = \nu e^{-u_i/kT} \tag{3.8}$$

using the Boltzmann condition. Therefore the strain rate due to intersection is

$$\dot{\gamma} = NAb\nu e^{-u_i/kT} \tag{3.9}$$

where U_i is defined by Eq. 3.7.

3D. Seeger's Approximation

It is advisable to discuss first, the simple case where the dislocations are undissociated. Since no constriction is involved in this example, the total activation energy for intersection is the jog energy.

$$u_j = u_{j0}\frac{G}{G_0} \tag{3.10}$$

The work done by the local stress in this case is $(\tau-\tau_0^* G/G_0)Lb^2$. And consequently the energy that must be supplied by a thermal fluctuation to complete intersection is

$$u_i = u_{j0}G/G_0 - (\tau-\tau_0^* G/G_0)Lb^2 \tag{3.11}$$

Therefore for this simplification,

$$\dot{\gamma} = NAb\nu e^{-\frac{U_{jo}G/G_o}{kT}} e^{+\frac{(\tau - \tau_o^* G/G_o)Lb^2}{kT}} \quad (3.12)$$

The flow stress is therefore given by

$$\tau \frac{G_o}{G} = \tau_o^* + \frac{U_{jo}}{Lb^2} - \frac{kT G_o}{Lb^2 G} \ln \frac{NAb\nu}{\dot{\gamma}} \quad (3.13)$$

Since the thermal fluctuation only assists in overcoming U_{jo}, Eq. 3.13 only applies when $U_{jo} > \frac{kT G_o}{G} \ln \frac{NAb\nu}{\dot{\gamma}}$. For temperatures where $U_{jo} < \frac{kT G_o}{G} \ln \frac{NAb\nu}{\dot{\gamma}}$ successful thermal fluctuations are immediate and in this range

$$\tau \frac{G_o}{G} = \tau_o^* \quad (3.14)$$

The critical temperature T_c at which the flow stress changes from that given by Eq. 3.13 to that in Eq. 3.14 is given by

$$U_{jo} = kT_c \frac{G_o}{G_{T_c}} \ln \frac{NAb\nu}{\dot{\gamma}} \quad (3.15)$$

and the temperature, T_c, therefore is independent of the activation volume Lb^2. Introducing Eq. 3.15 into Eq. 3.12 gives

$$\tau \frac{G_o}{G} = \tau_o^* + \frac{U_{jo}}{Lb^2}\left\{1 - \frac{T}{T_c}\frac{G_{T_c}}{G_T}\right\} \quad T < T_c \quad (3.16a)$$

and

$$\tau G_o/G = \tau_o^* \quad T > T_c \quad (3.16b)$$

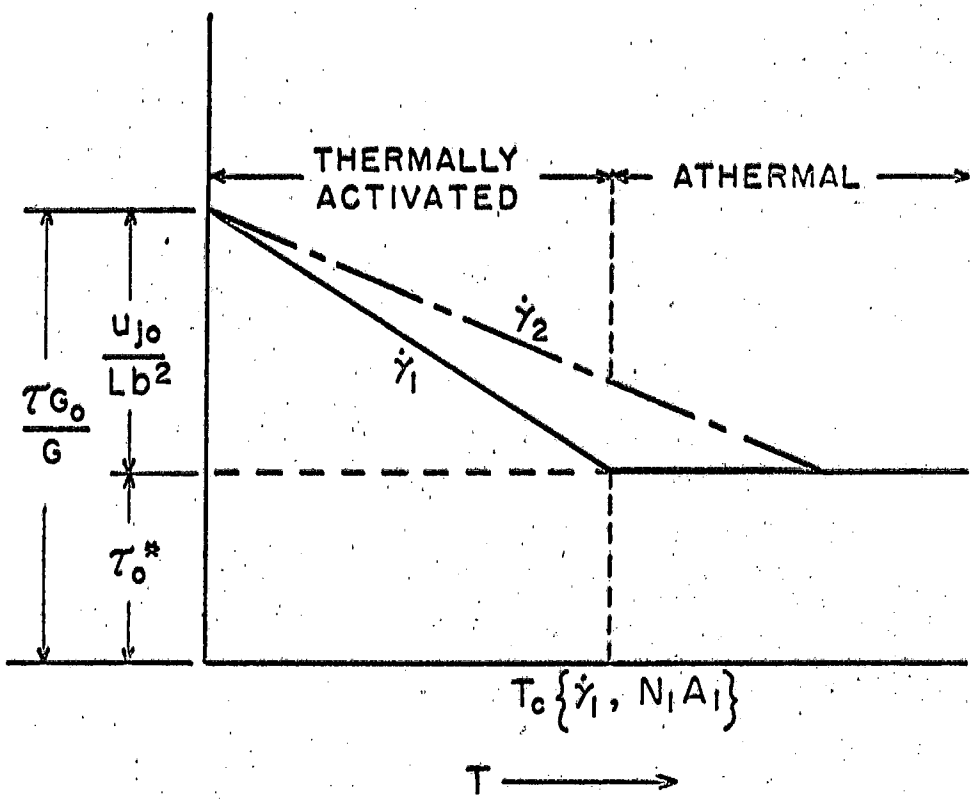

FIGURE 3.4. STRESS-TEMPERATURE RELATIONSHIP FOR INTERSECTION.

where the three quantities τ_o^*, U_{jo}/Lb^2 and T_c are directly determinable from experimental data. Whereas the independent externally controllable variables are $\dot{\gamma}$ and T and the dependent measurable variable is τ, the internally significant quantities are four in number, namely, τ_o^*, L, U_{jo}, and (NA). Obviously these four internal quantities cannot be deduced from the three measurable external variables. Therefore an additional independent experimental measurement is required. In order to obtain the needed quantity, we define the experimentally determinable quantity β as

$$\beta = \left(\frac{\partial \ln \dot{\gamma}}{\partial \tau} \right)_T = \frac{Lb^2}{kT} \qquad (3.17)$$

the last equality resulting from the differentiation of Eq. 3.12. The method of determining β experimentally from a tension test is illustrated in Fig. 3.5A[8] for the case of Al single crystals at 77°K. The activation volume $Lb^2 = \beta kT$ is shown as a function of the flow stress at 77°K in Fig. 3.5B.[8] As the single Al crystal strain hardens, the activation volume and therefore L decreases, illustrative of the fact that additional dislocations are introduced during straining or that the significant existing dislocations are more closely spaced as would occur in forming the entanglements to be described later. The added information on Lb^2 now permits all of the quantities τ_o^*, L, U_{jo} and NA to be determined. The deduced quantities for Al are in good agreement with those suggested by the intersection mechanism. This is significant inasmuch as other mechanisms can also give flow stress that decreases linearly with temperature as suggested by Eq. 3.16a.

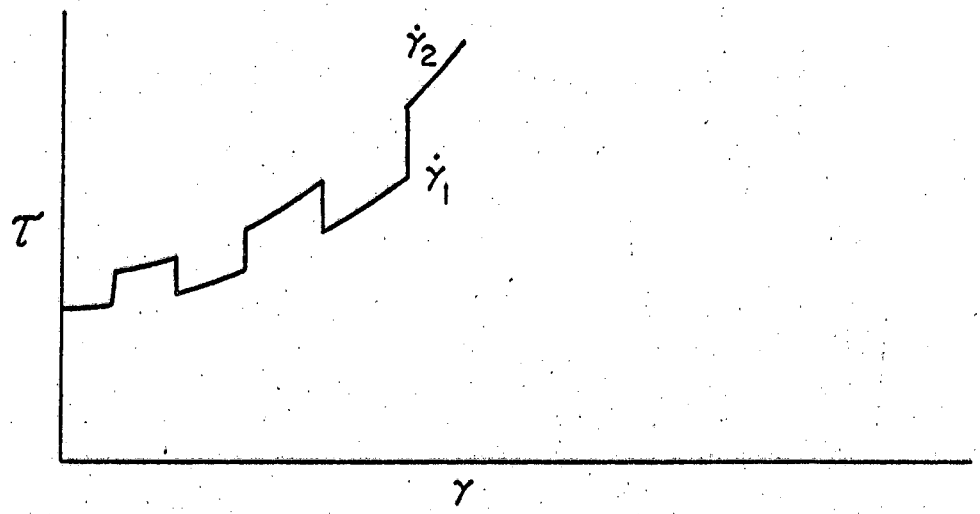

(A) SCHEMATIC OF TENSION TEST ON SINGLE Al CRYSTALS SUBJECTED TO A CHANGE IN STRAIN RATE.

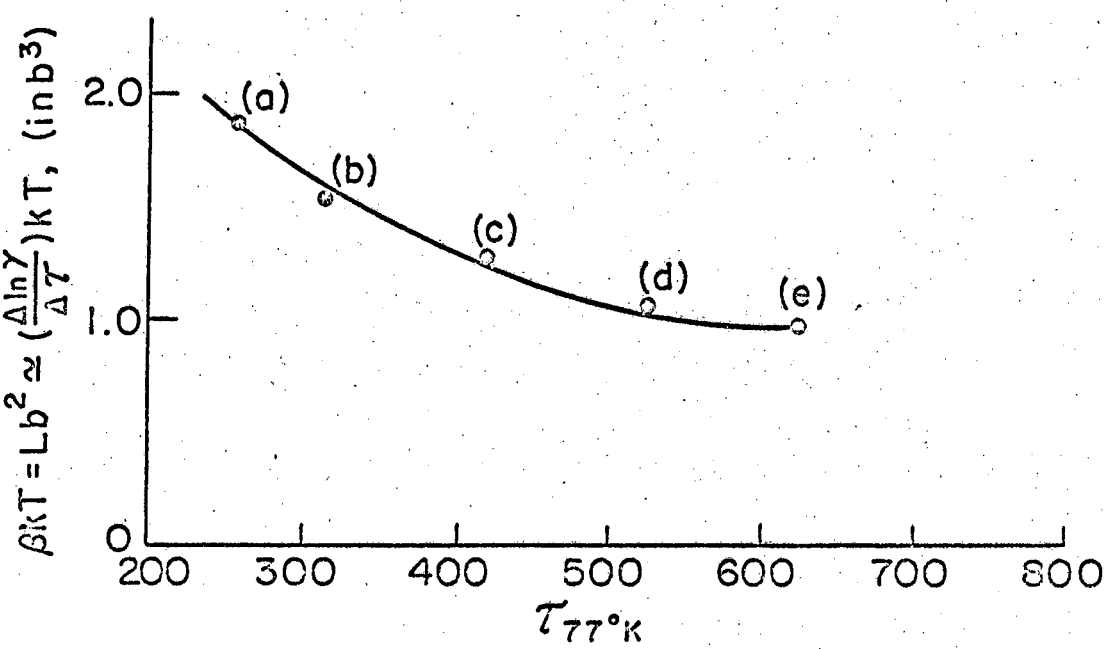

(B) ACTIVATION VOLUME.

FIGURE 3.5. DETERMINATION OF β.[8]

BCC metals also exhibit almost a linear decrease in τ with an increasing T at low temperatures. But the τ - T curve is much steeper than that for Al. If intersection controls the deformation of BCC metals U_{jo}/Lb^2T_c must be much greater for these metals than for Al. But T_c is about the same in both cases and U_{jo} for BCC metals can only be about twice that for Al. Consequently, L must be much smaller in BCC metals than in Al. This deduction is confirmed by the experimental fact that $\beta kT = Lb^2 \simeq 20b^3$ to $40b^3$ for Fe, giving $L \simeq$ 20b to 40b. If intersection is the controlling mechanism the experimental value of U_{jo} for Fe is calculated to be about 1.13×10^{-12} to 2.26×10^{-12} ergs.

It is yet commonly believed that the extremely low value of L is inconsistent with the average density of dislocations that are usually present in annealed Fe. The assumption has been made that perhaps the deformation of BCC metals at low temperatures arises from the activation of the Peierls mechanism. In this mechanism, dislocations lying in their potential energy valleys bow out and advance one Burgers vector to the next valley. This is accomplished by the formation of two kinks and has a theoretical activation energy of approximately $2U_k - (\tau - \tau^*)\ell_p b^2$, where U_k is the kink energy and ℓ_p is about 10b. Several factors, however, suggest that Peierls mechanism cannot account for the plastic deformation of BCC metals. First $2U_k$ is estimated theoretically to be much smaller than the value deduced for this quantity experimentally. Second, the observed activation volume is usually several times the estimated $10b^3$. The most pertinent evidence that serves to disqualify the Peierls mechanism is the fact that dislocations in mildly cold worked BCC metals do not lie along the potential energy troughs, as would be

necessary if the Peierls mechanism were valid, but have irregular shapes illustrating that they are already severely kinked.

Recently Schoeck[39] suggested that the plastic deformation of BCC metals at low temperatures might be controlled by the thermally activated motion of jogged screw dislocations. His argument stems from the thought that since the a/2 [111] dislocations in BCC metals are undissociated, their jog energy is very small. Consequently such dislocations would be severely jogged. As will be described in more detail later, when a jogged screw dislocation moves, it leaves either a trail of vacancies or a trail of interstitials in its wake. In this event the least possible activation energy is $U_f = (\tau - \tau^*)\ell_j b^2$ where U_f is the energy of formation of a vacancy and ℓ_j is the mean distance between jogs. There are several difficulties in accepting this interpretation. First, the experimentally evaluated value for U_f is much less than the energy of formation of a vacancy, and secondly, if this were the mechanism, it should also be operative in a high stacking fault FCC metal such as Al. Because the constriction energy in Al is small, the value of ℓ_j for Al should not be much different from that in BCC metals. Consequently, the exact mechanism of low temperature deformation in BCC metals is not yet well understood.

Until it was rationalized by Basinski,[37] one experimental fact regarding the activation volume of FCC metals embarrassed the theory. The experimentally determined activation volumes $Lb^2 = \beta kT$, for these metals, particularly Cu which has the lower stacking fault energy, increased with increasing temperatures. Theoretically, since L is constant for a given strain-hardened state, the activation volume for that state should therefore have been independent of the temperature. As we will demonstrate in the following section, this apparent anomaly is resolved

when the constriction energy of dislocations that are separated into their partials is taken into consideration.

The intersection theory assumes that the strain hardened state is described in terms of the variables τ_o^*, L and NA. Various strain hardened states, however, give about the same value of T_c for the same strain rate. Reference to Eq. 3.15 reveals that the product NA therefore does not change sufficiently during strain hardening to influence the analysis. This result might have been expected because, first, T_c is only logarithmically related to NA and second, because as N increases, A can be expected to decrease. For these reasons, the assumption that NA does not vary materially during strain hardening is justified.

Since, however, L and τ_o^* appear in the exponential term of Eq. 3.12, their changes during strain hardening have a pronounced effect on the flow stress. This is illustrated schematically in Fig. 3.6 where $\tau G_o/G$ vs. T curve at the same $\dot{\gamma}$ is shown for two different strain hardened states a and b. During strain hardening τ_o^* increases and L decreases, but T_c remains approximately constant. Therefore strain-hardening causes a more rapid decrease of $\tau G_o/G$ with an increase in T over the range $0 < T < T_c$.

The actual activation energy for intersection must increase linearly with the absolute temperature according to

$$u_i = kT \ln \frac{NAbv}{\dot{\gamma}} \qquad (3.18)$$

for tests conducted at a constant strain rate. The experimentally determinable apparent activation energy q_i for intersection, however, as defined by Eq. 1.3 of Section 1A, is

$$q_i = u_i + \frac{1}{kT}\frac{\partial u_i}{\partial \frac{1}{kT}} = u_i - T\frac{\partial u_i}{\partial T} \quad (3.19)$$

where $\frac{\partial U_i}{\partial T}$ plays the role of the entropy of activation and q_i is correlatable with the free energy of activation. When the dislocations are undissociated Eq. 3.11 applies and

$$\frac{\partial u_i}{\partial T} = \left(\frac{u_{j_0}G}{G_0} + \frac{\tau_0^* L b^2 G}{G_0}\right)\frac{1}{G}\left(\frac{\partial G}{\partial T}\right) \quad (3.20)$$

$$= \left(\frac{u_i + \tau^* L b^2}{G}\right)\left(\frac{\partial G}{\partial T}\right)$$

Therefore

$$q_i = u_i\left\{1 + \frac{T}{G}\left(-\frac{\partial G}{\partial T}\right)\right\} + \tau^* L b^2 \frac{T}{G}\left(-\frac{\partial G}{\partial T}\right)$$

$$= kT\left\{1 + \frac{T}{G}\left(-\frac{\partial G}{\partial T}\right)\right\}\ln\frac{NAb\nu}{\dot{\gamma}^2} + \tau^* L b^2 \frac{T}{G}\left(-\frac{\partial G}{\partial T}\right) \quad (3.21)$$

Since $\left(\frac{-\partial G}{\partial T}\right)$ is always positive $q_i > U_i$ and increases more rapidly than linearly with the temperature.

3E. Intersection Theory as Applied to Crystals Containing Dissociated Dislocations

The idealized intersection theory described in the preceding section assumed that the dislocations were undissociated. When dislocations are dissociated, as in the case of dislocations on the (111) plane of FCC metals or on the basal planes of HCP metals, the F - x curve for intersection is no longer rectangular but has the shape given in Fig. 3.3. In this case:

$$\beta = \frac{\partial \ln \dot{\gamma}^2}{\partial \tau} = -\frac{1}{kT}\frac{\partial u_i}{\partial \tau} \quad (3.22)$$

as shown by Eq. 3.9. But in terms of Eq. 3.7

$$\frac{\partial U_i}{\partial \tau} = -x L b \tag{3.23}$$

and therefore, the activation volume is given by

$$x L b = \beta k T \tag{3.24}$$

At low temperatures, say 4°K, U_i is small, since it is directly proportional to T for a constant strain rate test, as required by Eq. 3.9. Reference to Fig. 3.3 reveals that in this range $x \simeq b$ and therefore the activation volume approximates Lb^2. But for the same strain rate, U_i increases linearly with T. Consequently x increases with T as U_i increases with T as deduced from Fig. 3.3. Therefore, in agreement with the experimental facts, the activation volume for intersection of dissociated dislocations increases as the temperature increases.

We will now consider the determination of the smeared average F_o - x curve for the intersection mechanism in Al from deductions based on experimental facts. The data to be described were obtained by Mitra Osborne, and Dorn[8] from Al single crystals, all having the intial orientation shown in the unit stereographic triangle given in Fig. 3.7. The experimental procedure involved ccnsisted of prestraining one of a series of single crystals to one of a series of strain-hardened states over the easy glide and linear hardening ranges at 77°K. Each such state is, of course, characterized by a τ_o^* and an L value, NA, as discussed previously, being insensitive to the straining. The test temperature was then changed to a new value and β was determined as a function of strain (or stress).

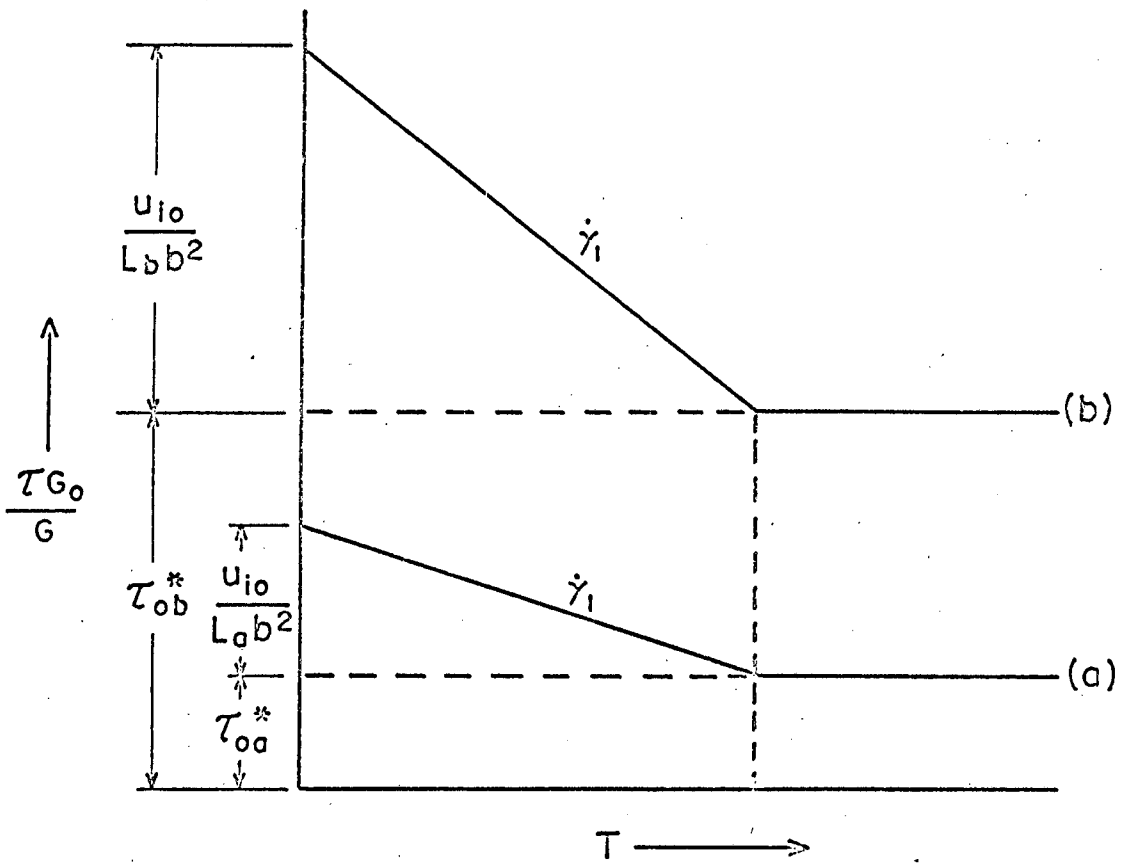

FIGURE 3.6. EFFECTS OF STRAIN HARDENING ON THE FLOW-STRESS TEMPERATURE RELATIONSHIP ACCORDING TO THE INTERSECTION MECHANISM.

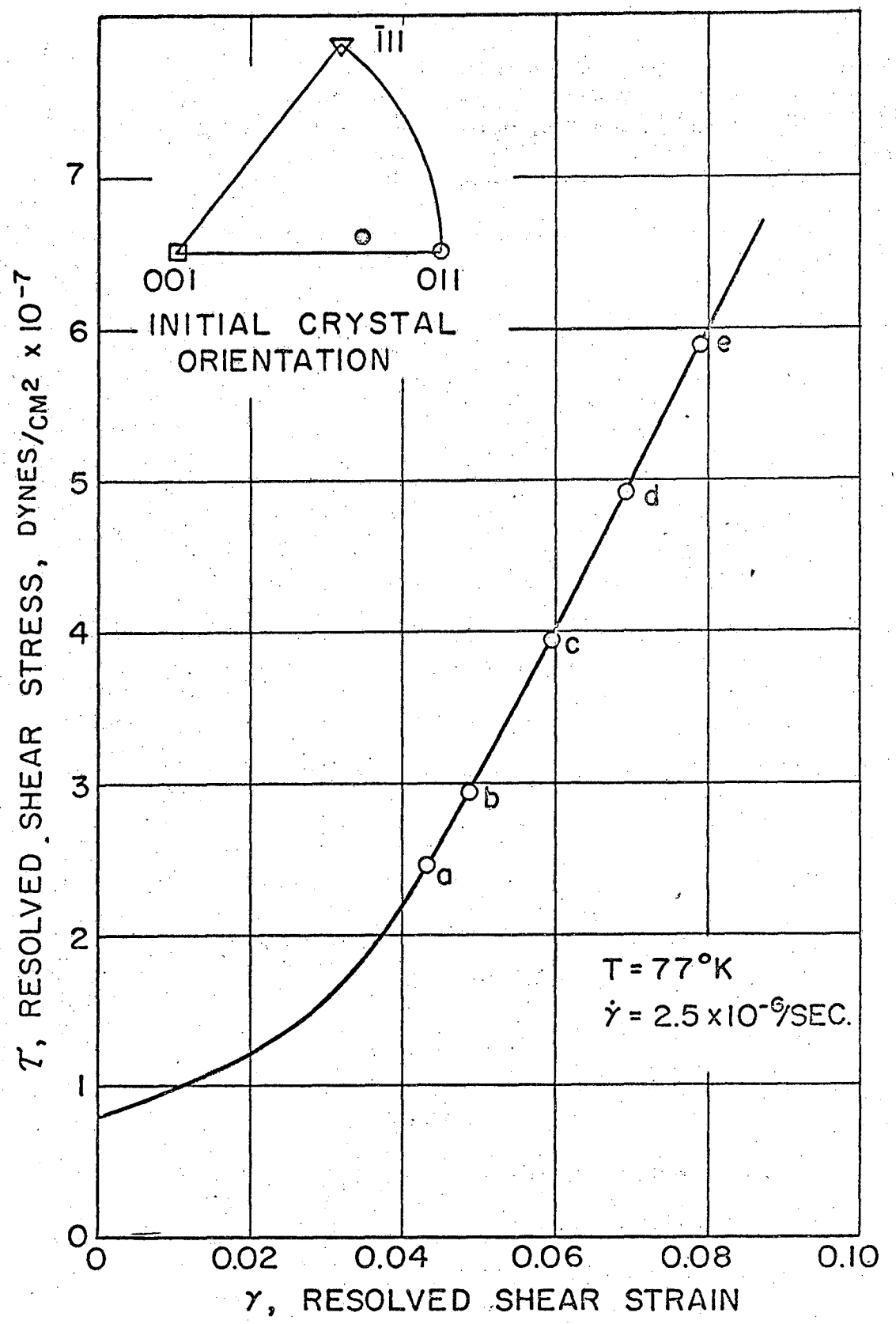

FIGURE 3.7. STRESS-STRAIN CURVE FOR SINGLE Al CRYSTALS AT 77°K.[8]

The value of β was then extrapolated to the value it had at the new test temperature at zero additional strain at that temperature. Thus βkT and $\tau G_o/G$ could be determined for a prescribed work-hardened state, at each of a series of temperatures. The results so obtained are shown in Fig. 3.8.[8] Each solid curve refers to a specific strain-hardened state, and each broken curve joins the series of tests for various strain-hardened states made at a given temperature. The curves for higher strain-hardened states reveal a more rapid decrease in $\tau G_o/G$ with βkT. At a given test temperature U_i is constant, since $\dot{\gamma}$ is constant. Therefore, F and x are also constant, as noted in Fig. 3.3. Therefore, the decreasing value of $\beta kT = x\,Lb$ with strain hardening along a constant temperature curve must be ascribed principally to decreases in L. At the lowest test temperatures, however, U_i is very small and x approaches b. Consequently for the 4°K values $x\,Lb \simeq Lb^2$. In this way L can be determined for each strain-hardened state. The values of 1/L so obtained are documented in Fig. 3.9[8] as a function of the strain at 77°K. Over easy glide 1/L remains substantially constant whereas it increases almost linearly with strain in the linear hardening region.

Knowing the values of L for each state as given in Fig. 3.9, the values of x for each point in Fig. 3.8 are determinable from $n = \frac{\beta kT}{Lb}$. Therefore, the data recorded in Fig. 3.8 could be recast in terms of $\tau G_o/G\,Lb$ vs x as shown in Fig. 3.10 for Al. The fact that these curves are identical, except as regards a vertical displacement, is in complete harmony with the intersection theory. For a given value of x, the value of F_o is constant as shown in Fig. 3.3 and from Eq. 3.4

$$\tau G_o/G\,Lb = F_o\{x\} + \tau_o^* Lb \qquad (3.25)$$

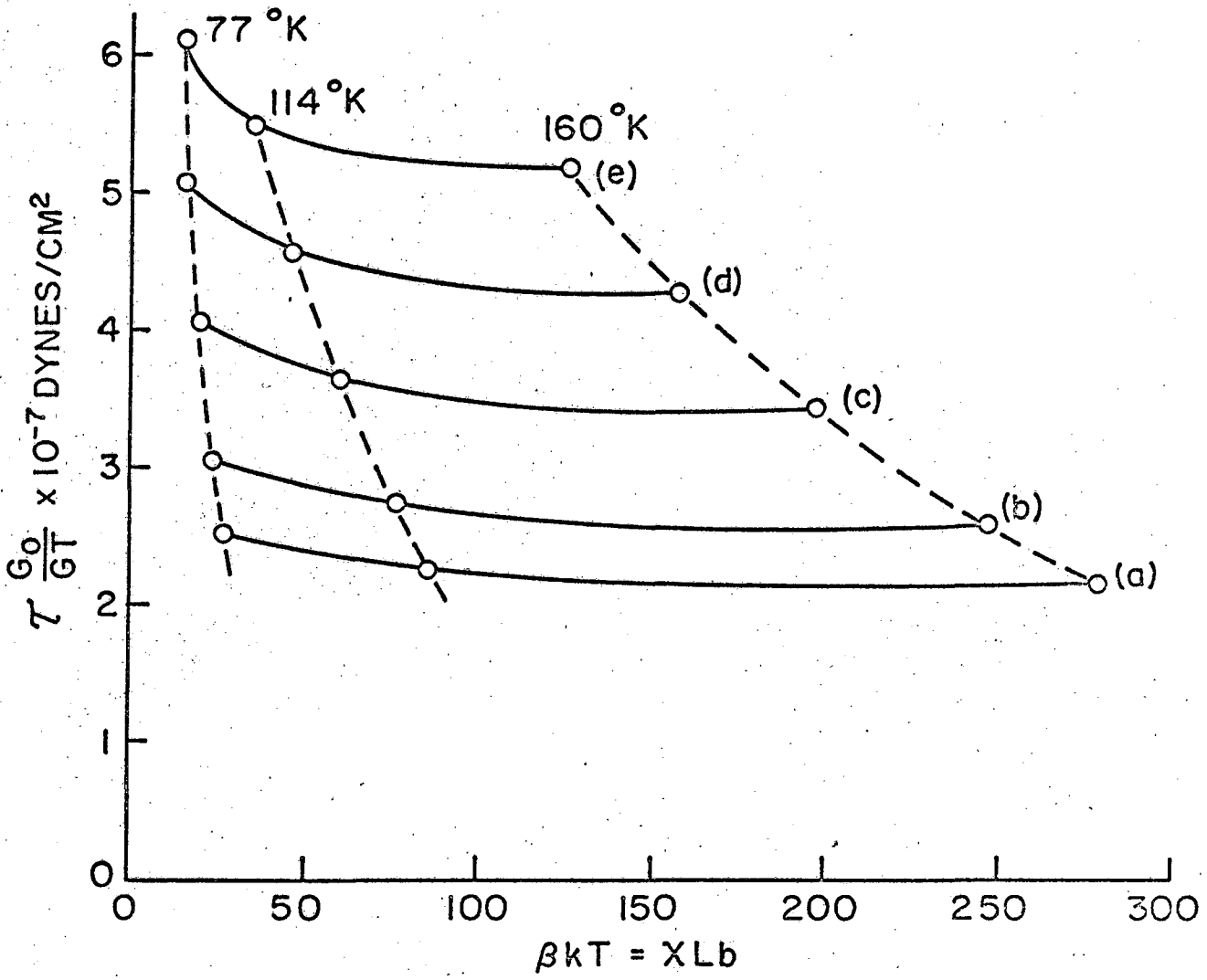

FIGURE 3.8. STRESS VERSUS ACTIVATION VOLUME CURVES FOR Al STRAIN HARDENED TO VARIOUS STATES. $\dot{\gamma} = 2.5 \times 10^{-6}$/SEC. [8]

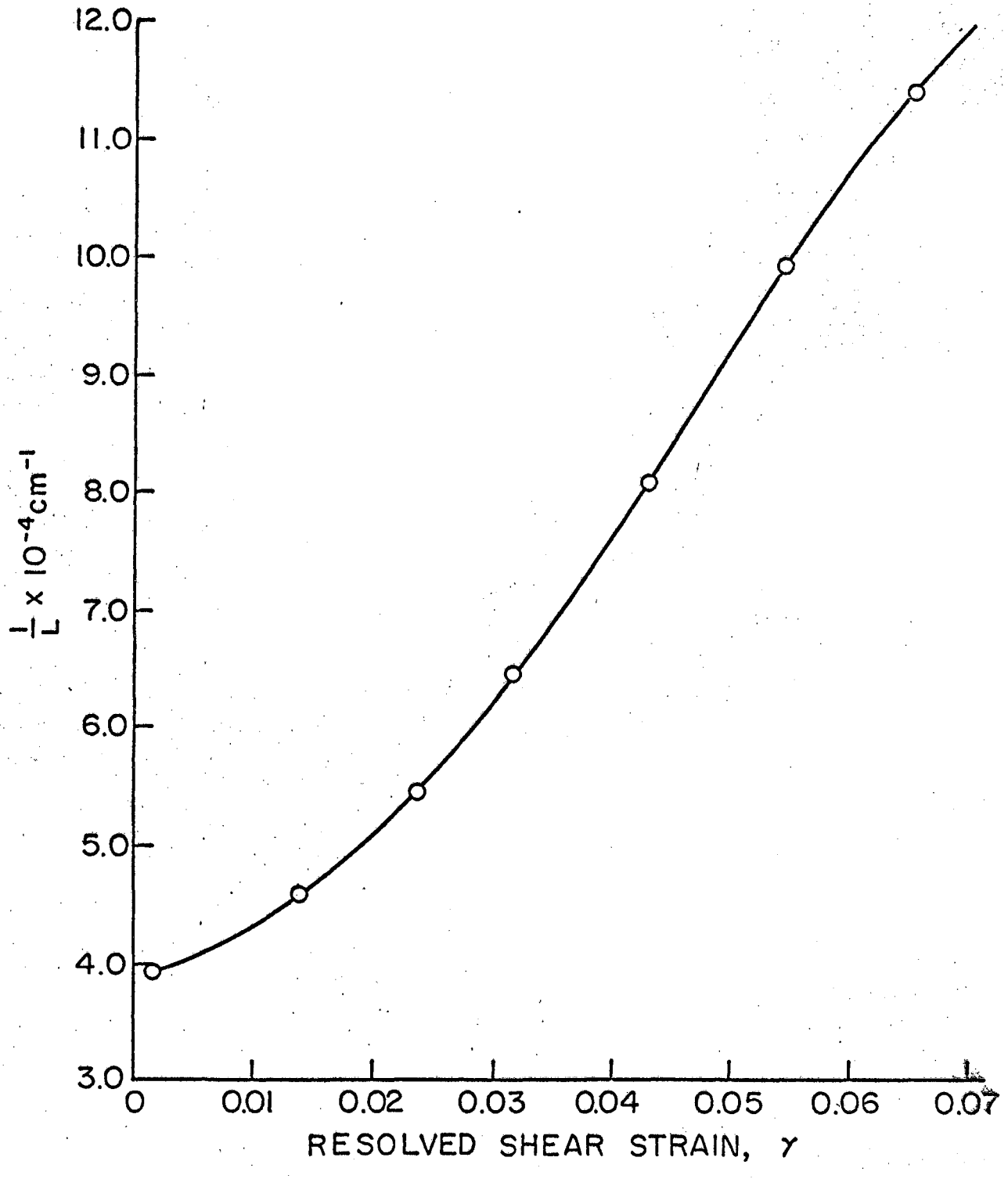

FIGURE 3.9. VARIATION OF $\frac{1}{L}$ WITH STRAIN AT 77 °K. [8]

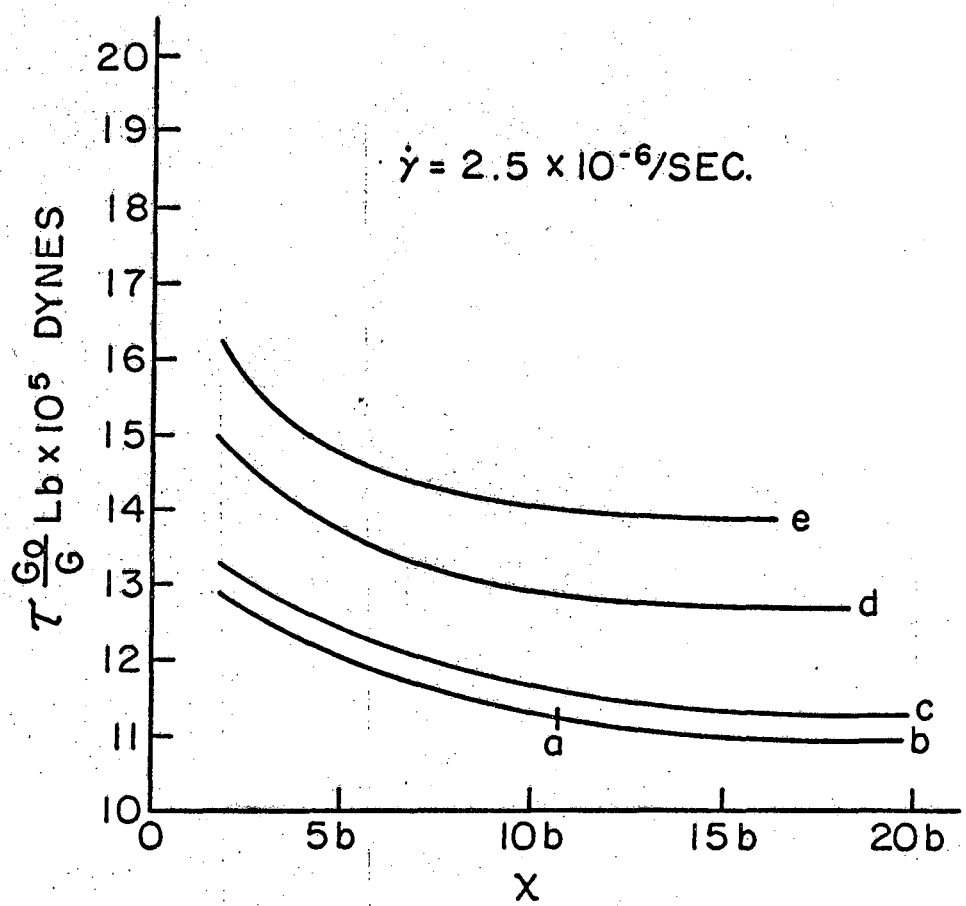

FIGURE 3.10. $\frac{\tau G_0}{G}$ Lb VERSUS X CURVES FOR Al.[8] (b ≡ BURGERS VECTOR).

whereas $F_o\{x\}$ is only a function of x, the value of $\tau_o^* Lb$ depends uniquely on the strain-hardened state. Therefore, the difference in vertical displacement of the curves in Fig. 3.10[8] for two states d and a is

$$\left(\tau \frac{G}{G_o} Lb\right)_d - \left(\tau \frac{G}{G_o} Lb\right)_a = \left(\tau_o^* Lb\right)_d - \left(\tau^* Lb\right)_a \quad (3.26)$$

Therefore, τ_o^* could be determined for the various states provided τ_o^* were known at one state, say the initial yeild strength.

It is possible that τ_o^* can arise from two sources such that

$$\tau_o^* = \tau_{oi}^* + \tau_{ol}^* \quad (3.27)$$

where τ_{oi}^* results from local repulsions of intersecting dislocations, and τ_{ol}^* arises from longer range back stress due to other dislocations than the specific pair involved in intersection. At initial yielding, however, τ_{ol}^* must be negligibly small and τ_o^* must result almost exclusively from τ_{oi}^*. But as discussed previously in Section 3B,

$$\tau_{oi}^* = \frac{\alpha G b}{L} \quad (3.28)$$

where $\alpha \simeq 0.04$ as obtained by using the lowest datum value of $\tau G_o/G\ Lb$ for initial yielding that is given in Fig. 3.10. On this basis the values of τ_{oi}^* and τ_{ol}^* shown in Fig. 3.11[8] were obtained. The total back stress by this approach appears to be almost equally due to the local interaction and the long-range stress fields. For the Al single crystal tested here τ_{ol}^* also varies almost linearly with 1/L. For Cu single crystals a vertical displacement between the various work-hardened states is also

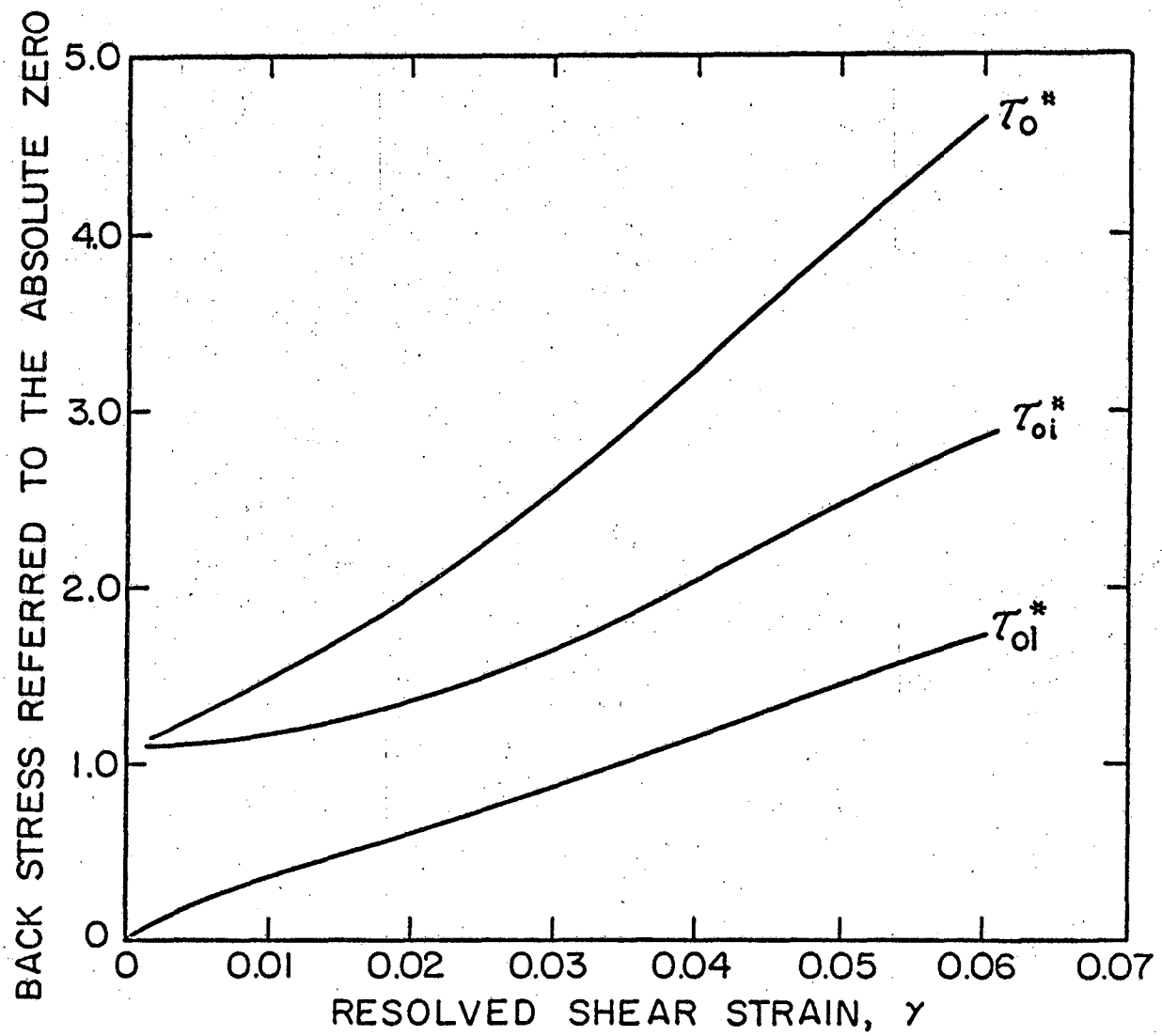

FIGURE 3.11. EFFECTS OF STRAINING ON THE BACK STRESSES.[8]

obtained. The F_o - x curve for Al, obtained by subtracting the estimated values of $(\tau_{oi}^* + \tau_{o\ell}^*)Lb$ from $\tau(G_o/G)Lb$ according to

$$F_o = (\tau G_o/G)Lb - (\tau_{oi}^* + \tau_{o\ell}^*)Lb \quad (3.20)$$

is shown in Fig. 3.12.[44]

Because of its high stacking fault energy, the two partial dislocations in Al are separated only about 2b. Therefore, the value of F_o might have been expected to be zero at about $x \simeq 3b$. In contrast, however, it continues to decrease slowly for $x > 3b$. This is due to the fact that thermal activation can assist in overcoming some of the interaction back stresses at points, and under the geometric conditions, where those are small.

In his 1961 Institute for Metals Lecture, Mott[40] suggested that most of the strain hardening during low temperature deformation might arise from the restraints to motion of jogs on screw dislocations. He argued that inasmuch as dislocation entanglements are observed and no arrays of piled-up dislocations are noted in deformed Al or Cu, there can be no long-range back stresses. But the absence of piled-up dislocation arrays does not constitute proof of the absence of long-range back stresses. Such stresses can also arise as a result of concentrations of dislocations of the same sign in one region. Furthermore, dislocation entanglements are probably produced because the energy of the entanglement is lower than the energy of other possible configurations. Therefore, when a dislocation segment is forced to leave an entanglement, work must be done against the attractive forces arising from the remaining dislocations in the entanglement. The net result is, therefore, equivalent

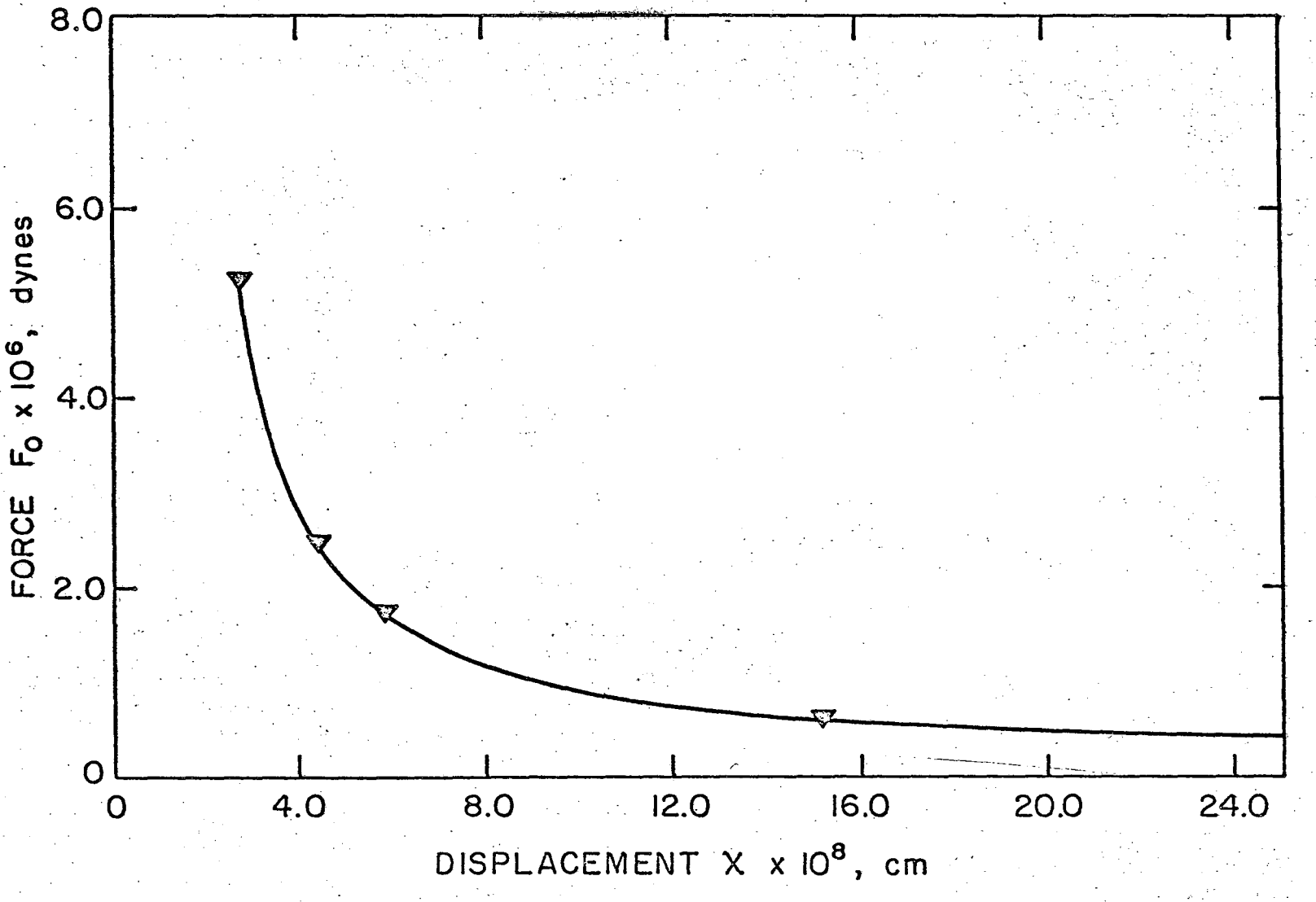

FIGURE 3.12. THE $F_0 - X$ CURVE FOR INTERSECTION IN Al.[44]

to a long-range back stress. Seeger and Mader[41] have demonstrated the presence of long-range back stresses in ferromagnetic metals by determining the effect of cold work on magnetic saturation. This property is not affected by local interactions and therefore constitutes rather good proof of the presence of long-range back stresses in cold-worked metal.

Mitra and Dorn[8] have also detected the effect of long range back stresses from analyses of data obtained during the determination of β in a single tension test. Since the temperature and average strain rate were held constant, U_i was essentially constant, and, therefore, F_o and x must also have remained constant throughout the test. The data obtained are shown plotted on a log-log graph as shown in Fig. 3.13.[8] But

$$\tau G_o/G = \frac{F_o}{Lb} + \left(\tau^*_{ol} + \tau^*_{oi}\right) = \frac{F_o}{Lb} + \frac{\alpha G_o b^2}{Lb} + \tau^*_{ol} \quad (3.30)$$

If τ^*_{ol} were zero, therefore, over the range from the initial yield strength at (a) to higher work-hardened states, the log-log plot of $\tau G_o/G$ vs βkT would have been given by the broken line at 45°. Therefore, long-range back stresses are present that are not related linearly to the reciprocal of Lb. The values of τ^*_{ol} as a function of x Lb can be obtained directly as shown in Fig. 3.12. Using the value of x appropriate for the strain rate and test temperature that was employed gives the same values of τ^*_{ol} that were deduced from the alternate procedure employed in determining the F_o - x curve as are already recorded in Fig. 3.11.

Since the same F_o - x curves are obtained in Stage I of easy glide and Stage II of linear hardening, plastic flow in these regions must be

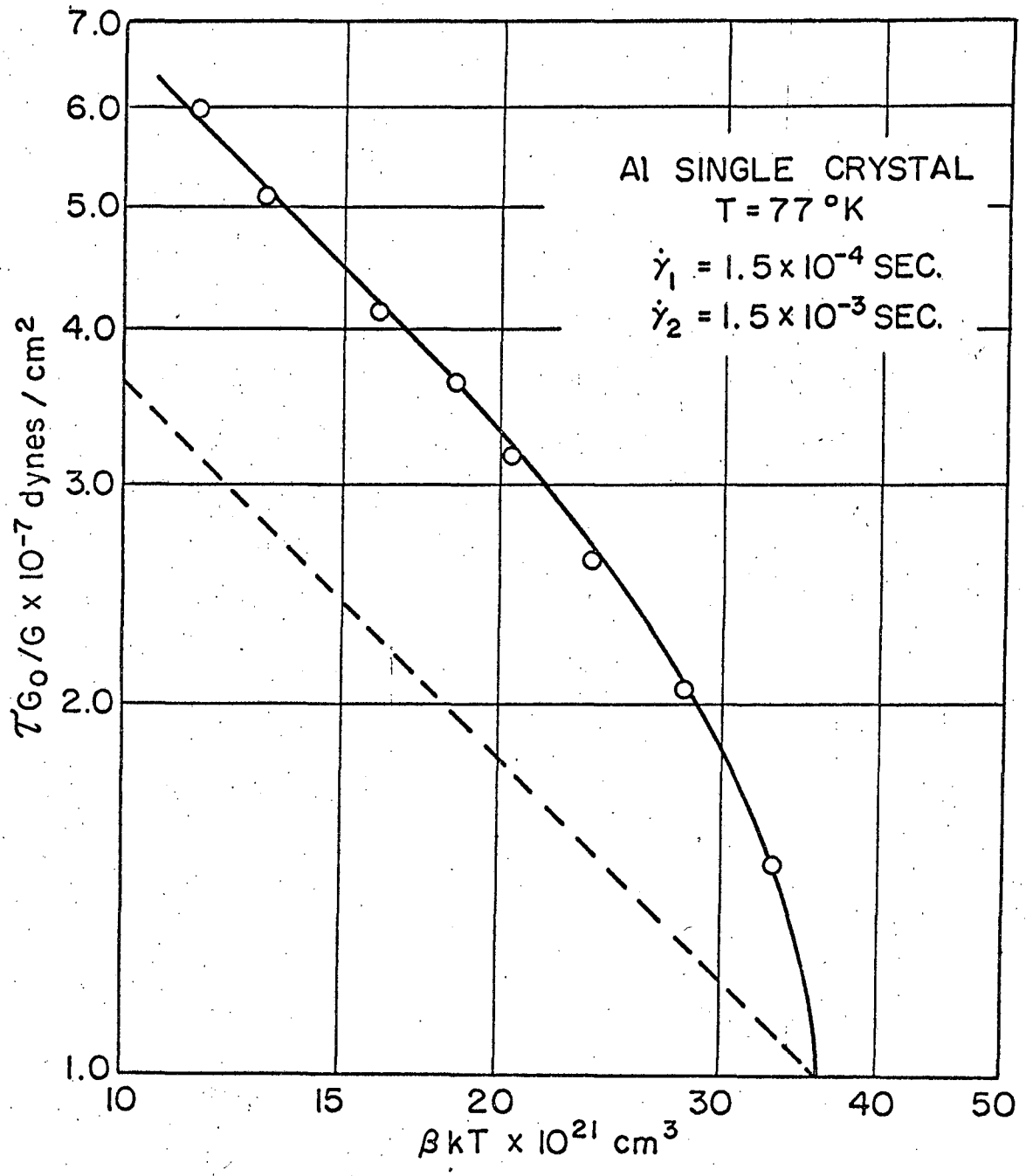

FIGURE 3.13. STRESS vs. ACTIVATION VOLUME AS DETERMINED FROM A SINGLE TEST.

ascribed to the same thermally activated process. During Stage I, 1/L and therefore the local interaction stresses change slowly whereas the long-range back stresses appear to build up almost immediately and almost, but not quite, linearly with 1/L. During the transition from Stage I to Stage II the values of 1/L increase, promoting an increase in the local interaction stresses. This transition is also reflected in the transition of the Cottrell-Stokes[42] ratio, as shown in Fig. 3.14, in going from easy glide to linear hardening. Over the linear hardening range the Cottrell-Stokes ratio is substantially constant. Solving Eqs. 3.7, 3.18, and 3.28 explicitly for the flow stress, and formulating the Cottrell-Stokes ratio gives

$$\frac{\tau_1}{\tau_2} = \frac{\tau_{0\ell}^* G_1/G_0 + \frac{1}{Lb}\left[\alpha G_1 b^2 - \psi\left\{kT_1 \ln \frac{NAb\nu}{\dot{\gamma}}\right\}\right]}{\tau_{0\ell}^* G_2/G_0 + \frac{1}{Lb}\left[\alpha G_2 b^2 - \psi\left\{kT_2 \ln \frac{NAb\nu}{\dot{\gamma}}\right\}\right]} \qquad (3.31)$$

The substantial constancy of this ratio with strain demands either that $\tau_{0\ell}^*$ vary approximately linearly with 1/L or that $\tau_{0\ell}^*$ be zero, in which case all back stresses arise from local interactions between intersecting dislocations. Whereas several investigators have emphasized the second alternative, the first is supported by the analyses made here. Further confirmation of this internally self-consistent separation of local interaction and long-range back stresses will be given in the discussion on polycrystalline Al covered in the following section.

Whelan et al[43] have observed that glide dislocations can combine with some forest dislocations over a length ℓ as shown in Fig. 3.15. This occurs only for those geometric conditions which lead to a decrease in energy when combinations take place. Saada has shown that an average stress τ_r^* given by

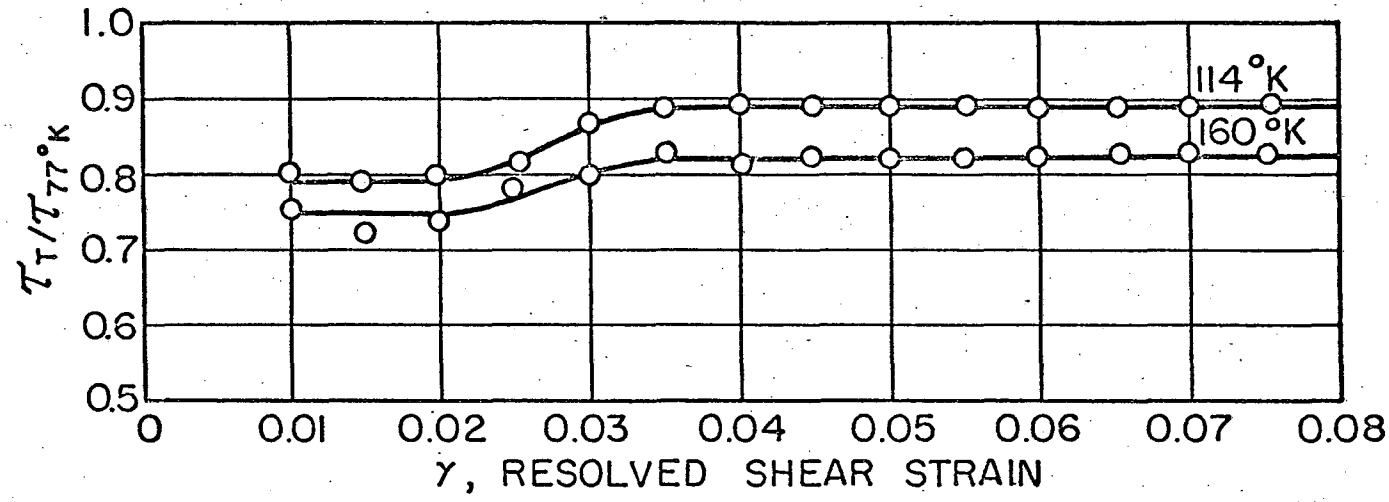

FIGURE 3.14. COTTRELL-STOKES RATIO FOR SINGLE Al CRYSTALS.

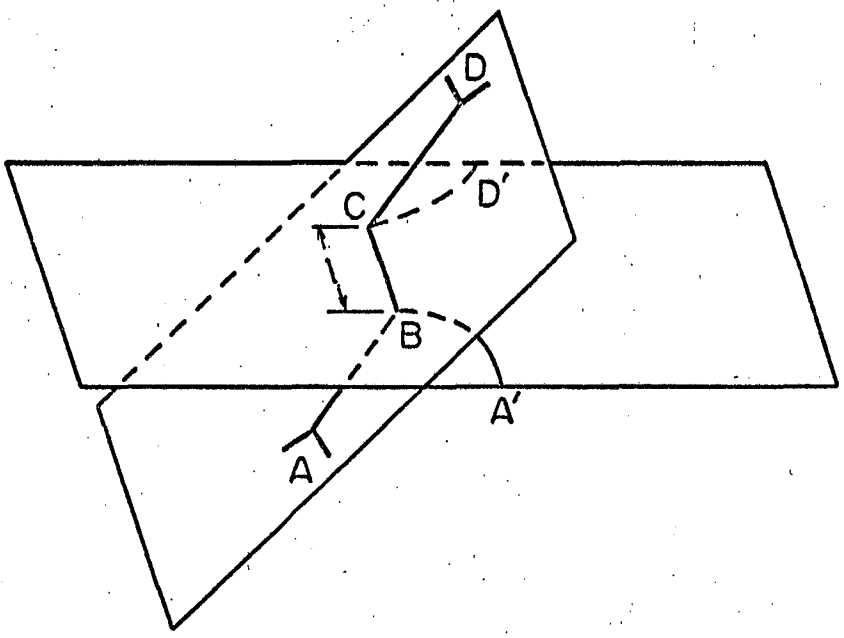

FIG. 3.15 COMBINATION OF A FOREST DISLOCATION, ABCD, WITH A GLIDE DISLOCATION, A'BCD', OVER LENGTH l.

$$\tau_r^* G/G_o = \frac{\alpha' G b}{L} \qquad (3.32)$$

is required to separate the combined dislocations where all terms have their usual meaning and $\alpha \simeq 0.20$. Thus α' is more than the α deduced experimentally for the local interactions. Since Hirsch's observations on combinations and Saada's theory are highly reliable, it becomes necessary to rationalize these factors in terms of the previous discussion. Such combinations must occur and contribute to strain hardening. First if thermal fluctuations assisted the applied stress to overcome the combination energy so as to complete intersection, the F_o - x curves for all FCC metals should be identical. But the F_o - x curve for Cu is substantially different from that for Al in just the way that would be expected for the previously described intersection mechanism in terms of the lower stacking fault energy of Cu and the resulting higher constriction energies. Consequently the strongly combined dislocations do not contribute to the thermally activated flow at low temperatures. Before combination can take place constriction must be completed. Also, it is quite possible that the thermal fluctuations required to complete the constriction introduces conditions more favorable to a reaction path that proceeds directly to intersection rather than one that has the intervening stage of combination. Consequently the possibility of combinations does not disqualify the simple intersection model presented here.

3F. Intersection Theory Applied to Pure Polycrystals, Alpha-Solid Solutions and Dispersions

The same experimental procedures for analysis of the intersection mechanism in single crystals, which were described in the preceding

section, have also been used to study the intersection mechanism in polycrystalline Al,[9] polycrystalline alpha-solid solutions of Mg in Al[9] and dispersions of $CuAl_2$ in an Al plus 0.19 atomic percent Cu matrix.[26] In spite of the fact that the von Mises[31] requirement demanded the operation of at least five slip systems in the polycrystal, and in spite of the fact that the stress levels were higher than those necessary to promote cross slip, the F_o - x curve deduced from the polycrystalline Al data coincided exactly with that previously obtained for single crystals in the easy glide and linear hardening ranges. Obviously the statistical distribution of the local interaction stresses must have been about the same regardless of the major differences in the amounts of polyslip in the two cases. Furthermore, cross slip, which must have been very prevalent in the polycrystalline aggregate, probably functioning to relieve the back stresses, thus promoting further operation of the rate controlling intersection mechanism. Under these conditions the strain rate due to cross slip could have been directly equated to the strain rate due to intersection, and the analysis could have been made in terms of either mechanism.

The F_o - x curves that were obtained from the Al-Mg alpha-solid solution alloys and the Cu-Al dispersion-hardened alloys differed only very slightly from that obtained for pure Al in a way that suggested these alloys exhibited slightly lower stacking fault energies and slightly higher constriction energies than pure aluminum.

Although the initial effective spacing of the forest dislocations was about the same for the single and polycrystalline specimens of pure Al, 1/L was greater for the Al-Mg alloys and yet greater for the Al-Cu dispersion alloys as shown in Fig. 3.16. The values of 1/L increased

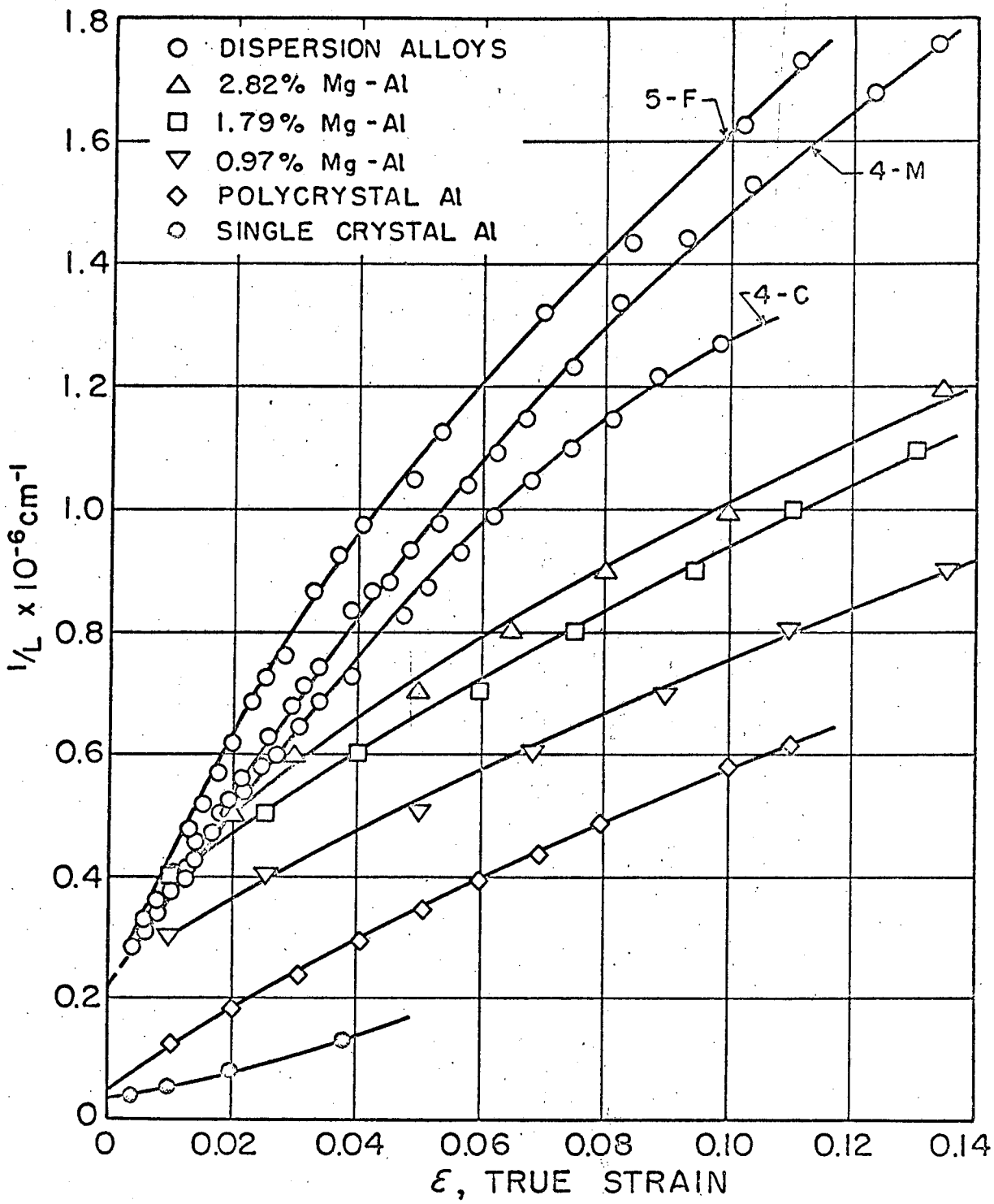

FIGURE 3.16. VARIATION OF $1/L$ AND τ_{oi} WITH TRUE STRAIN.

most rapidly with strain for the dispersion-hardened Cu-Al alloys and least for the Al single crystals. The local interaction stress $\tau_{oi}^{*} = 0.04 G_o b/L$, increases linearly with 1/L and is also shown in Fig. 3.16. The effect of strain on the long-range back stresses $\tau_{o\ell}^{*}$ is shown in Fig. 3.17. The pronounced differences between the trends of the local interaction stresses τ_{oi}^{*} and the long-range back stress fields $\tau_{o\ell}^{*}$ leave no doubt as to the separate origin and trends of these two separable quantities.

Polycrystalline aluminum strain hardens more rapidly than single crystals for the following three reasons:

1. The von Mises requirement for the operation of at leave five slip systems in polycrystalline Al causes the forest density to increase more rapidly than in single crystals.
2. The same factor results in correspondingly higher values of the local interaction stresses, τ_{oi}^{*}.
3. The long-range back stress fields, $\tau_{o\ell}^{*}$, are much greater for the polycrystalline Al. As shown in Fig. 3.18, the total flow stress σ (p) for polycrystals is about 3.10 τ (s) that for single crystals at the same value of 1/L as suggested by Taylor's theory for polycrystalline aggregates.

The slightly higher initial values of 1/L for the Al-Mg solid-solution alloys may have resulted from the stabilization of higher dislocation densities in these alloys as a result of Cottrell[44] and Suzuki[45] locking plus short-range ordering effects. These factors may also have contributed to the higher initial values and greater increases in both the local interaction stresses and the long-range back stresses with straining.

Orowan's[25] theory for the effects of incoherent dispersions on the yield strength of precipitation-hardened alloys was discussed in

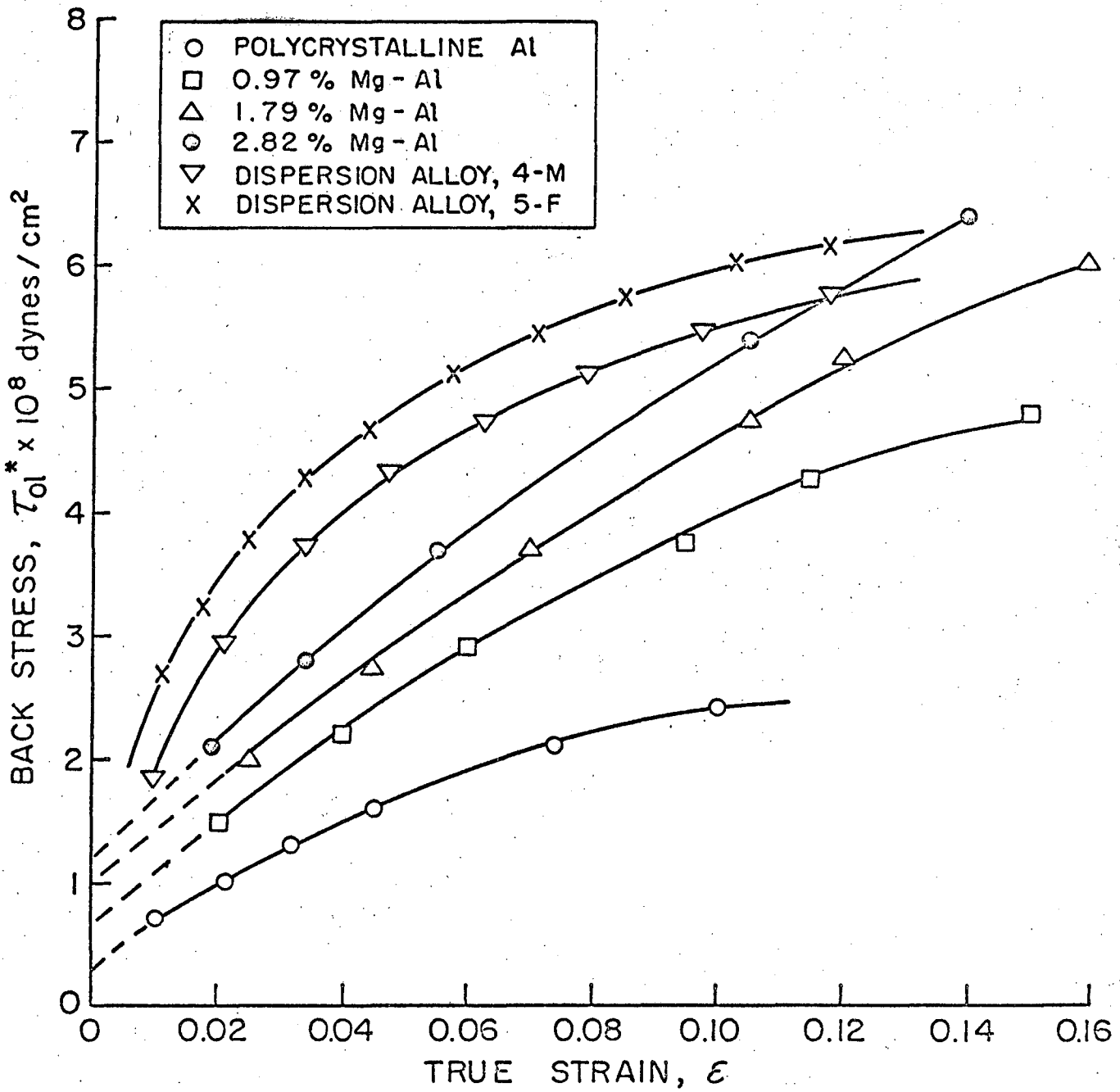

FIGURE 3.17. EFFECT OF TRUE STRAIN ON THE LONG RANGE BACK STRESSES.

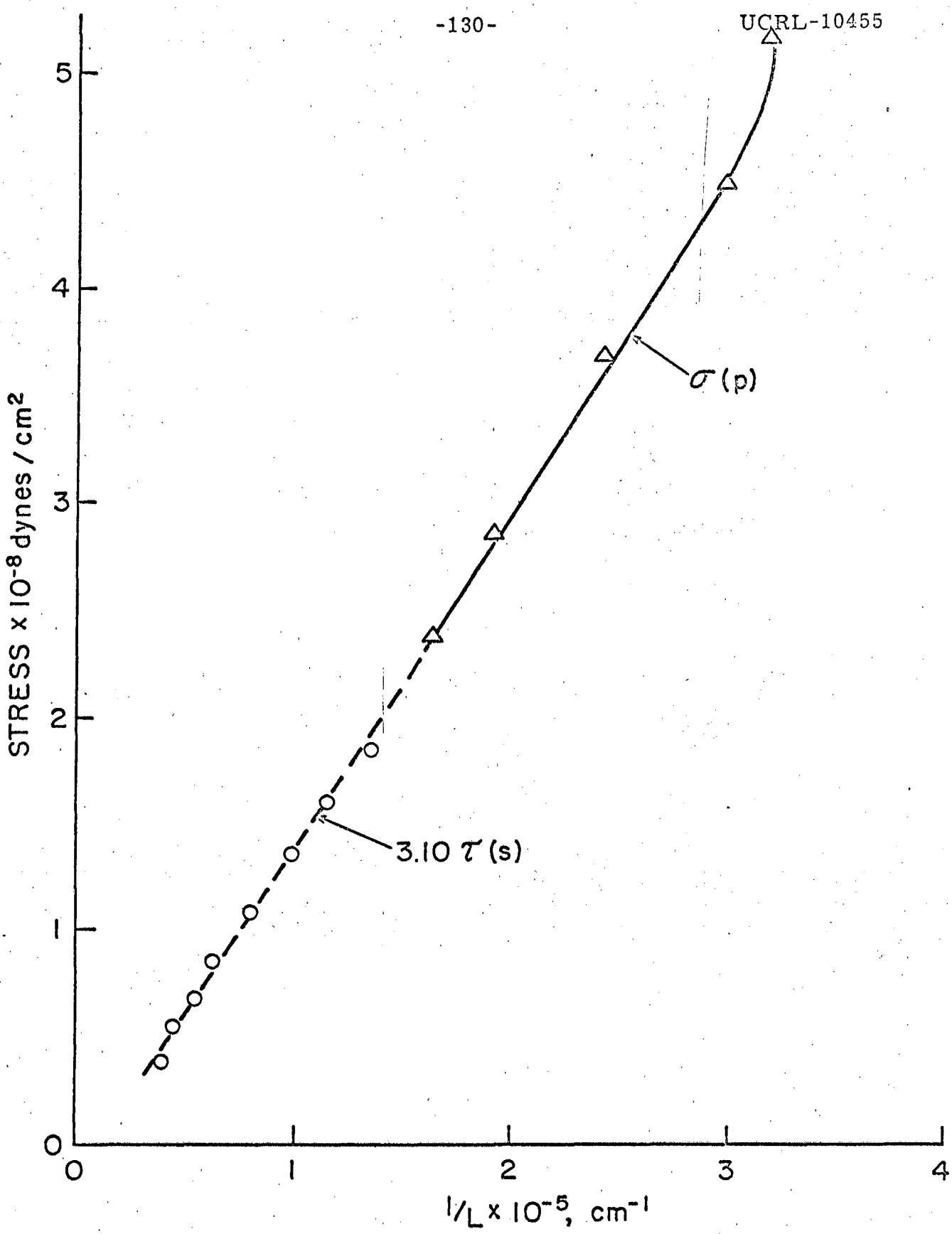

FIGURE 3.18. COMPARISON OF THE STRESS $\sigma(p)$ FOR THE DEFORMATION OF POLYCRYSTALLINE Al WITH 3.10 $\tau(s)$ FOR SINGLE CRYSTALS.

Section 2I. Fisher, Hart and Pry[27] extended Orowan's theory to include the effects of strain hardening. They assumed that as dislocations passed the dispersed particles they left loops about each particle which contributed to the strain hardening, primarily by increasing the long-range back stresses. Reference to the data recorded in Figs. 3.16 and 3.17, however, reveals that the major contribution to strain hardening of dispersion strengthened alloys arises not from $\tau_{0\ell}^*$ but from τ_{0i}^*. Electron microscopic observations show that dislocation entanglements form about the dispersed particles and that the observed values of L can be associated with dislocation segments in the entanglements. Furthermore the leveling off of $\tau_{0\ell}^*$ at the higher values of the strain is probably due to the relief of the back stresses due to cross slip.

3G. Nucleation of Cross Slip

Dislocations in BCC metals undertake extensive cross slip, whereas cross slip of dislocations in FCC metals becomes more infrequent as the stacking fault energy decreases . Undissociated dislocations can cross slip as soon as they are in screw orientation since the activation energy for cross slip of complete dislocations is zero. But dissociated dislocations in screw orientation must recombine and form constrictions before they can cross slip. The activation energy for cross slip is equal to the recombination and constriction energies. Among the several theories for cross slip that have been proposed, only Friedel's[46], which will be reviewed here, is satisfactorily formulated.

We will consider first slip on the prismatic plane of HCP metals. Dislocations in the prism planes are undissociated but those lying in the basal planes dissociate into partials as previously described in Section 2M.

Consequently when a dislocation on a prism plane moves into screw orientation it will spontaneously dissociate into its two partials on the basal plane with a corresponding decrease in energy. Consequently any extensive prismatic slip must involve regeneration of dislocations on the prismatic plane by thermal activation of cross slip. The path for nucleation of cross slip is illustrated in Fig. 3.19. The two partials B_1 and B_2 on the basal plane recombine over a length L and produce one constriction. The recombined segment bows out to P on the prismatic plane under the action of the applied stress. Consequently the activation energy for cross slip, U_x, is given by

$$U_x = U_c + U_R + \Delta U_L - W_\tau \qquad (3.33)$$

where U_c is the constriction energy, U_R is the recombination energy, ΔU_L is the increase in the line energy due to bowing of the dislocation, and W_τ is the work done by the local stress, $(\tau - \tau^*)$ acting on the prismatic plane in the direction of the Burgers vector. If Γ equals the line energy per unit length of the total dislocation, and R is the recombination energy,

$$U_x = U_c + (2R\sin\theta)R + (2R\theta - 2R\sin\theta)\Gamma + (\tau - \tau^*)b\left\{\frac{2\theta}{2\pi}(\pi R^2) - R^2\sin\theta\cos\theta\right\} \qquad (3.34)$$

where the last term in the brackets is the area swept out by the dislocation on the prismatic plane as a result of bowing. Both U_c and R will depend on the local resolved shear stress on the basal plane as shown by Eqs. 2.68 and 2.67b. But in single crystals so oriented that the resolved shear stress on the basal plane is zero, these quantities depend only on the elastic constants and the stacking fault energy. τ^* is also negligible for single

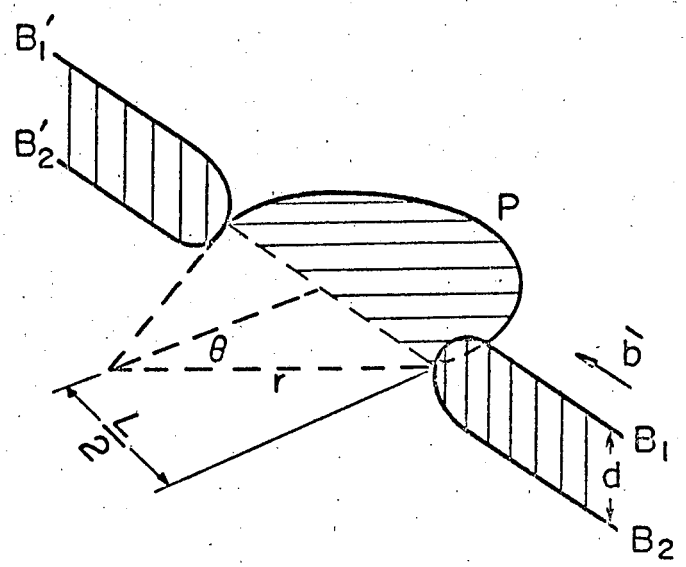

FIG. 3.19 NUCLEATION OF CROSS SLIP AS A RESULT OF RECOMBINATION OF THE PARTIALS B_1 AND B_2 ON THE BASAL PLANE ALONG LENGTH L AND BOWING OUT OF THE RECOMBINED SECTION P ON THE PRISM PLANE.

crystals. Furthermore the radius of curvature of the bowed dislocation is given by the well-known expression

$$R = \frac{\Gamma}{\tau b} \tag{3.35}$$

Under these circumstances the only unspecified quantity in Eq. 3.34 is θ. As θ increases the recombined length increases, the line energy increases and more work is done by the applied stress. At a critical value of $\theta = \theta_c$, however, U_x acquires a maximum value. Any thermal fluctuation greater than this critical value will nucleate cross slip. Applying $\partial U_x / \partial \theta = 0$ in order to ascertain the critical value of θ_c gives

$$\cos\theta_c = 1 - R/\Gamma \tag{3.36}$$

But $R < \Gamma$; therefore expanding $\cos\theta_c$ into a Taylor's series reveals that

$$\theta_c \simeq \left(\frac{2R}{\Gamma}\right)^{1/2} \tag{3.37}$$

Since θ_c is small, Eq. 3.35 for the activation energy becomes

$$U_x \simeq U_c + 2R\theta_c R \tag{3.38}$$

the remaining terms being negligibly small. Therefore, introducing Eqs. 3.34 and 3.37 into Eq. 3.38 gives

$$U_x = U_c + \frac{2(2\Gamma R^3)^{1/2}}{b\tau} \tag{3.39}$$

The critical length L that must be recombined in order to nucleate cross slip is

$$L_c = 2R\sin\theta_c = \frac{2\Gamma}{\tau b}\theta_c = \frac{2(2\Gamma R)^{1/2}}{\tau b} \qquad (3.40)$$

Therefore the higher the stress is, the shorter is the length that must recombine and the lower is the activation energy for cross slip.

Let N be the total number of screw segments of dislocations, each having an average length L_s, in a unit volume of the crystal. Then the total number of segments of length L_c per unit volume of the crystal is crudely about NL_s/L_c. The frequency with which each segment L_c vibrates is

$$\nu' \simeq \nu b/L_c \qquad (2.41)$$

where ν is approximately the Debye frequency. If then, A is the average area swept out by the dislocation following each successful fluctuation, the strain rate due to cross slip, $\dot{\gamma}^{c}_{x}$, will be given by

$$\dot{\gamma}^{c}_{x} = \left(\frac{NL_s}{L_c}\right) Ab \left(\frac{\nu b}{L_c}\right) e^{-U_x/kT} \qquad (3.42)$$

Introducing Eqs. 3.40 and 3.39 for L_c and U_x gives

$$\dot{\gamma}^{c}_{x} = \frac{NL_s Ab^4 \nu \tau^2}{8\Gamma R} e^{-\left\{\frac{U_c}{kT} + \frac{2(2\Gamma R^3)^{1/2}}{\tau b kT}\right\}} \qquad (3.43)$$

Obviously there is no simple relationship between the flow stress and temperature for cross slip as was observed previously for intersection. Perhaps the most easily adapted method of analysis is obtained by rewriting Eq. 3.43 as

$$\frac{1}{\tau T} = \frac{kb}{2(2\Gamma R^3)^{1/2}} \ln\left(\frac{NL_s A b^4 \nu}{\dot{\gamma}_x^e 8\Gamma R}\right) + \frac{2kb}{2(2\Gamma R^3)^{1/2}} \ln \tau - \frac{b U_c}{2(2\Gamma R^3)^{1/2} T} \tag{3.44}$$

which suggests that, neglecting the variation in $\ln \tau$,

$$\frac{1}{\tau T} \simeq C_1 - \frac{C_2}{T} \tag{3.45}$$

where C_1 and $C_2 = b U_c / 2 (2\Gamma R^3)^{1/2}$ are constants. A typical result of such a correlation is shown for Mg in Fig. 3.20,[47] where $\frac{1}{\tau T}$ decreases linearly with 1/T when prismatic slip takes place. From the slope of this plot, one deduces

$$\frac{U_c}{\Gamma^{1/2} R^{3/2}} = 15.0 \text{ cm}^2/\text{dyne} \tag{3.46}$$

This expression will subsequently be used to estimate the separation of the partial dislocations on the basal plane in Mg.

When the activation energy decreases linearly with the stress, as in the case of intersection, βkT is the activation volume. But when the activation energy for a mechanism is not such a simple function of the stress, as in the case of cross slip, this interpretation is no longer valid. It is nevertheless useful, in such cases, to call βkT the apparent activation volume. Therefore, from Eq. 3.43

$$\beta kT = kT\left(\frac{\partial \ln \dot{\gamma}_x^e}{\partial \tau}\right)_T = \frac{2kT}{\tau} + \frac{2(2\Gamma R^3)^{1/2}}{\tau^2 b} \tag{3.47}$$

or

$$\left(\beta - \frac{2}{\tau}\right) kT = \frac{2(2\Gamma R^3)^{1/2}}{\tau^2 b} = \frac{C_3}{\tau^2} \tag{3.48}$$

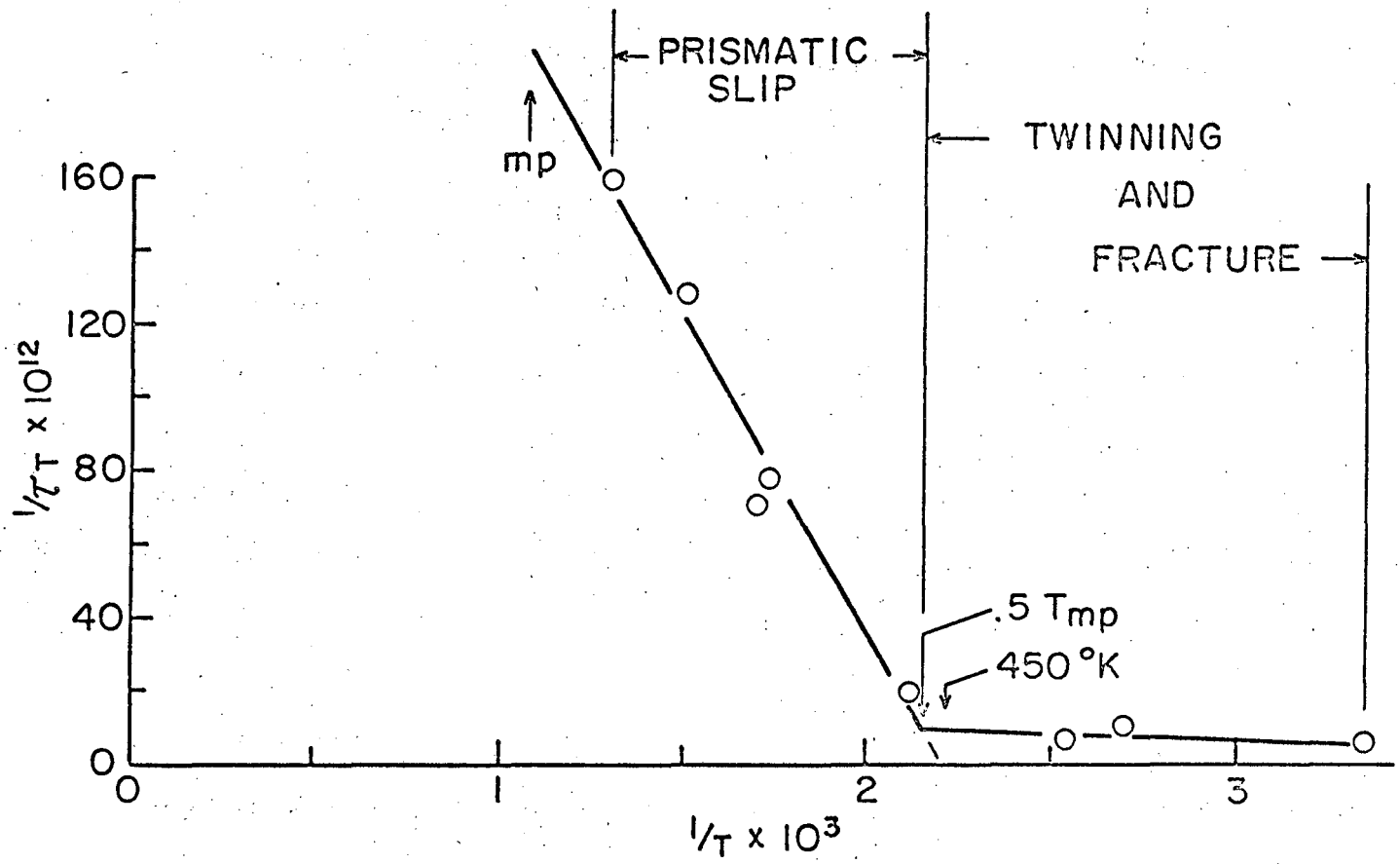

FIGURE 3.20. EFFECT OF TEMPERATURE ON THE YIELD STRENGTH OF Mg SINGLE CRYSTALS ORIENTED FOR PRISMATIC SLIP.[47]

A typical experimental result is shown in Fig. 3.21 for prismatic slip of Mg. As given by Eq. 3.48 the slope of Fig. 3.21 is $2(2\Gamma R^3)$ b, therefore, using the expression[48]

$$\frac{R}{\Gamma} \simeq \frac{1}{16} \ln \frac{d}{eb} \qquad (3.49a)$$

the separation of the partials on the basal plane was estimated to be $d \simeq 2.3b$. Also $U_c = C_2 C_3$, hence from the expression[34]

$$U_c = \frac{Gb^2 d}{30} \left(\ln \frac{d}{b} \right)^{1/2}$$

and the data of Fig. 20 (Eq. 3.46) the separation of the partials was estimated to be d 6.6 b which is in good agreement with that estimated from the data of Fig. 3.20.

The activation energy for cross slip in FCC metals differs slightly from that in HCP metals as revealed in Fig. 3.22. As the dislocation cross slips, it dissociates into its partials on the cross slip plane. Consequently the activation energy for cross slip is about twice the constriction energy (i.e., $2U_c$), and the segment of the dislocation over which this occurs is about 4d, where d is the separation distance of the partials. Therefore,

$$\dot{\gamma}_x^e = \left(N \frac{L_s}{4d} \right) Ab \left(\frac{\nu b}{4d} \right) e^{-\frac{2U_c}{kT}} \qquad (3.49b)$$

where both d and U_c are dependent on the local stresses as previously described. Up to the present there has been no completely satisfactory experimental verification of the cross-slip mechanism in FCC metals. As previously described, however, in the range of conditions where cross

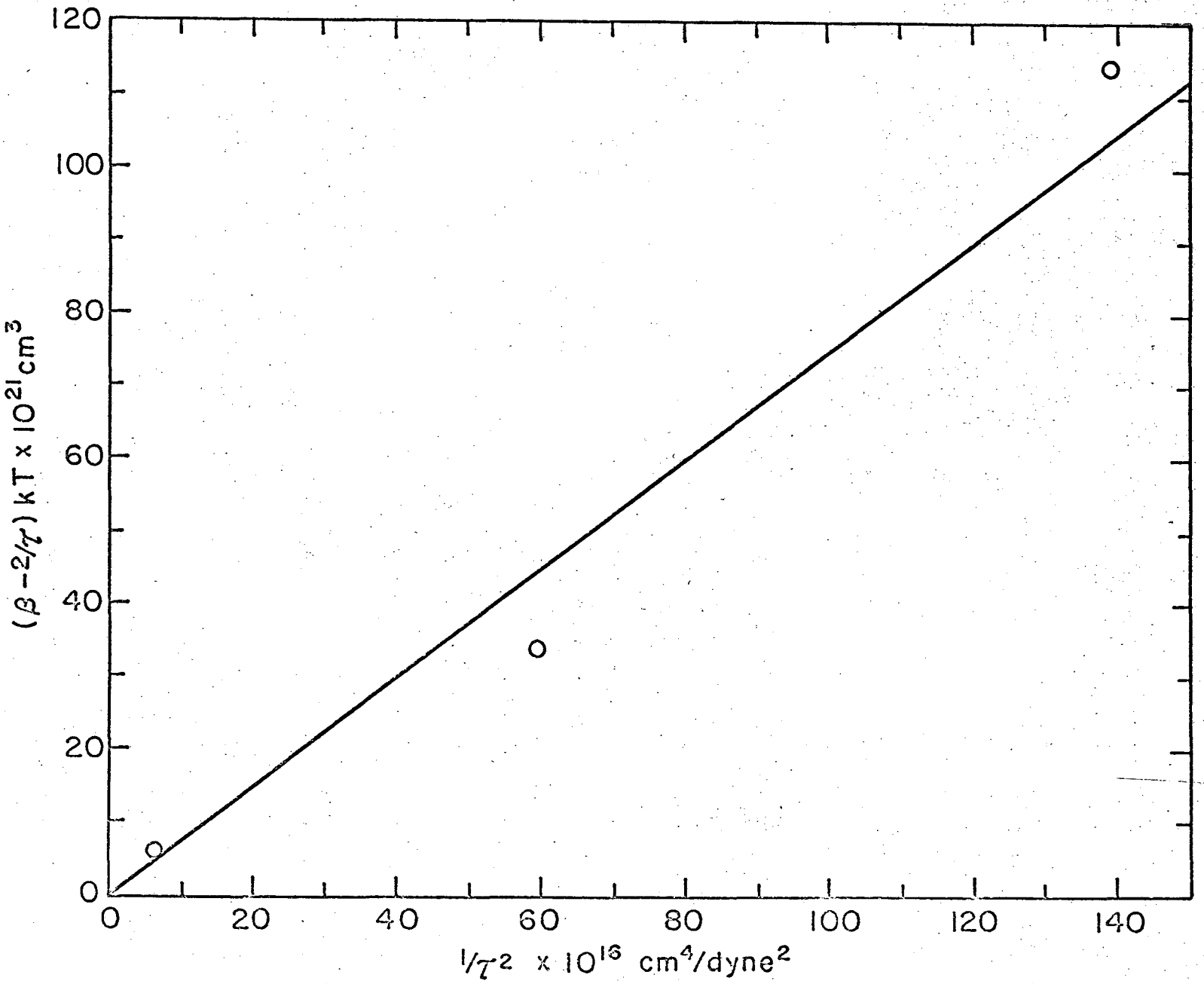

FIGURE 3.21. CORRELATION OF APPARENT ACTIVATION VOLUME WITH FLOW-STRESS AND TEMPERATURE FOR CROSS-SLIP IN Mg.

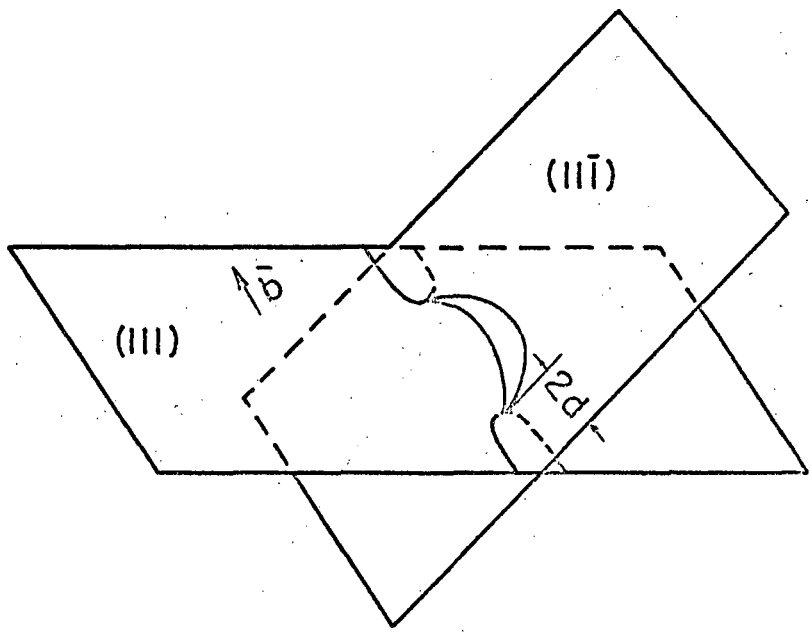

FIG. 3.22 CROSS SLIP IN FCC METALS.

slip merely relieves the back stresses so that dislocations can proceed to undertake intersection, $\gamma_x^* = \gamma_i^*$, and the analysis can be more readily made in terms of the intersection mechanism.

3H. Energy of Formation and Motion of Vacancies

As the test temperature is increased, the lower activation energy mechanisms such as intersection and cross slip take place with increased facility so that they no longer serve as barriers to the motion of dislocations. At this stage additional creep takes place by thermal activation of more difficult processes, and the experimentally determined activation energy begins to approximate those for self diffusion. A brief review of diffusion will be given here in order to provide the basis for describing such mechanisms.

Diffusion can take place by several mechanisms. As documented in a number of recent reviews[49-51] on this subject, however, the volume diffusion in pure metals, and substitutional alloys as well, is now known to occur principally by the vacancy mechanism as shown in Fig. 3.23. The rate at which the radioactive atoms (shown by *) move is directly related to the number of vacancies that are present. The equilibrium number of single vacancies in a crystal is easily deduced from statistical thermodynamics.[52-54] Since the equilibrium number of vacancies are independent of the mechanism whereby they are produced, it is permissible to view their production as given in the transition from (a) to (b) of Fig. 3.23. When an atom is removed from the near center of a crystal, the bonds with the adjacent coordinated atoms must be broken and when that atom is placed on the surface one-half of these bonds are restored. The total work involved in making a vacancy, therefore, is the work U_f

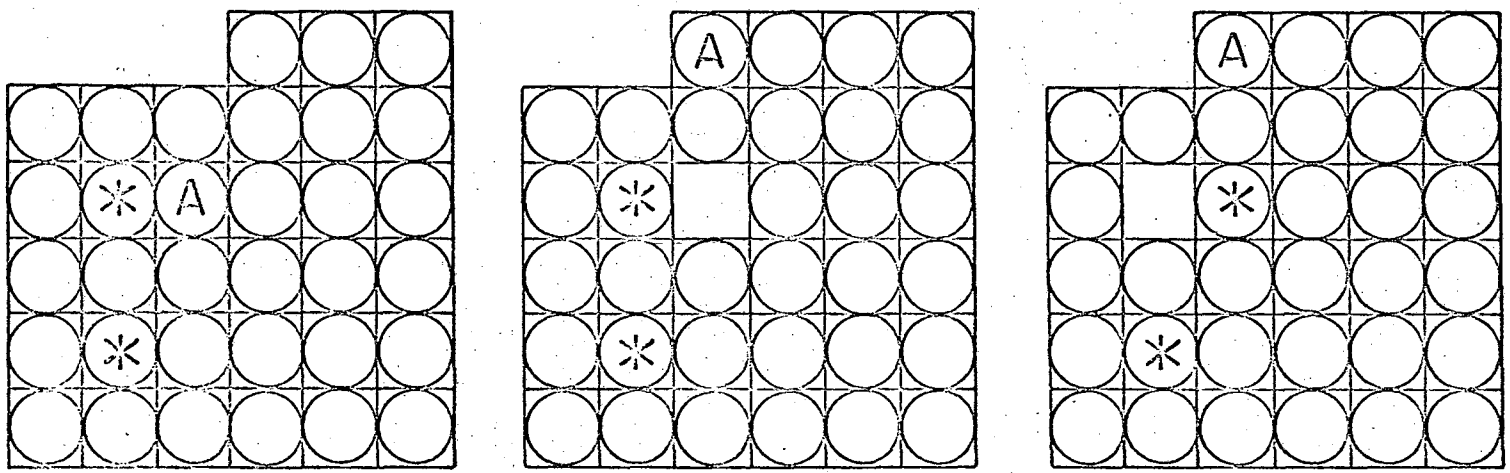

(a) THE PRODUCTION OF A VACANCY

(b) RADIOACTIVE * ATOM ADJACENT TO A VACANCY

(c) ATOM VACANCY EXCHANGE OR MOTION OF A VACANCY

FIGURE 3.23. VACANCIES AND DIFFUSION.

of breaking one-half of the atomic bonds plus the work $p\Omega_f$ done against the surroundings where p is the pressure and Ω_f is the volume expansion per vacancy produced, a quantity almost equal to the atomic volume. The atoms adjacent to the vacancy now have a lower frequency of vibration than before. Consequently the vibrational entropy changes an amount s_f per vacancy produced and the work that must be done to produce a single vacancy at a given site is

$$f_f = u_f + p\Omega_f - Ts_f \tag{3.49c}$$

where f_f is the free energy of formation of a vacancy. On the other hand, the total increase in free energy upon introduction of n independent and noninteracting vacancies at random among n_A atoms is

$$F = nf_f - kT \ln \frac{(n_A + n)!}{n_A!\, n!} \tag{3.50}$$

where the last term arises from the configurational entropy of random mixing of n vacancies among n_A atoms. Therefore, the average work that must be done in adding a vacancy to a random mixture of n vacancies and n_A atoms is

$$\frac{\partial F}{\partial n} = f_f - kT \ln \left(\frac{n + n_A}{n} \right) \tag{3.51}$$

Since the free energy is a minimum at equilibrium, the equilibrium number of vacancies, n_o, in a solid is given by $(\partial F/\partial n)_{n=n_o} = 0$ and consequently

$$n_o/n_s = e^{-f_f/kT} \tag{3.52}$$

where $n_s = n_A + n$ the total number of lattice sites.

The extra work that must be done in creating a vacancy in a crystal that contains n vacancies as referred to one that contains the equilibrium number of vacancies is given by the chemical work

$$W_c = \left(\frac{\partial F}{\partial n}\right)_n - \left(\frac{\partial F}{\partial n}\right)_{n_0} = kT \ln \frac{n}{n_0} \qquad (3.53)$$

This is, therefore, the constant pressure isothermal work that a system which is supersaturated with vacancies can do.

Diffusion is a random walk phenomenon and, in the simple case of self diffusion, it can be described in terms of the mass migration of tagged, radioactive atoms. When the concentration of such tagged atoms is uniform, their random walk causes no net mass transfer. But when the situation is as shown in Fig. 3.24, a mass migration will take place in the direction opposite to the concentration gradient. Here N^* is the number of tagged atoms per cm^2 of a crystal plane, and λ is the jump distance. Since all atoms are chemically identical, each atom jumps with the same frequency ν' in any one fixed direction. Therefore, the increase in the number of tagged atoms on the plane at x in time δt is given by

$$\delta N^* = \{N^*(x-\lambda) + N^*(x+\lambda) - 2N^*\} f \, \delta t$$

or

$$\frac{\delta N^*}{\delta t} = D \left(\frac{\partial^2 N^*}{\partial x^2}\right) \qquad (3.54)$$

where

$$D = \nu' \lambda^2 \qquad (3.55)$$

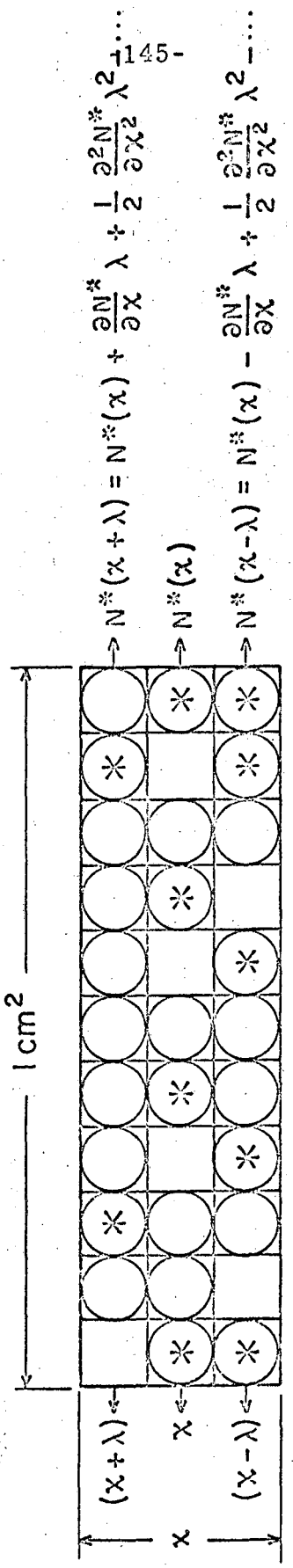

FIGURE 3.24. DIFFUSION OF TRACER ATOMS.

is the diffusivity as defined by Fick's second law for diffusion.

The frequency ν' depends on the mechanism of diffusion that takes place. For the vacancy mechanism of diffusion the frequency is given by the frequency ν of an atom adjacent to a vacancy times the probability that it has enough energy to move into a vacant site,

$$e^{-g_m/kT} = e^{-\frac{u_m + p\Omega_m - s_m T}{kT}}$$

times the probability that the atom is moving in a given direction α, times the probability n/n_s that a vacancy is in that direction. Therefore,

$$D = \alpha \lambda^2 \nu \frac{n}{n_s} e^{-\frac{u_m + p\Omega_m - s_m T}{kT}} \qquad (3.56)$$

For the simple cubic lattice the factor α, giving the probability of motion in any one of the six possible directions is 1/6. The same type of analysis reveals that the diffusivity of a vacancy is

$$D_v = \alpha \lambda^2 \nu e^{-\frac{u_m + p\Omega_m - s_m T}{kT}} \qquad (3.57)$$

where the subscript m refers to the values of the variables pertaining to the motion of a vacancy which is of course identical to those for the motion of an atom.

When the diffusivity is determined under conditions where the concentration of vacancies is given by thermal equilibrium, the value n/n_s in Eq. 3.56 must be replaced by n_o/n_s of Eq. 3.52. Therefore,

$$D_o = \alpha \lambda^2 \nu e^{\frac{s_f + s_m}{k}} e^{-\left\{\frac{u_f + u_m + p(\Omega_f + \Omega_m)}{kT}\right\}} \qquad (3.58)$$

$$= \alpha \lambda^2 \nu e^{s_d} e^{-\frac{u_d + p\Omega_d}{kT}}$$

where the subscript d refers to the values for diffusion. Consequently the activation enthalpy for diffusion, $U_d + p\Omega_d$ is equal to the sums of the enthalpies of formation and motion of vacancies. The fact that the activation enthalpies for high temperature creep begin to approximate those for self-diffusion, strongly suggests that this creep is dictated by atomistic mechanisms that involve the formation and migration of vacancies.

Three different theories for high temperature creep that are based on the formation and migration of vacancies have now been postulated. The first, originally conceived by Nabarro[17] and elaborated upon by Herring,[55] is known as stress directed diffusion of vacancies. It is applicable at very high temperatures, those approaching the melting temperatures, and at very low stresses, presumably below those which are required to operate a Frank-Read dislocation source or to generate dislocations by other means. The theory is quite accurately and completely formulated. It concerns the formation of vacancies under an applied stress at the grain boundaries normal to the applied stress and migration of the vacancies through the grain volume to the boundaries parallel to the applied stress. Atoms, of course, migrate in the opposite direction to the vacancies and thus provide the permanent strain. Several investigations give creep rates that are in good agreement with the theory. In view of the fact, however, that this mechanism of creep is not dependent on dislocation processes, it will not be presented in detail here.

The remaining two theories, (a) thermally activated motion of jogged screw dislocations, and (b) the climb of edge dislocations are limited to crystalline materials and both depend on dislocation processes. The applicability of these theories

to creep is not nearly so well established as that for the stress-directed diffusion of vacancies; and consequently attempts are continuing to isolate these mechanisms experimentally for individual study.

31. Creep Due to the Motion of Jogged Screw Dislocations

Jogs in edge dislocations do not materially restrain the motion of an edge dislocation because the jogs also lie in slip planes. But jogs on screw dislocations are edge jogs, and if the screw dislocation is forced to move, such jogs must move from one slip plane to the next adjacent slip plane. This is only possible as a result of atom transfer known as climb. Two types of unit jogs are shown in Fig. 3.25. Under the applied stress, the screw dislocation, shown dissociated into its partials, will bow out, as shown, and move to the right. If the upper jog also moves to the right one atomic plane, it will have to form a vacancy V_1 at the lower part of the extra half plane of atoms A comprising the edge jog. When the lower jog moves to the right, it must leave the last atom B_1 of the half-plane in an interstitial position. Whereas the upper jog, for the configuration shown, is a vacancy forming jog, the lower jog is an interstitial forming jog.

Jogs can form by means of a number of mechanisms: As we have seen when a glide screw dislocation intersects a forest screw dislocation, unit jogs are produced; when a screw dislocation cross slips from plane A_1 to some other slip plane B and then back to A_2, which is parallel to A_1, superjogs of many planes in height are formed by the dislocation segments left in plane B; when the two nodal points of a dislocation segment lie on different slip planes this segment must contain superjogs. Since the free energy of a jog in dissociated dislocations is equal to the jog energy U_j plus the constriction energy U_c, the equilibrium distance

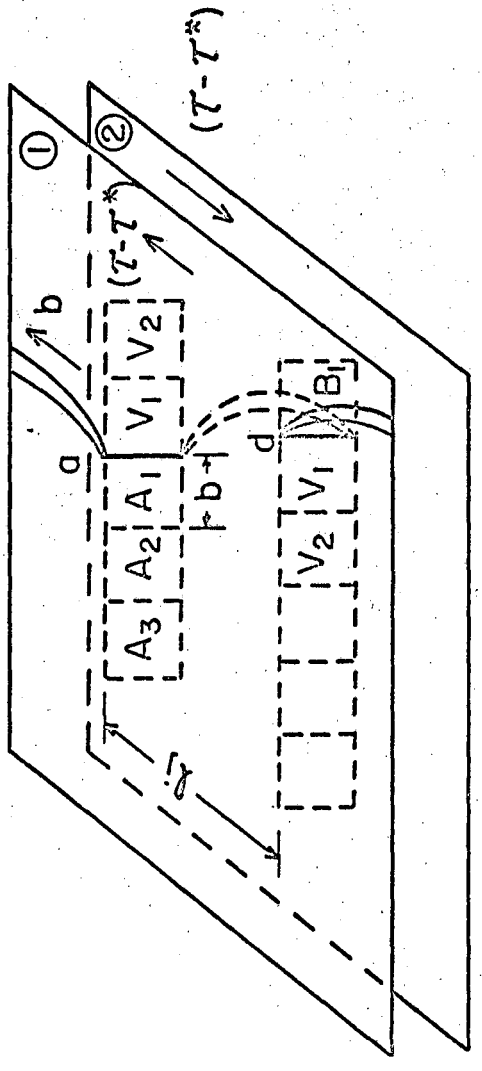

FIGURE 3.25. MOTION OF JOGS.

between jogs is given by the Boltzmann expression

$$b/l_j = e^{-\frac{U_j + U_c}{kT}} \qquad (3.59)$$

Jogs can be created by absorption or liberation of vacancies.

Jogs in screw dislocations can glide on their slip planes parallel to the screw dislocation. Thus interstitial and vacancy jogs can annihilate each other or they can glide to the nodes. Jogs on edge dislocations can be eliminated by climb resulting from absorption or liberation of vacancies. The thermally activated motion of jogged screw dislocations has been described by Mott,[56] Seeger,[57] Friedel[58] and van Bueren.[59] The following analysis is taken, with minor modifications, principally from the recent investigations by Hirsch and Warrington.[60]

As shown in Fig. 3.25, screw dislocation segments bow out between the jogs under an average local stress $\tau - \tau^*$, the dislocation being held up at the jogs. In view of the high energy, however, of forming interstitials, the operative process of creep must depend primarily on the vacancy mechanism. At both "a" and "b" a force $(\tau - \tau^*) l_j b^2$ is operative where l_j is the mean distance between the jogs. If the jog at "a" is to move forward one Burgers vector, an atom must occupy position V_1 and liberate a vacancy. Consequently point "a" is a source of vacancies. In order for the jog at "b" to move forward, a lattice vacancy must exchange with the atom at B_1. Consequently point "b" is a vacancy sink. Throughout the lattice there are many sources and sinks. For example, edge dislocations and grain boundaries can also serve as sources and sinks for vacancies.

The question now arises as to how vacancies, generated at sources, diffuse to the nearby sinks. For example, Lothe[61] recently suggested that inasmuch as the energy to form a vacancy on a dislocation is smaller than that to form a vacancy some distance from a dislocation, and inasmuch as pipe diffusion along the dislocation is so much more rapid than volume diffusion, pipe diffusion must control the process. Although such a mechanism undoubtedly contributes to the all-over process, there are several factors that suggest it may not be important. First, pipe diffusion would lead to an activation enthalpy for creep that is considerably below that for volume self-diffusion. Secondly, pipe diffusion must take place along the single atomic path coincident with the dislocation line, whereas volume diffusion may proceed along many paths, a factor which compensates for the higher activation energy of volume diffusion. Furthermore, the osmotic work that can be done by supersaturation in the vicinity of a vacancy forming jog may be sufficient to cause large numbers of vacancies to leave the dislocation pipe to undertake volume diffusion.

For superjogs having a height of h atomic planes, the average force acting on each atomic height of the jog is $(\tau - \tau^*) l_j b^2/h$. The energy that must be supplied by a thermal fluctuation in order to form a vacancy is, therefore, $f_f - (\tau - \tau^*) l_j b^2/h$ where f_f is the free energy of the formation of a vacancy and the last terms represent the work contributed mechanically by the force acting at the jog. But to provide a permanent forward motion of the jog, the vacancy so produced will have to move away. Consequently the frequency ν_{vj}^+ with which a vacancy-forming superjog moves forward one Burgers vector is given by

$$\nu_{vj}^+ = \frac{\nu}{h} e^{\frac{-f_f - (\tau - \tau^*) l_j b^2/h}{kT}} z e^{-f_m/kT} \qquad (3.60)$$

where ν is only slightly less than the Debye frequency, and Z is the coordination number. Having so jumped forward, the jog may now jump back again. This frequency depends on the probability that a vacancy is next to the last atom on the jog times the probability that it will exchange with that atom and thus return the jog to its original position. Consequently, the frequency ν_{vj}^{-} for the reverse action is

$$\nu_{vj}^{-} = \frac{\nu}{h} Z \frac{n^{+}}{n_s} e^{-f_m/kT} \tag{3.61}$$

where n^{+}/n_s is the actual probability of finding a vacancy adjacent to a vacancy-forming jog. But

$$n^{+}/n_s = n^{+}/n_o \; n_o/n_s = \frac{n^{+}}{n_o} e^{-f_f/kT} \tag{3.62}$$

And therefore the net frequency of the forward motion of a vacancy-forming jog, $\nu_{vj} = \nu_{vj}^{+} - \nu_{vj}^{-}$, is

$$\nu_{vj} = \frac{\nu}{h} Z e^{-f_d/kT} \left\{ e^{\frac{(\tau - \tau^*) l_j b^2/h}{kT}} - \frac{n^{+}}{n_o} \right\} \tag{3.63}$$

The forward frequency of motion for an interstitial-forming jog is obtained by the same type of analysis. Since the interstitial-forming jog is a vacancy sink the probability of finding a vacancy adjacent to the terminal atom on the jog is n^{-}/n_s. Therefore, the net frequency for the forward motion of the interstitial-forming jog is

$$\nu_{ij} = \frac{\nu}{h} Z e^{-f_d/kT} \left\{ \frac{n^{-}}{n_o} e^{\frac{(\tau - \tau^*) l_j b^2/h}{kT}} - 1 \right\} \tag{3.64}$$

Eqs. 3.63 and 3.64 suggest, at first, that the interstitial-forming jog might lag behind the vacancy forming jog since $n^+/n_s > 1$, and $n^-/n_o < 1$. But it is easily shown that as one jog moves ahead of the other, the forces acting on the jogs so readjust themselves that the two jogs will move with the same velocity. Consequently, either Eq. 3.63 or 3.64 gives a good estimate of the frequency of the forward motion of a jog. The strain rate, $\dot{\gamma}^{\ell}$, is given by

$$\dot{\gamma}^{\ell}_s = \frac{\rho_s}{\ell_j}(\ell_j b) b \nu_{vj} = \rho_s b_s^2 \nu_{vj} \qquad (3.65)$$

where ρ_s is the total length of screw dislocations per cm^3, (ρ_s/ℓ_j) is the number of jogs per cm^3 on screw dislocations, and $(\ell_j b)$ is the area swept out per activation.

Excess vacancies have a very short lifetime even below atmospheric temperatures. At higher temperatures, where jogged screw dislocations might move, the lifetime of a vacancy is so short that a supersaturation of vacancies is difficult to maintain. Therefore, n^+/n_o can be approximated by unity. It is difficult in this case to prescribe, á priori, whether the long-range back stresses τ^* will be significant or not. In cases where the stacking fault energy is high or even intermediate, screw dislocations will cross slip with relative ease. Furthermore, screw dislocations may also enter twist boundaries which exhibit only very local stress fields and may not therefore contribute significantly to τ^*. Piled up edge dislocations, however, may introduce long-range back stresses. The creep rate, retaining the back stress term, is given by

$$\dot{\gamma}^{\ell}_s = \rho_s b^2 \frac{\nu}{h} e^{\Delta s} e^{-\frac{u_d + p\Omega_d}{kT}} \left\{ e^{\frac{(\tau-\tau^*)\ell_j b^2/h}{kT}} - 1 \right\} \qquad (3.66)$$

When $(\tau-\tau^*)\, l_j b^2/h \gg kT$, the flow stress becomes

$$\tau=\tau^*+\frac{U_d+p\Omega_d}{l_j b^2/h}-\frac{kT}{l_j b^2/h}\ln\left(\frac{\rho_s b^2 \nu e^{S_d/k}}{h\dot{\gamma}_s^e}\right) \quad (3.67)$$

and it decreases linearly with the absolute temperature. An alternate viewpoint is also possible, namely that the presence of local back stresses reduces the number of operative screw dislocations to $\rho_s' < \rho_s$. Then

$$\tau=\frac{U_d+p\Omega_d-S_dT}{l_j b^2/h}-\frac{kT}{l_j b^2/h}\ln\frac{\rho_s' b^2 \nu}{h\dot{\gamma}_s^e} \quad (3.68)$$

The only satisfactory experimental confirmation of the possible operation of the jog screw dislocation mechanism for deformation was presented in a report by Hirsch and Warrington. They contended that below about one-half of the melting temperature, where diffusion rates are negligibly slow, motion of jogged screws resulting in the formation of vacancies is an athermal process. Therefore, the flow stress is independent of the temperature and strain rate being given by

$$\tau_a=\frac{f_f}{l_j b^2/h}=\frac{U_f+p\Omega_f-S_fT}{l_j b^2/h} \quad \text{for } T<T_c \quad (3.69)$$

Consequently τ_a is less than τ at low temperatures and $\tau_a=\tau$ at the critical temperature T_c, when

$$\frac{U_f+p\Omega_f-S_fT_c}{l_j b^2/h}=\frac{U_d+p\Omega_d-S_dT}{l_j b^2/h}-\frac{kT_c}{l_j b^2/h}\ln\left(\frac{\rho_s' b^2 \nu}{h\dot{\gamma}_s^e}\right)$$

giving

$$U_m + pV_m - \Delta_m T_c = kT_c \ln \frac{\rho' b^2 \nu}{h \dot{\gamma}_s} \qquad (3.70)$$

Therefore,

$$\tau = \frac{U_d + pV_d - \Delta_d T}{l_j b^2/h} - \left(\frac{U_m + pV_m - \Delta_m T}{l_j b^2/h} \right) \frac{T}{T_c} \qquad (3.71)$$

for $T > T_c$

where the entropy and work terms are small. The activation volume is $\beta kT = l_j b^2/h$.

A schematic diagram of the expected results are shown in Fig. 3.26 and actual data for Al are reproduced in Fig. 3.27. The experimentally determined flow stress for a specified strain-hardened state decreases almost linearly with an increase in temperature as suggested by this theory. The range of temperatures for which the flow stress decreases almost linearly with the temperature, coincides closely with that shown over region D of Fig. 1.4 where the activation energy for creep increases almost linearly with the absolute temperature. This relationship also follows from Eq. 3.66 for tests at different temperatures when $\dot{\gamma}_s^e$ is about constant. But in spite of these confirmations of the theory, several questions must yet be answered before it can be assumed operative for the case in question. The major issue concerns whether or not vacancies can be produced athermally over the lower temperature range.

3J. Creep as a Result of Climb of Edge Dislocations

The theory for creep due to climb of edge dislocations is much more difficult to formulate accurately than that due to the motion of a

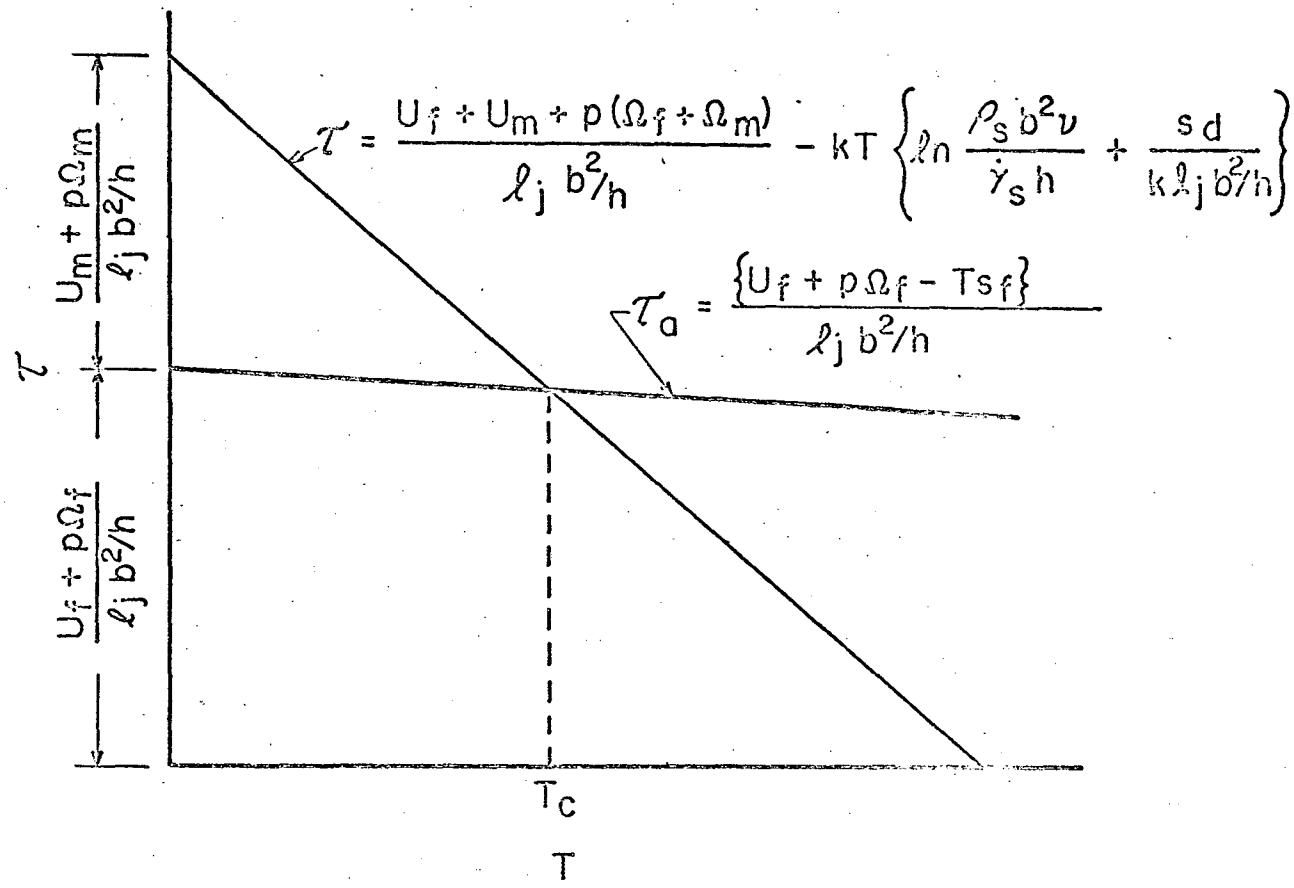

FIGURE 3.26. EFFECT OF TEMPERATURE ON THE FLOW STRESS FOR THE MOTION OF JOGGED SCREW DISLOCATIONS.

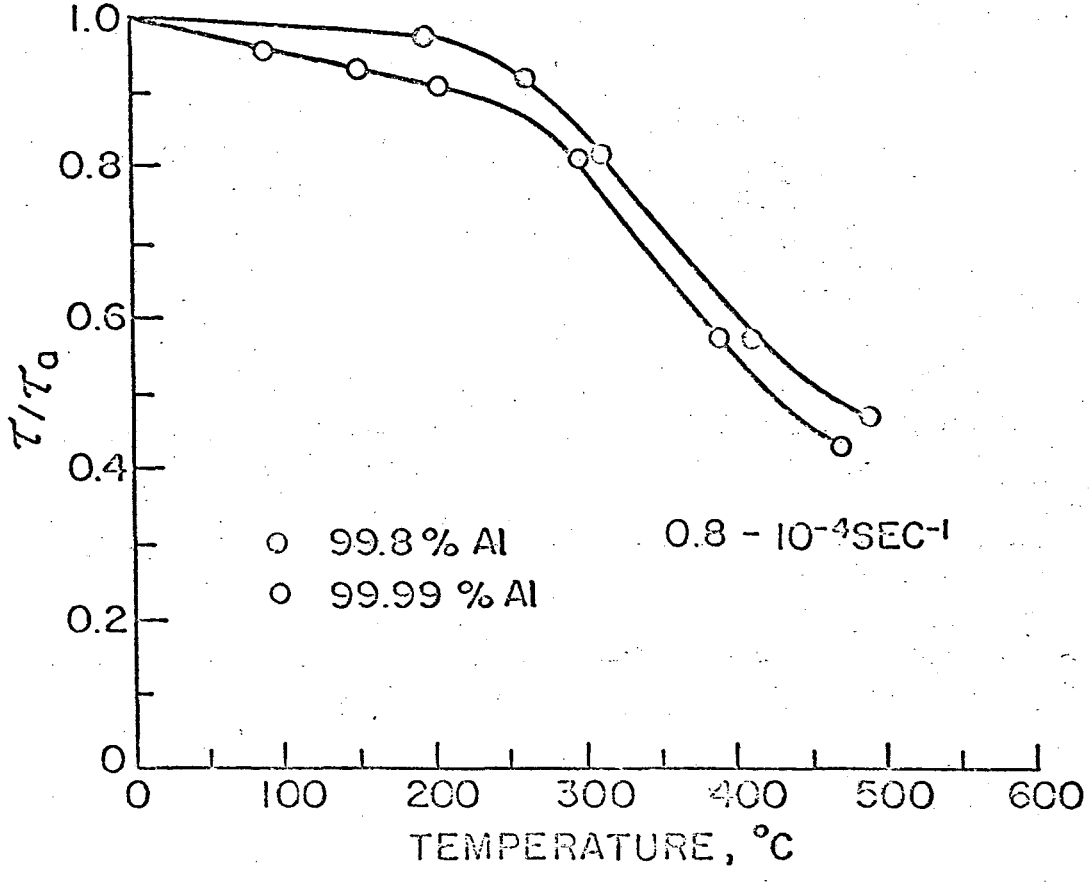

FIGURE 3.27. TEMPERATURE DEPENDENCE OF τ/τ_a FOR TWO PURITIES OF POLYCRYSTALLINE Al (99.8% AND 99.9 %).

jogged screw dislocation. This arises from the fact that the rate at which edge dislocations climb depends intimately on the geometric details of dislocation patterns that are produced under stress in the vicinity of the climbing dislocation. These patterns have not yet been sufficiently well documented to provide unambiguous guides to formulation of the climb process in detail. The following analysis, based on a specific model, therefore, can only suggest the general trends. The theory for climb of dislocations has been discussed by Mott,[56, 62] Seeger,[63] and Weertman.[64] Recently Christy[65] has elaborated on the model, but inasmuch as his approach is only a minor variation on the same theme presented in detail by Weertman, the following analysis with the exceptions of minor innovations, will be based on Weertman's formulation.

The process for climb, as illustrated in Fig. 3.28, is somewhat analogous to the motion of jogged screw dislocations. As shown under a tensile stress normal to the extra half plane and atom can jump into position at the bottom of the extra half plane, leaving a vacancy, $\square$, in its former site. This, of course, can only happen easily at a jog, because of geometric and energetic considerations. When the vacancy migrates away from the core of the dislocation by diffusion, a unit climb will have resulted. Under compression stresses, climb will take place in the opposite direction. But in either case the formation or the absorption of a vacancy can only occur with relative ease at a jog.

As seen, climb involves the formation of a vacancy at a jog under the action of a stress σ_{xx} followed by its migration away from the dislocation. Therefore the frequency for climb in the positive direction (i.e., under a tensile stress) is

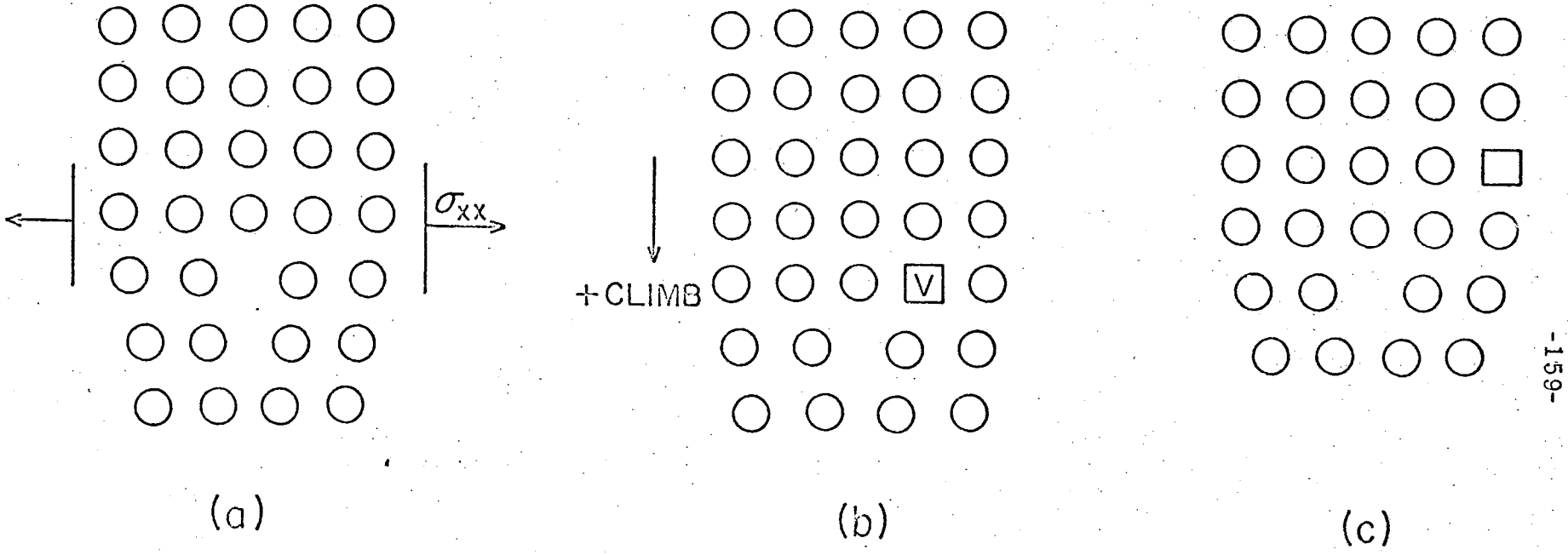

FIGURE 3.28. CLIMB OF AN EDGE DISLOCATION.

$$\nu_c^+ = \nu p_j \left\{ e^{-f_f/kT} e^{\frac{\sigma_{xx}\Omega}{kT}} \right\} \left\{ (Z-1) e^{f_m/kT} \right\} \quad (3.72)$$

where ν is almost equal to the Debye frequency, p_j is the probability a jog is present, $e^{-f_f/kT}\, e^{\sigma_{xx}\Omega/kT}$ is the probability of having enough thermal energy to form a vacancy (where $\sigma_{xx}\Omega$ is the work done by the local stress and Ω is the atomic volume) $e^{f_m/kT}$ is the probability of a sufficiently high thermal fluctuation to move the vacancy, Z is the coordination number and (Z-1) is the number of directions the vacancy can move without reversing the climb. If, however, a vacancy exchanges positions with the terminal atom on the extra half plane, the direction of climb will be reversed. Since vacancies are being produced at the jog, the probability of finding a vacancy adjacent to the jog is $(Z-1)\, n^+/n_s$ where n^+ is the total number of vacancies on n_s atomic sites in the near vicinity of the jog. Therefore, the frequency of reversed climb is

$$\nu_c^- = \nu p_j (Z-1) \frac{n^+}{n_s} e^{-f_m/kT} \quad (3.73)$$

But

$$n^+/n_s = \frac{n^+}{n_o} \frac{n_o}{n_s} = \frac{n^+}{n_o} e^{-f_f/kT} \quad (3.74)$$

as shown by Eq. 3.52. Consequently

$$\nu_c^- = \nu p_j (Z-1) e^{-f_d/kT} \frac{n^+}{n_o} \quad (3.75)$$

The net rate of positive climb v_c where

$$v_c = v_c^+ - v_c^-$$

$$v_c = \nu(z-1)\rho_j e^{f_d/kT}\left\{e^{\frac{\tau_{xx}\Omega}{kT}} - \frac{n^+}{n_0}\right\} \quad (3.76)$$

But as previously discussed $n^+/n_0 \simeq 1$. And since the atomic volume Ω is so very small, the value of $\tau_{xx}\Omega$ that can be achieved is also small relative to kT. Therefore, expanding the exponential in terms a Taylor series gives

$$v_c = \nu(z-1)\frac{\tau_{xx}\Omega}{kT}\rho_j e^{f_d/k} e^{-\frac{U_d + p\Omega_d}{kT}} \quad (3.77)$$

Whereas the above analysis is quite reliable for any climb mechanism, in the following details only one of a series of possible models will be analyzed. We will assume that dislocations formed at two unspecified sources on slip planes a distance h apart are arrested as shown in Fig. 3.29. If h is greater the h_m, as shown in Section 2J, the dislocations will pass each other. But if h is less than this critical value, additional motion of the dislocations can only occur when the two leading dislocations of the array climb together so as to annihilate each other. The rate of climb, of course, depends on τ_{xx}. Since the applied stress is usually quite small, the major contribution to τ_{xx} arises from the stress concentration factors from the piled-up arrays of dislocations as discussed previously in Section 2K.

Letting $\dot{y}$ be the rate of climb in the vertical direction,

$$\dot{y} = b v_c \quad (3.78)$$

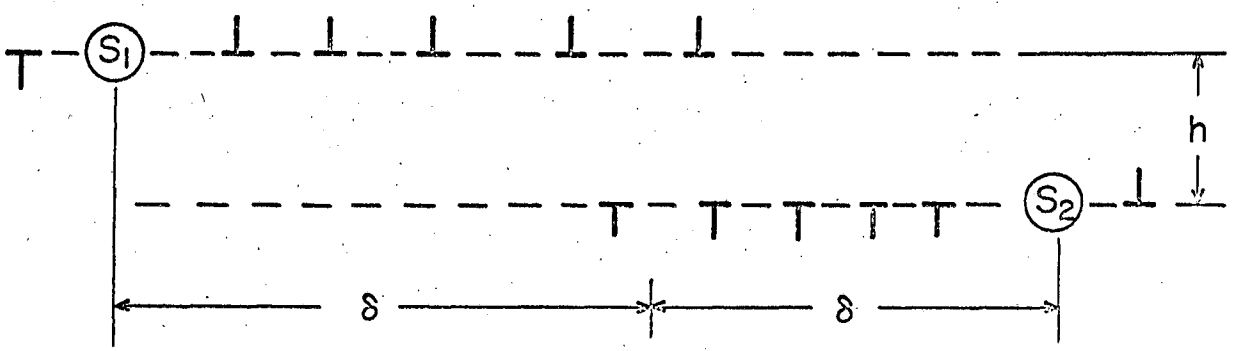

FIGURE 3.29. ARRESTED ARRAYS OF EDGE DISLOCATIONS.

A brief reflection on the stress σ_{xx} will reveal that the two leading dislocations climb toward each other, each climbing a height h/2 before they can annihilate each other. Therefore, the time for climb is

$$t_c = \frac{h}{2\dot{y}} = \frac{h}{2b\nu_c} \tag{3.79}$$

If N are the number of such pairs of arrested arrays per unit volume, the creep rate due to climb is given by

$$\dot{\gamma}_c = \frac{N(4\delta)^2 b}{t_c} = \frac{2N(4\delta)^2 b^2 \nu_c}{h} \tag{3.80}$$

or, introducing ν_c .

$$\dot{\gamma}_c \doteq 2N(4\delta)^2 b^2 \Omega (z-1) \frac{\sigma_{xx}}{h\,kT} p_j e^{\Delta d/k} e^{-\frac{(u_1 + p\Omega_1)}{kT}} \tag{3.81}$$

Thus, in order to complete the formal part of the analysis, some measure of how σ_{xx} and $1/h$ depend on the applied stress must be estimated.

In accord with the deductions made by Eschelby, Frank and Nabarro,[29] as discussed in Section 2J, σ_{xx} is given by

$$\sigma_{xx} = 2\sqrt{\frac{\delta}{h}}\ \frac{Gb}{2\pi(1-\mu)h} \tag{3.82}$$

where the factor 2 arises from the two arrays $\sqrt{\delta/2h}$ is approximately the stress concentration, and $\frac{Gb}{2\pi(1-\mu)h}$ is the stress field σ_{xx} , of the leading dislocation of the array. Furthermore, as shown by Eq. 2.42 in Section 2J, the number of edge dislocations in the array is given by

$$n = \frac{6\pi\tau(1-\mu)}{4Gb} \tag{3.83}$$

giving a local shear stress at the leading dislocation of the array of $n\tau$ or

$$\frac{6\pi\delta\tau^2(1-\mu)}{4Gb}$$

when this stress is equal to the repulsion stress due to dislocations in the other array the dislocations arrays will be arrested. Therefore,

$$\frac{6\pi\delta\tau^2(1-\mu)}{4Gb} = \tau\sqrt{\frac{\delta}{2h_m}} \tag{3.84}$$

Consequently,

$$h_m = \frac{2}{9}\frac{G^2b^2}{\pi^2\delta\tau^2(1-\mu)^2} \tag{3.85}$$

Since arrays will be separated all heights between $0 < h < h_m$, we will crudely let $h = h_m/2$ in order to obtain a reasonable average value. Consequently,

$$\frac{\sigma_{xx}}{h} = \frac{\delta^{1/2}Gb}{\pi(1-\mu)h^{5/2}} = \frac{3^5\pi^4\delta^3\tau^5}{\{Gb/(1-\mu)\}^4} \tag{3.86}$$

$$\dot{\gamma}_c \simeq 7800N\delta^5\frac{\Omega(z-1)\pi^4\tau^5}{b^2kT\{G/(1-\mu)\}^4}D_j e^{\frac{A_d}{k}e}e^{-\frac{U_d+p\Omega_d}{kT}} \tag{3.87}$$

Sherby[66] has attempted to justify this version of the dislocation climb theory as shown by the data assembled in Fig. 3.30. In general, the creep rate for many metals follows the τ^5 law as shown. But this analysis neglects the possible effect of stress on $N\delta^5$.

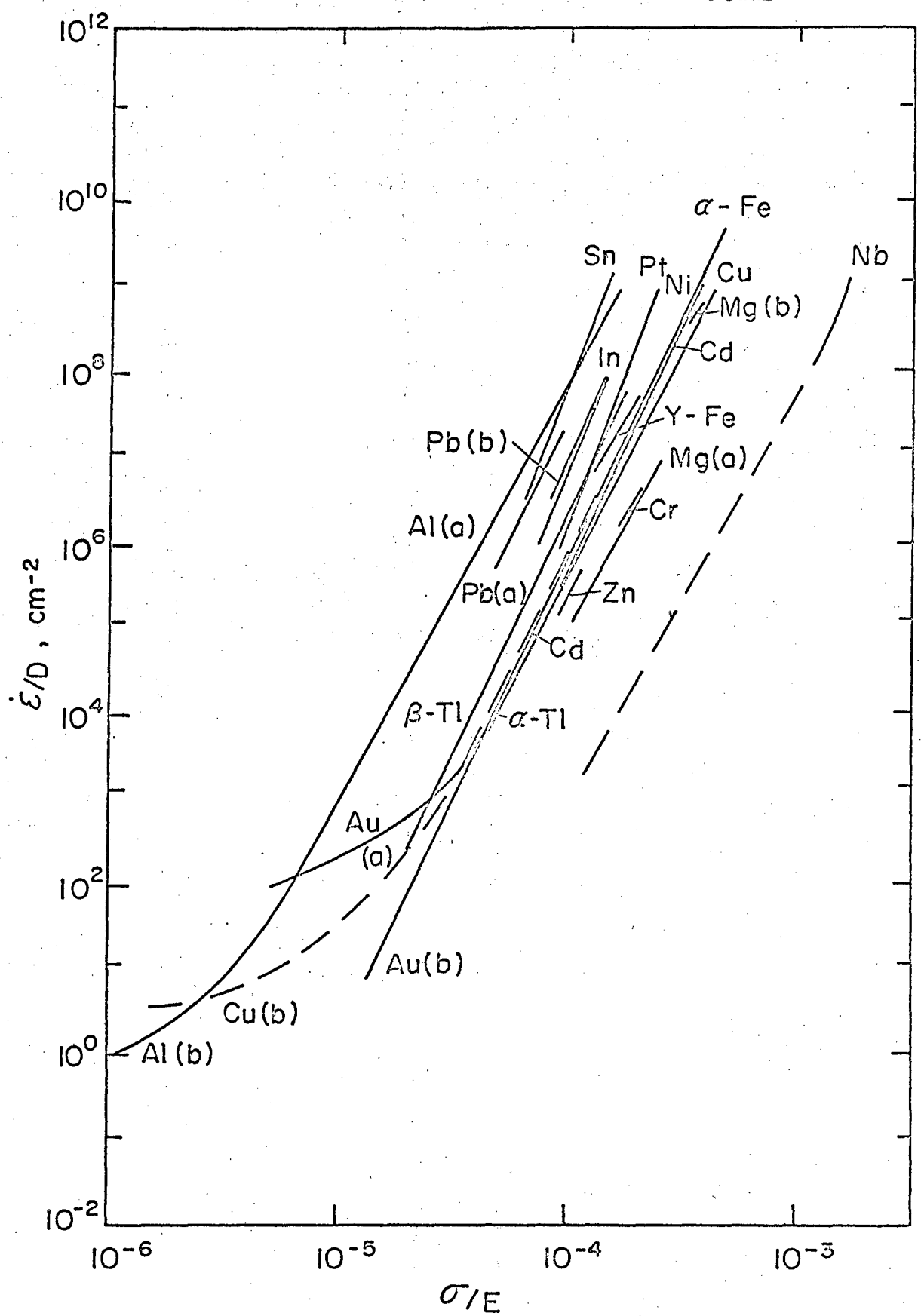

FIGURE 3.30. STEADY-STATE CREEP RATE PROVIDED BY DIFFUSION RATE vs. CREEP STRESS DIVIDED BY ELASTIC MODULUS FOR VARIOUS PURE METALS.[66]

The activation energies for high temperature creep have been shown in a number of cases to be insensitive to the applied stress as suggested by Eq. 3.86. And, as shown in Fig. 3.31, they are approximately equal to that for self diffusion. But, at the high temperatures and slow strain rates for creep, it is expected that the equilibrium number of jogs is approximated, and $p_j \simeq e^{\frac{-U_j + U_c}{kT}}$. Consequently the theoretically estimated activation energy for climb equals $U_d + U_j + U_c$, a quantity that is always somewhat greater than the experimentally determined value of U_d. Although the general correlations for high temperature creep appear to agree with the theory for climb, the lack of detailed agreement between theory and experiment need yet to be rationalized.

Other factors that are significant in high temperature creep concern subgrain formation, grain boundary migration and grain boundary shearing. These have been discussed elsewhere and will not be reviewed here.

4. SOLUTE ATOM STRENGTHENING

4A. Introduction

In general, solid-solution alloys are stronger than the base metals from which they are prepared. Empirical correlations suggest that such strengthening might be related to the differences in atomic radii and valency of the solute and solvent atomic species. Such empirical observations, however, must be rationalized in terms of dislocation theory.

Solid-solution effects can be classified into two major categories. First, additions of solute atoms can introduce perturbations of the details of the same mechanisms of deformation that apply to pure metals. And second, solid-solution alloying can introduce new mechanisms of strengthening.

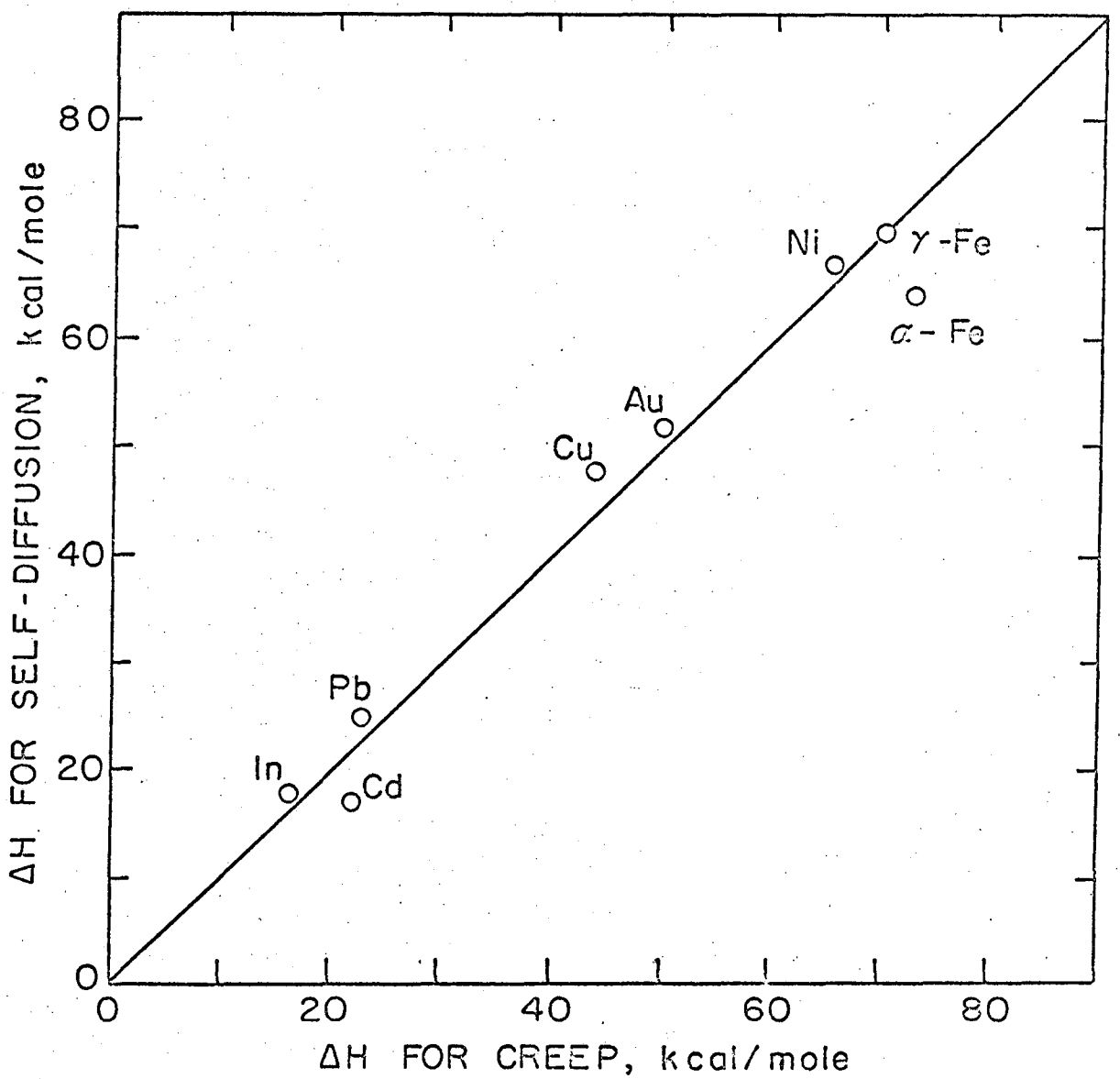

FIGURE 3.31. ACTIVATION ENERGIES FOR HIGH TEMPERATURE CREEP AND SELF-DIFFUSION.

Solid-solution alloying generally causes a decrease in the modulus of elasticity which, of course, is reflected in appropriate small changes in the activation energies and flow stresses for all of the previously discussed mechanisms of deformation. Furthermore, as described in Section 3F, alloying can also increase the density of dislocation in annealed metals, undoubtedly as a result of operation of one or more of the several unique interactions to be discussed later. It appears, at present, that in specific alloys much of strengthening found in the low temperature deformation of FCC metals arises from this fact. Solid-solution alloying also changes the stacking fault energy and thereby modifies the constriction and recombination energies of dissociated dislocations.

Several uniquely different interactions also result from solid-solution alloying. At high temperatures, solute atoms can inhibit climb, motion of jogged screw dislocations and introduce a diffusion controlled viscous drag on moving dislocations. At lower temperatures, solute atoms can interact with strain energy fields of dislocations (Cottrell locking[44]) or provide chemical interactions with stacking faults (Suzuki locking[45]), or result in short-range order strengthening (Fisher hardening[67]). We shall be content here to review only the last three mentioned mechanisms.

4B. Cottrell Locking

Substitutional atoms that have atomic radii that differ from the solvent species, introduce local dilations and contractions in the lattice. Such strain centers can interact elastically with the hydrostatic tension stress fields of dislocations. As shown by Eqs. 2.6 and 2.10, the mean hydrostatic tension stress field due to an edge dislocation is

$$\frac{\sigma_{rr}+\sigma_{\theta\theta}+\sigma_{zz}}{3}=\left(\frac{1+\mu}{3}\right)\left(\sigma_{rr}+\sigma_{\theta\theta}\right)=\frac{-(1+\mu)Gb\sin\theta}{3\pi(1-\mu)r} \quad (4.1)$$

and therefore edge dislocations will interact with substitutional solute atoms. A small interaction, which will be neglected here, also arises from electronic effects. But the mean hydrostatic tension stress arising from screw dislocations is zero. Nevertheless a screw dislocation segment near a solute atom can reorient somewhat to acquire a small edge component which will then interact with the solute atom.

Interstitial atoms not only cause local increases in volume but also introduce local shear distortions. Consequently interstitials interact elastically with both edge and screw components and for this reason give much higher locking effects than substitutionals.

The interaction of interstitials with dislocations has been analyzed by Cochardt, Schoeck, and Weidersich.[68] But we shall be content here to review the interaction of substitutional alloying elements with dislocations as first described by Cottrell.[44]

Consider an atom at r and θ from the core of an edge dislocation where the mean hydrostatic tension is given by Eq. 4.1. In order to ascertain the strain energy between a solute atom at this point and the dislocation we consider blowing the atom up from a radius R corresponding to that of the radius of solvent atom to a size R_1 appropriate for the radius of the solute. Work must be done during this process against the constant mean hydrostatic tension given by Eq. 4.1. This work is equal to the pressure times the change in volume. Therefore, assuming R_1 - R is not too large

$$U_{cB} = p\Delta V = \frac{-(\sigma_{rr}+\sigma_{\theta\theta}+\sigma_{zz})}{3} 4\pi R^2 (R_1 - R) \qquad (4.2)$$

When the strain due to the differences in atomic radius is given by

$$\varepsilon = (R_1 - R)/R \qquad (4.3)$$

the interaction strain energy reduces to

$$U_{cB} = -\left(\frac{\sigma_{rr}+\sigma_{\theta\theta}+\sigma_{zz}}{3}\right) 4\pi R^3 \varepsilon \qquad (4.4)$$

Introducing Eq. 4.1 gives

$$U_{cB} = 4/3\, R^3 \varepsilon \frac{1+\mu}{1-\mu} \frac{Gb \sin\alpha}{r} \qquad (4.5)$$

The above derivation, however, neglects the compressibility of the solute atom. When this is taken into consideration, as suggested by Bilby,[69]

$$U_{cB} = \frac{A}{r}\sin\alpha = 4\pi R^3 \varepsilon \frac{Gb}{r}\sin\alpha \qquad (4.6)$$

Introducing cartesian coordinates $r^2 = x^2 + y^2$ and $\sin\alpha = y/r$, Eq. 4.6 can be written as

$$U_{cB} = \frac{Ay}{r^2} = \frac{Ay}{x^2+y^2}$$

or

$$x^2 + y^2 - \frac{A}{U_{cB}} y = 0 \qquad (4.7)$$

Each constant potential energy, therefore, is represented by a circle that is tangent to the line y = 0 and is centered on the line x = 0 as shown in Fig. 4.1. The interaction force to which the atom is subjected, therefore, acts normal to the equiponential lines in the direction of the conjugate set of circles shown as broken curves. Consequently at temperatures where diffusion can take place solute atoms will migrate along the broken circles toward the core of the dislocation. Solute atoms larger than the host will migrate in the direction shown by the arrow to the lower or extended part of the dislocation. Solute having a smaller atomic radius than the host will migrate in the opposite direction. In either case such migration results in a decrease in the free energy of the system.

It was suggested at one time that the dislocation core becomes saturated when the solute atoms satisfy its strain field. On this basis it was believed that the dislocation could accommodate only a single line of solute atoms along its core. A brief review of how the preceding calculation was made will reveal that this concept simply is not true. The interaction between a dislocation and a solute atom is unmodified by the presence of other solute atoms. Of course, the other solute atoms can independently react with the one under consideration. And therefore an equilibrium atmosphere is produced when the chemical potential gradient along the broken circle is equal and opposite to the potential energy gradient arising from the presence of the dislocation. Consequently Cottrell atmospheres are much broader than originally visualized. And in some cases, e.g., when there is an excess of N and C in steels, the chemical potential gradient never completely countermands the elastic interaction energy. For this reason, as shown so clearly in electron

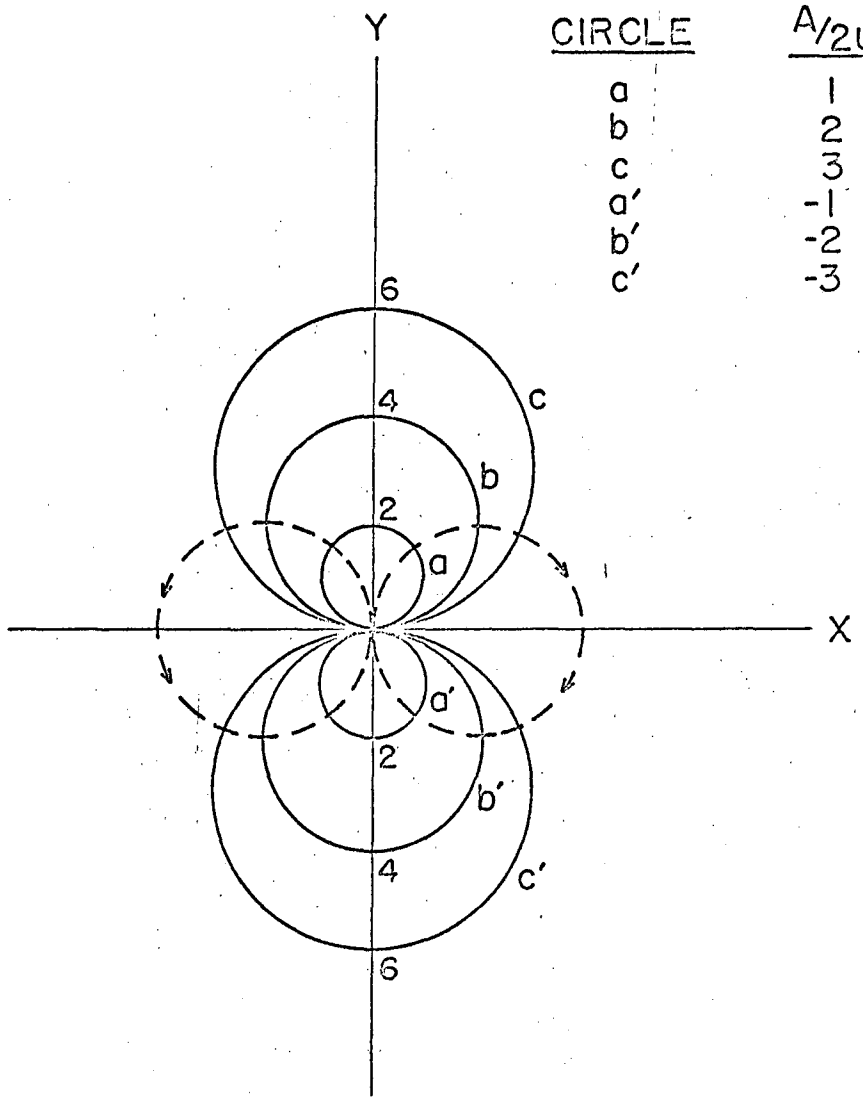

FIGURE 4.1. CIRCLES OF CONSTANT INTERACTION ENERGY.

microscopic investigations, the solute atoms continue to feed into the dislocation core producing precipitates of nitrides and carbides on the dislocations.

When a dislocation is moved away from its atmosphere, the energy of the system must be increased. Early consideration of single atom atmospheres illustrated that this energy was not excessive and therefore solute atom locked dislocations could be moved from their atmosphere with the aid of thermal fluctuations. It was thought that once a dislocation segment were so unlocked it would multiply, impinge on other locked dislocations and thus initiate an avalanche which would result in a Luders band. But it can now be shown that the locking is in general so severe that locked dislocations do not move. Therefore the usual yield point phenomena must be associated with the generation and multiplication of new unlocked dislocations. This model is in complete agreement with the observations that the activation energies for the preyield creep strains, delayed yielding, and the propagation of Luders bands agree well with the activation energy for deformation per se.

Precipitates on dislocations, of course, block the motion of newly formed dislocations. When a dislocation is separated from a mild atmosphere, the atmosphere will interact with other moving dislocations. In these ways Cottrell atmospheres cause strengthening even when new dislocations are introduced.

4C. Suzuki Interactions

As we have seen in Section 2M, dislocations on the (111) plane in FCC metals on those on the basal planes of HCP metals dissociate into partials leaving a strip of stacking fault 2 atomic layers high between them. Whereas the stacking fault in FCC metals consists of two atomic

layers of CPH stacking, that in CPH metals consists of two atomic layers of FCC stacking. When a metal containing stacking faults is heated into the temperature range where diffusion can take place, the solute atoms will redistribute themselves between the stacking faults and the ideal crystal. During such redistribution the separation of the partials will increase slightly because the stacking fault energy decreases. Since the volume occupied by the stacking faults is small, the mole fraction of solute atoms remains about equal to the average composition in the crystal c, whereas the mole fraction of the faulted region becomes c_f.

The situation then is as shown in Fig. 4.2. If then a unit length of the dislocation is moved a distance δ, assumed to be identical for both partials in this approximation, the work done is $(\tau-\tau^*)b\delta$. This work must equal the increase in chemical free energy. In moving the partial dislocations an amount δ, the volumes of the phases changed $2h\delta$; for the first dislocation this volume of the matrix phase was produced at a composition c_f resulting in the disappearance of the same stacking fault volume of the same composition; and at the second dislocation this volume of the stacking fault was produced resulting in the disappearance of the same volume of the matrix phase at the composition c. Consequently

$$(\tau-\tau^*)b\delta = \frac{2h\delta}{V}\left\{(F-F^f)_{c_f}+(F^f-F)_c\right\} \qquad (4.8)$$

where V is the molar volume, assumed identical regardless of stacking, F is the free energy per mole of the matrix, F_f, the free energy per mole of the faulted region, and the subscripts c_f and c refer to the compositions at which the free energies must be evaluated. Therefore

$$(\tau-\tau^*) = \frac{2h}{bV}\left\{(F^f-F)_c-(F^f-F)_{c_f}\right\} \qquad (4.9)$$

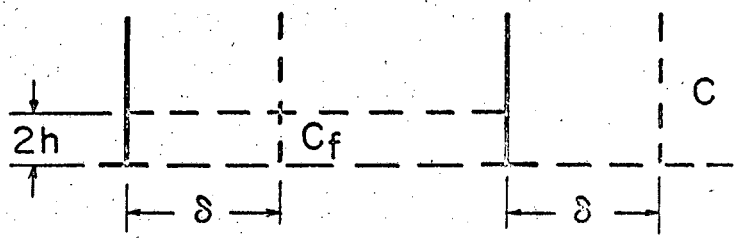

FIG. 4.2 STACKING FAULT IN SUZUKI LOCKED ALLOY.

In general both $(F^f - F)_c$ and $(F^f - F)_{c_f}$ are positive as, e.g., in the case of Ni-Cu alloys where the stable phase is always FCC, the faulted region having the higher free energy regardless of composition. But $(F^f - F)_{c_f} < (F^f - F)_c$ since the composition c_f was obtained as a result of equilibrium. Consequently the total term in the braces of Eq. 4.9 is always positive.

An additional relationship between the variables of Eq. 4.9 is obtained by invoking quasi-equilibrium conditions between the matrix phase and the faulted region. Complete equilibrium, of course, is never achieved inasmuch as this would demand the disappearance of the faulted regions. We consider, therefore, open matrix and faulted phases for which, at equilibrium, the virtual change in free energy $\delta F_t'$ for the total system is

$$\delta F_t' = \left(\frac{\partial F'}{\partial n_a}\right)\delta n_a + \left(\frac{\partial F'}{\partial n_a}\right)\delta n_b + \left(\frac{\partial F'^f}{\partial n_a^f}\right)\delta n_a^f + \left(\frac{\partial F'^f}{\partial n_b^f}\right)\delta n_b^f$$

where F' refers now to the free energy of the matrix containing n_a "a" atoms and n_b "b" atoms, etc. The partials derivatives are therefore the chemical potentials. At equilibrium, $\delta F_t'$, for the total system is zero. To arrive at the equilibrium condition we let $\delta n = \delta n_a = -\delta n_b = \delta n_b^f = \delta n_a^f$. This is merely the expression for conservation of mass which yet permits atom species transfer of δn atoms of type "a" from the fault to the matrix and δn atoms of type "b" from the matrix to the fault. For equilibrium, therefore,

$$\frac{\partial F'}{\partial n_a} - \frac{\partial F'}{\partial n_b} - \frac{\partial F'^f}{\partial n_a^f} + \frac{\partial F'^f}{\partial n_b^f} = 0 \qquad (4.10)$$

In general, the thermodynamic data that are needed to achieve a simultaneous solution of Eqs. 4.9 and 4.10 are not available. Furthermore, theories on the thermodynamics of solid solutions have not yet been well enough developed to provide reliable analyses of the thermodynamics of unstable solid solutions (e.g., hexagonal Cu-Ni alloys). But in order to obtain an initial concept of possible trends, the regular solution laws might be invoked. To simplify the analysis this will be done not only for the matrix but equally for the faulted volume, in spite of the fact that the stacking fault region should be treated as a surface.

The free energy of an open regular solution consisting of n_a "a" atoms and n_b "b" atoms can be written as

$$F' = \frac{n_a F_a}{N} + \frac{n_b F_b}{N} + \left(\frac{n_a + n_b}{N}\right) \Delta H_m - kT \ln \frac{(n_a + n_b)!}{n_a! + n_b!} \qquad (4.11)$$

where N is Avogadro's number, F_a and F_b are the free energies per mole of pure "a" and pure "b", ΔH_m is the change in enthalpy upon mixing a mole of "a" and "b" atoms and the last term refers to the contribution of the entropy for random mixing. A similar expression applies to the faulted region. When C is defined as

$$C = \frac{n_b}{n_a + n_b} \qquad (4.12)$$

Eq. 4.11, written for one mole of the alloy, reduces to

$$F_c^f = (1-c) F_a^f + C F_b^f + \Delta H_m(c) + RT\{c \ln c + (1-c) \ln (1-c)\} \qquad (4.13)$$

with similar expressions for the remaining free energies in Eq. 4.9. Then

$$(F^f - F)_c = (1-c)(F_a^f - F_a) + c(F_b^f - F_b) + (\Delta H_m^f - \Delta H_m)_c \quad (4.14)$$

where the entropy terms vanish. Also

$$(F^f - F)_{c_f} = (1-c_f)(F_a^f - F_a) + c_f(F_b^f - F_b) + (\Delta H_m^f - \Delta H_m)_{c_f} \quad (4.15)$$

Introducing Eqs. 4.14 and 4.15 into 4.9 gives

$$(t-t^*) = \frac{2h}{bV}\left\{(c-c_f)\left[(F_b^f - F_b) - (F_a^f - F_a)\right] + (\Delta H_m^f - \Delta H_m)_c - (\Delta H_m^f - \Delta H_m)_{c_f}\right\} \quad (4.16)$$

For equilibrium conditions, we apply Eqs. 4.11 etc. to the condition given by Eq. 4.10. For example

$$\frac{\partial F'}{\partial n_a} = \frac{F_a}{N} + \frac{\Delta H_m}{N} + \frac{n_a+n_b}{N}\frac{\partial \Delta H_m}{\partial c}\frac{\partial c}{\partial n_a} + kT \ln \frac{n_a+n_b}{n_a} \quad (4.17a)$$

and

$$\frac{\partial F'}{\partial n_b} = \frac{F_b}{N} + \frac{\Delta H_m}{N} + \frac{n_a+n_b}{N}\frac{\partial \Delta H_m}{\partial c}\frac{\partial c}{\partial n_b} + kT \ln \frac{n_a+n_b}{n_b} \quad (4.17b)$$

Recalling that

$$\frac{\partial c}{\partial n_a} = -\frac{n_b}{(n_a+n_b)^2} \quad \text{and} \quad \frac{\partial c}{\partial n_b} = \frac{1}{n_a+n_b} - \frac{n_b}{(n_a+n_b)^2} \quad (4.18)$$

and similarly for the faulted region

$$\frac{\partial F'^{f}}{\partial n_a^f} + \frac{\partial F'^{f}}{\partial n_b^f} = \frac{F_a^f - F_b^f}{N} - \frac{1}{N}\left(\frac{\partial \Delta H_m^f}{\partial c^f}\right) - kT \ln \frac{c_f}{1-c_f} \quad (4.20)$$

Consequently the equilibrium condition, obtained by introducing Eqs. 4.19 and 4.20 into 4.10 is given by

$$\frac{c_f}{1-c_f} = \frac{c}{1-c} \exp\left\{-\frac{1}{kT}\left[(F_b^f - F_b) - (F_a^f - F_a) + \left(\frac{\partial \Delta H_m^f}{\partial c_f} - \frac{\partial \Delta H_m}{\partial c}\right)\right]\right\} \quad (4.21)$$

Eqs. 4.16 and 4.21 therefore constitute the solution to the problem. An explicit expression for c_f is not obtainable from Eq. 4.21 since $\frac{\partial}{\partial c^f}(\Delta H_m^f)$ also depends on c_f. But the quantities in the braces of the exponential term will be positive and therefore c_f will be somewhat smaller than c. This difference will be greatest at the absolute zero and as the temperature increases c_f will increase very slowly to approach c.

When the solution is ideal the ΔH_m's are zero and Eqs. 4.16 and 4.21 reduce to the simple expressions, respectively, of

$$(\tau - \tau^*) = \frac{2h}{bV}(c - c_f)\Delta F \quad (4.22)$$

$$\frac{c_f}{1-c_f} = \frac{c}{1-c} e^{-\Delta F/kT} \quad (4.23)$$

where

$$\Delta F = (F_b^f - F_b) - (F_a^f - F_a) \qquad (3.24)$$

and

$$\frac{2h}{V}\Delta F = \gamma_b^f - \gamma_a^f \qquad (3.25)$$

γ_b^f and γ_a^f being the stacking fault energies in pure b and a. Therefore $(\tau - \tau^*)$ can vary mildly with temperature depending on the variation in stacking fault energies of pure a and pure b with temperature.

Excepting when the stacking fault width is only a few Burgers vectors, Suzuki locked alloys cannot be thermally activated. An example of the insensitivity of the flow stress to strain rate and temperature is shown in Fig. 1.6. These results cannot be ascribed to Cottrell locking since the atomic radii of Ag and Al are almost identical. Furthermore short-range order hardening would have resulted in decreasing flow stress with increasing temperature. The increase in flow stress with temperature and the presence of a yield point could only be rationalized in terms of Suzuki locking.

4D. Fisher Strengthening

When A and B atoms are mixed to produce a solid solution alloy the bond reaction

$$\tfrac{1}{2}\,A\text{-}A + \tfrac{1}{2}\,B\text{-}B \longrightarrow A\,B \qquad (4.26)$$

takes place. The change in energy of the system is given by

$$\mathcal{E} = \mathcal{E}_{AB} - \tfrac{1}{2}\mathcal{E}_{AA} - \tfrac{1}{2}\mathcal{E}_{BB} \qquad (2.27)$$

per A - B bond produced. Consequently if $\mathcal{E}$ is negative the reaction will tend to go to the right. Under these conditions the atoms in the alloy will so arrange themselves that the largest number of A - B bonds will be produced. Consequently the number of A atoms about a B atom or the number of B atoms about an A atom will become greater than that appropriate for an ideal solution. Such an alloy exhibits short-range ordering. Conversely, if the energy $\mathcal{E}$ increases, there will result more A - A and B - B bonds than in a random solution. Such an alloy is said to cluster. But ordering and clustering are only different facets of the same problem. Such ordering and clustering can only apply to near neighbors because the solution, as a whole, must have the average composition. In fact to a good first approximation only interactions between the atoms and their immediate neighbors need be considered. At greater atomic distances the alloy is random.

We will employ Cowley's[70] analysis for order here limiting our discussion only to interaction effects between nearest neighbors. Let α be the degree of order, and p_{AB} the probability that an A atom is next to a B atom. By definition of α

$$p_{AB} = m_A(1-\alpha) \qquad (4.28a)$$

where m_A is the mole fraction of A atoms. When the solution is random,

p_{AB} must be equal to m_A. When α is positive there are fewer than the average number of A atoms and about a B and the alloy exhibits clustering; when α is negative there are more than the average number of A atoms about a B atom and the alloy exhibits short-range ordering. Thus for an ordered alloy both ε and α are negative whereas for a clustered alloy both are positive. The product $\varepsilon\,\alpha$ is always positive or, in a random solid solution, zero. The range of α is limited. When $p_{AB} = 0$, α has its maximum value of 1 , and when p_{AB} is 1 , α has its minimum value of $\alpha = 1 - \frac{1}{m_A} = \frac{m_A - 1}{m_A} = -\frac{m_B}{m_A}$. The probabilities for the remaining arrangements, shown below, follow directly from the definition given in Eq. 4.28a, namely,

$$p_{BB} = 1 - p_{AB} = 1 - m_A + m_A\alpha = m_B + m_A\alpha \qquad (4.28b)$$

$$p_{BA} = m_B(1-\alpha) \qquad (4.28c)$$

$$p_{AA} = (1 - p_{BA}) = m_A + m_B\alpha \qquad (4.28d)$$

We now consider an alloy containing N atoms in a structure that has a coordination number Z. In this alloy there are a total of $\frac{NZ}{2}$ bonds and we plan to express the total energy of the alloy in terms of the degree of order α as

$$E\{\alpha\} = \frac{NZ}{2}\,\varepsilon\{\alpha\} \qquad (4.29)$$

where $\mathcal{E}\{\alpha\}$ is the average energy per bond in an alloy that has order α. The total energy of the alloy is the sums of the energies of the A - A, the B - B and the A - B bonds; which is

$$E\{\alpha\} = \left(m_A \frac{ZN}{2}\right) p_{AA} \mathcal{E}_{AA} + \left(m_B \frac{ZN}{2}\right) p_{BB} \mathcal{E}_{BB} + \left(m_A \frac{ZN}{2}\right) p_{BA} \mathcal{E}_{BA} + \left(m_B \frac{ZN}{2}\right) p_{AB} \mathcal{E}_{AB} \tag{4.30}$$

When Eqs. 4.28 are introduced, and Eq. 4.29 is solved,

$$\mathcal{E}\{\alpha\} = m_A^2 \mathcal{E}_{AA} + m_B^2 \mathcal{E}_{BB} + 2 m_A m_B \mathcal{E}_{AB} - 2 m_A m_B \alpha \mathcal{E} \tag{4.31}$$

where $\mathcal{E}$ is given by Eq. 4.27. Since α and $\mathcal{E}$ always have the same sign, $\mathcal{E}\{\alpha\}$ is always less than the average energy of a bond in the randomly arranged alloy where $\alpha = 0$.

When a dislocation moves through the lattice it displaces its nearest nieghbors across the slip plane and replaces them by next nearest neighbors. But next nearest neighbors are almost random. Consequently if two or more dislocations pass, the alloy becomes practically completely disordered across the slip plane. The average increase in energy per bond that is broken is

$$\bar{\mathcal{E}} = \mathcal{E}\{0\} - \mathcal{E}\{\alpha\} = 2 m_A m_B \alpha \mathcal{E} \tag{4.32}$$

In order to illustrate the determination of the flow stress, we will consider as shown in Fig. 4.3 slip on the (110) plane in the [111] of a BCC

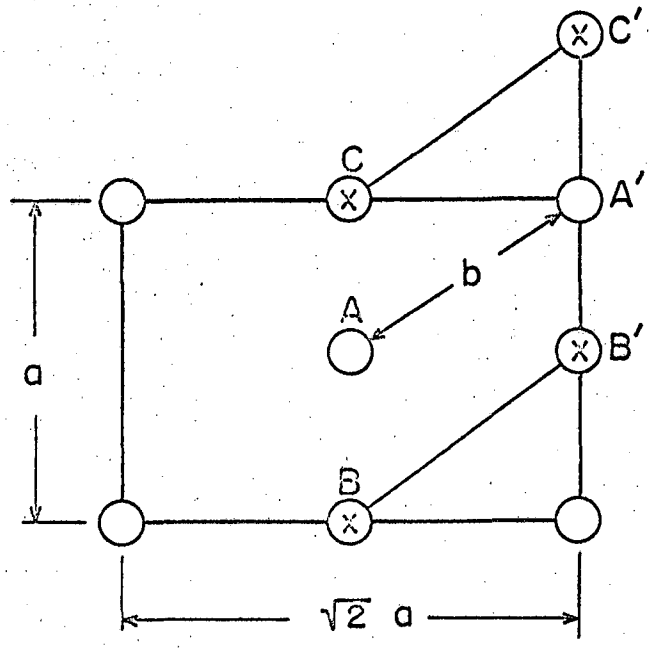

⊗ ATOMS BELOW

○ ATOMS ABOVE

WHEN ATOM A ABOVE SLIP PLANE MOVES TO A', IT IS NO LONGER CO-ORDINATED WITH ATOMS C AND B BELOW THE SLIP PLANE, BUT WITH ITS FORMER NEXT NEAREST NEIGHBORS B' AND C'.

FIGURE 4.3. CHANGE IN NEIGHBOR ARRANGEMENT DURING DEFORMATION OF A SHORT RANGE ORDERED ALLOY.

crystal. The dislocation line of length CD moves one $\bar{b}$ breaking the former bonds of A with B and C and making new bonds with B' and C'. Therefore, the work done

$$(\tau-\tau^*)\frac{\sqrt{3}}{2}a\,\frac{\sqrt{2}}{2}a^2 = 2\bar{\varepsilon} \tag{4.33}$$

Therefore,

$$(\tau-\tau^*) = \frac{16 m_A m_B \alpha\varepsilon}{\sqrt{6}\,a^3} \tag{4.34}$$

This can indeed be quite a large quantity.

It has been shown that the equilibrium degree of order α_o is given by[71]

$$\frac{(m_A + m_B\alpha_o)(m_B+m_A\alpha_o)}{m_A m_B (1-\alpha_o)^2} = e^{2\varepsilon/kT} \tag{4.35}$$

Therefore, at sufficiently high temperatures, where diffusion is possible, the absolute value of the degree of order α_o decreases slowly with increasing temperatures. Below this temperature, however, the flow stress $(\tau-\tau^*)$ is dependent on the "frozen in" degree of order α and therefore is insensitive to the temperature. An example of the effect of short-range order hardening is shown in Fig. 4.4 where short range ordering controls the deformation over Region II.

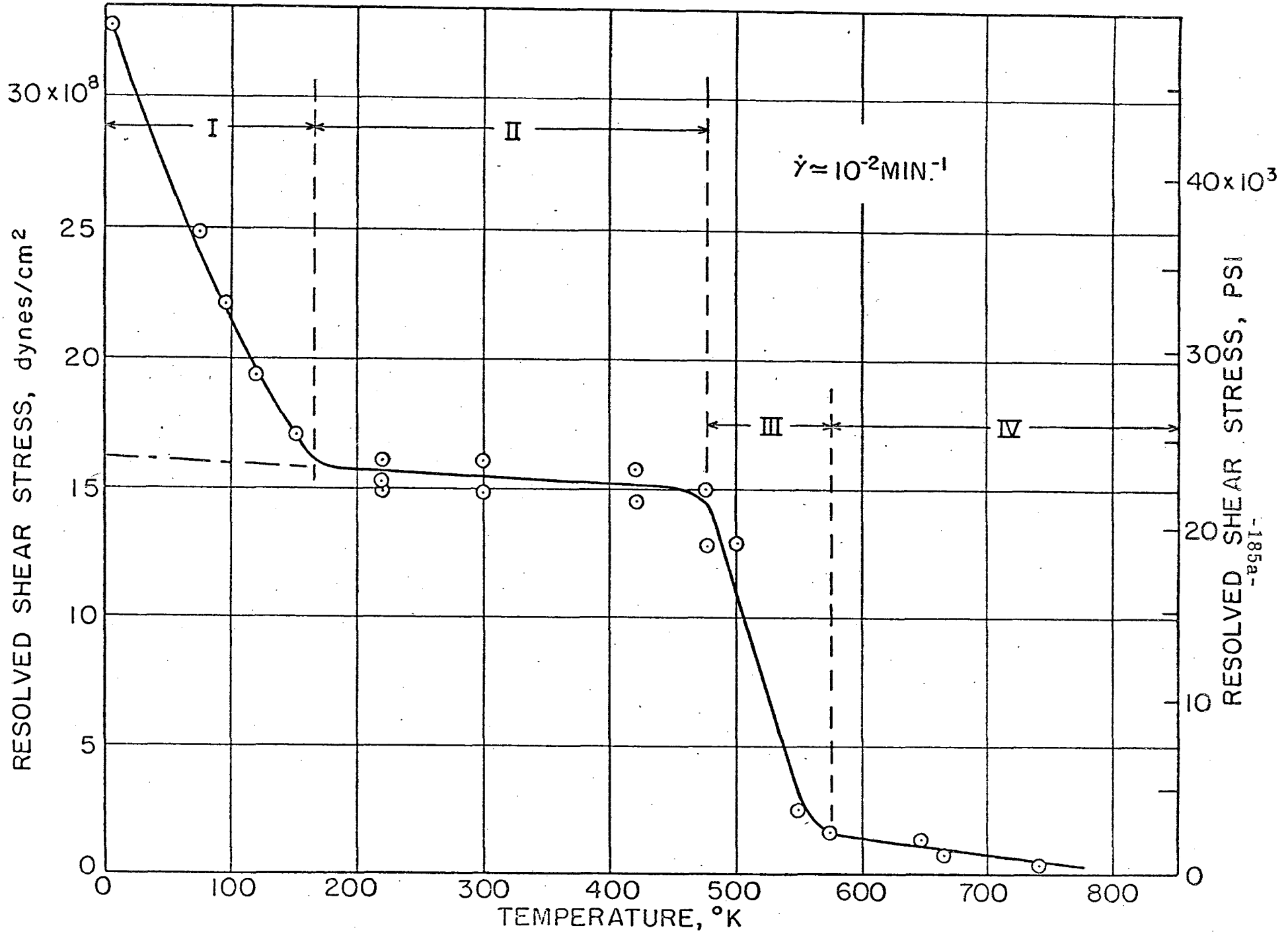

FIG. 4.4. EFFECT OF TEMPERATURE ON THE CRITICAL RESOLVED SHEAR STRESS FOR PRISMATIC SLIP OF Ag - 33 AT. % Al SINGLE CRYSTALS.[72]

ACKNOWLEDGMENTS

The author wishes to express his appreciation for the encouragement hiven him by the Inorganic Materials Research Division of the Lawrence Radiation Laboratory and by the United States Atomic Energy Commission in his research on dislocation mechanics. He gratefully acknowledges the cooperation of his graduate students in this endeavour. He particularly wishes to thank Mr. J. Mote for his advice and assistance in preparing this survey.

General References

A. A.H.Cottrell, "Theory of Dislocations"
(a) Progress in Metal Physics, 1, 77 (1949)
(b) Progress in Metal Physics, 4, 205 (1953)

B. A.H.Cottrell, Dislocations and Plastic Flow in Crystals (Oxford Press, 1952)

C. W.T.Read, Jr., Dislocations in Crystals (McGraw-Hill Co., 1953)

D. A.S.M.Symposium on the Relation of Properties to Microstructure, (American Society for Metals, 1953)

E. AIME Symposium on the Dislocations in Metals (American Institute of Mining and Metallurgical Engineers, 1954)

F. J. Friedel, Les Dislocations (Gauthiers-Villars, 1956)

G. National Physics Laboratory Symposium on the Creep and Fracture of Metals at High Temperatures (Her Majesty's Stationary Office, London, 1956)

H. J.C.Fisher, W.G.Johnston, R.Thomson and T. Vreeland, Jr., Lake Placid Conference on the Dislocations and Mechanical Properties of Crystals, 1956

I. J.D.Eshelby, "The Continuum Theory of Lattice Defects," Solid State Physics 3, 79 (1956)

J. A.S.M.Symposium on Creep and Recovery (American Society for Metals, 1957)

K. A. Seeger, Handbuch der Physik (1958)

L. R.H.Doremus, B.W.Roberts and D.Turnbull, Growth and Perfection of Crystals (John Wiley and Sons, 1958)

M. Symposium on the Vacancies and Other Point Defects in Metals and Alloys (The Institute of Metals, 1958)

N. Symposium on the Internal Stresses and Fatigue in Metlas (Elsevier Publishing Company, 1959)

O. Swampscott Seminar on the Conference on Fracture (National Research Council, 1959)

P. S. Amelinckx and W. Dekeseyer, "The Structure and Properties of Grain Boundaries," Solid State Physics 8, 325 (1959)

Q. F. de Wit, "The Continuum Theory of Stationary Dislocations," Solid State Physics 10, 249 (1960)

R. H.G. van Beuren, Imperfections in Crystals, (North Holland Publishing Company, Amsterdam, 1960)

S. A.S.M. Seminar on the Strengthening Mechanisms of Solids (American Society for Metals, 1960)

T. Mechanical Behavior of Materials at Elevated Temperatures (McGraw-Hill Book Company, 1961)

U. R.W.K. Honeycombe, "The Effect of Temperature and Alloying Additions on the Deformation of Metal Crystals," Progress in Metal Physics 9, 93 (1961)

V. I.R. Kramer and L.J. Demer, "Effects of Environment on Mechanical Properties of Metals," Progress in Metal Physics 9, 133 (1961)

References

1. T. A. Trozera, O. D. Sherby and J. E. Dorn, "Effect of Strain Rate and Temperature on the Plastic Deformation of High Purity Aluminum," Trans. Am. Soc. Metals 49, (1956)

2. T. E. Tietz and J. E. Dorn, "The Effect of Strain Histories on the Work-hardening of Metals," Trans. Am. Soc. Metals 41A (1949)

3. N. F. Mott, "A Theory of Work-Hardening of Metal Crystals," Phil. Mag. 43, 1151 (1952)

4. A. H. Cottrell, "The Time Laws of Creep," J. Mech. and Phys. Solids 1, 53 (1952)

5. J. Friedel, Les Dislocations (Gauthier-Villars, Paris, 1956)

6. A. Seeger, "Theorie der Kristallplastizitat," I. Grundzuge der Theorie, Z. Naturforsch. 9A, 758 (1954); II. Die Grundstruktur der dichtest gepockten Metalle und ihr Einfloss auf die plastische Verformung, Z. Naturforsch. 9A, 856 (1954); III. Die Temperatur-- und Geschwindigkeitsabhangigkeit der Kristallplastizitat, Z. Naturforsch. 9A, 870 (1954); "The Generation of Lattice Defects by Moving Dislocations and its Application to the Temperature Dependence of the Flow-Stress of FCC Crystals," Phil. Mag. 46, 1194 (1955)

7. Z. S. Bosinski, "Thermally Activated Glide in Face-Centered Cubic Metals and its Application to the Theory of Strain Hardening," Phil. Mag. 4, 393 (1959)

8. S. K. Mitra, P. W. Osborne and J. E. Dorn, "On the Intersection Mechanism of Plastic Deformation in Aluminum Single Crystals," Trans. AIME 221, 1206 (1961)

9. S. K. Mitra and J. E. Dorn, "On the Nature of Strain Hardening in Face-Centered Cubic Metals," Trans. AIME 224, 1062 (1962)

10. S. K. Mitra and J. E. Dorn, "On the Nature of Strain Hardening in Polycrystalline Aluminum and Aluminum-Magnesium Alloys," submitted for publication in Trans. AIME

11. J. Lothe and J. P. Hirth, "Dislocation Dynamics at Low Temperature," Phys. Rev. 115, 543 (1959)

12. J. Weertman, "Steady-State Creep of Crystals," J. Appl. Phys. 28, 1185 (1957)

13. H. I-Lieh Huang, O. D. Sherby and J. E. Dorn, "Activation Energy for High Temperature Creep of High Purity Aluminum," Trans. AIME 206, 1385 (1956)

14. O. D. Sherby, J. L. Lytton and J. E. Dorn, "Activation Energies for Creep of High-Purity Aluminum," Acta Met. 5, 219 (1957)

15. N.R.Borch, L.A.Shepard and J.E.Dorn, "Activation Energies for Creep of an Alpha Solid Solution of Magnesium in Aluminum," Trans. ASM 52, (1958)

16. S.L.Rajnak, T.Larsen, F.E.Hauser and J.E.Dorn, "The Effect of Strain Rate and Temperature on the Yield Strength in Ag-Al Single Crystals," Mat'l. Res. Lab., Inst. of Engineering Research, Univ. of Cal., Berkeley, 2nd Tech. Rept., Ser. 174, Issue 2, (1962)

17. F.R.N.Nabarro, "Deformation of Crystals by the Motion of Single Ions," Report of a Conference on the Strength of Solids, The Physi Soc., 75 (1948)

18. L. Prandtl, "Hypothetical Model for the Kennetic Theory of Solid Bodies," Z. Angew. Math und Mech. 8, 85 (1928)

19. U. Dehlinger, "Zur Theorie der Rekiestallisationreiner Metalle," Ann. Physik 2, 749 (1929)

20. E. Orowan, "Zur Kristallplastizitat III, Uber den Mechanismus Gleitvorganges," Z. Physik, 89, 634 (1934)

21. G. Taylor, "The Mechanism of Plastic Deformation of Crystals, Pt. I, Theoretical," Proc. Royal Soc., (London), A145, 362 (1934)

22. J. Diehl, "Zugverformung von Kupfer-Dinkristallen, I. Verfestigungenskurven und Oberflaschenersheinungen," Z. fur Metallkunde 47, 331 (1956)

23. F.C.Frank, "Crystal Dislocations - Elementary Concepts and Definitions," Phil. Mag. 42, 809 (1951)

24. F.C.Frank and W.T.Read, "Multiplication Processes for Slow Moving Dislocations," Phys. Rev. 79, 722 (1950)

25. E. Orowan, "Theory of Disperson Strengthening," Symposium on Internal Stresses in Metals and Alloys, Inst. of Metals, 451 (1948)

26. J. Mitchell, S.K.Mitra and J.E.Dorn, "Dispersed Particle Strengthening at Low Temperatures," submitted for publication in Trans. ASM

27. J.C.Fisher, E.W.Hart and R.M.Pry, "The Hardening of Metal Crystals by Precipitate Particles," Acta Met., 1, 336 (1953)

28. W.M.Lomer, "A Dislocation Reaction in the Face-Centered Cubic Lattice," Phil. Mag, 42, 1327 (1951);
A.H.Cottrell, "The Formation of Immobile Dislocations During Slip, Phil. Mag. 43, 645 (1952)

29. J.D.Eshelby, F.C.Frank and F.R.N.Nabarro, "The Equilibrium of Linear Arrays of Dislocations," Phil. Mag. 42, 351 (1951)

30. R. Armstrong, J. Codd, R. M. Douthwaite and N. J. Petch, "The Plastic Deformation of Polycrystalline Aggregates," Phil. Mag., 45 (1961)

31. R. von Mises, "Mechanik der Plastischein Formanderung von Kristallen," Z. aug. Matu. und Mech., 8, 161(1928)

32. A. N. Stroh, "Formation of Cracks as a Result of Plastic Flow," Proc. of the Roy. Soc., (London) A223, 404 (1954)

33. F. C. Frank, "The Growth of Carborundum: Dislocations and Polytypism," Phil. Mag. 42, 1014 (1951)

34. A. N. Stroh, "Constrictions and Jogs in Extended Dislocations," Proc. of the Phys. Soc. (London), B67, 427 (1951)

35. V. G. Saada, Thesis, Faculty of Science, University of Paris, (1960)

36. A. H. Cottrell, "The Time Laws of Creep," J. of Mech. and Phys. Solids, 1, 53 (1952)

37. Z. S. Bosinski, "Thermally Activated Glide in Face-Centered Cubic Metals and its Application to the Theory of Work Hardening," Phil. Mag. 4, 393 (1959)

38. P. R. Thornton and P. B. Hirsch, "The Effect of Stacking Fault Energy on Low Temperature Creep in Pure Metals," Phil. Mag., 738 (1958)

39. G. Schoeck, Theories of Creep, Mechanical Behavior of Materials at Elevated Temperatures, (McGraw-Hill Book Company, N. Y., 1961) pp. 79-107

40. N. F. Mott, "The Work-Hardening of Metals," 1960 Inst. of Metals Lecture, Trans. AIME 218, 962 (1960)

41. A. Seeger, S. Mader and H. Kronmuller, "Theory of Work-Hardening in FCC and HCP Single Crystals," Electron Microscopy and Strength of Crystals, (Interscience Publishers, Inc., N. Y., 1962) pp. 665-712

42. A. H. Cottrell, and R. J. Stokes, "Effects of Temperature on the Plastic Properties of Aluminum Crystals," Proc. of the Roy. Soc. (London), A233, 17 (1955)

43. M. J. Whelan, P. B. Hirsch, R. W. Horne and W. Bollmann, "Dislocations and Stacking Faults in Stainless Steel," Proc. of the Roy. Soc., (London) A240, 524 (1957)

44. A. H. Cottrell, "Effect of Solute Atoms on the Behavior of Dislocations," Report of a Conference on Strength of Solids, The Phy. Soc., 30 (1948)

45. H. Suzuki, "Chemical Interaction of Solute Atoms with Dislocations," Sci. Rep. Res. Insts., Tohoku University, Series A4, 455 (1952); The Yield Strength of Binary Alloys, Dislocations and Mechanical Properties of Crystals (John Wiley and Sons, N.Y., 1957) pp. 361-390

46. J. Friedel, "Dislocation Interactions and Internal Strains," Physiques des Solides, Sorbonne, Paris, pp. 220-262

47. P.W. Flynn, J.D. Mote and J.E. Dorn, "On the Thermally Activated Mechanism of Prismatic Slip in Magnesium Single Crystals," Trans. AIME 221, 1148 (1961)

48. F.R.N. Nabarro, "Mathematical Theory of Stationary Dislocations," Advances in Physics 1, 271 (1952)

49. A.D. LeClaire, "Diffusion of Metals in Metals," Prog. in Met. Phys. 1, 307(1949); 4, 265 (1953)

50. W.M. Lomer, "Point Defects and Diffusion in Metal and Alloys," Vacancies and Other Point Defects in Metals and Alloys, Inst. of Metals, 1958, pp. 79-98

51. D. Lazarus, "Diffusion in Metals," Solid State Physics 10, 71 (1960)

52. W.M. Lomer, "Defects in Pure Metals," Progress in Met. Phys. 8, 255 (1959)

53. A.H. Cottrell, "Point Defects and the Mechanical Properties of Metals and Alloys," The Inst. of Metals, 1 (1958)

54. T. Broom, "The Effects of Lattice Defects on Some Physical Properties of Metals," Vacancies and Other Point Defects in Metals and Alloys, Inst. of Metals, 41 (1958)

55. C. Herring, "Diffusional Viscosity of a Polycrystalline Solid," J. of Appl. Phys. 21, 437 (1950)

56. N.F. Mott, "A Theory of Work-Hardening of Metal Crystals," Phil. Mag. 43, 1151 (1952)

57. A. Seeger, "The Generation of Lattice Defects by Moving Dislocations and its Application to the Temperature Dependence of the Flow Stress in FCC Crystals," Phil. Mag. 46, 1194 (1955)

58. J. Friedel, "On the Linear Work-Hardening Rate of Face-Centered Cubic Single Crystals," Phil. Mag. 46, 1169 (1956)

59. H.G. van Bueren, "Theory of the Formation of Lattice Defects During Plastic Strain," Acta Met., 3, 519 (1955)

60. P.B. Hirsch and D.H. Warrington, "The Flow Stress of Aluminum and Copper at High Temperatures," Phil. Mag. 6, 735 (1961)

61. J. Lothe, "Theory of Dislocation Climb in Metals," J. of Appl. Phys. 31, 1077 (1960)

62. N. F. Mott, "The Mechanical Properties of Metals," Proc. Phys. Soc., (London) B63, 729 (1951) ;
"A Theory of Work-Hardening of Metals II: Flow Without Slip-Lines Recovery and Creep," Phil. Mag. 44, 741 (1953) ;
"Dislocations, Plastic Flow and Creep," Proc. Roy. Soc., (London) 220A, 1 (1953)

63. A. Seeger, "Jogs in Dislocation Lines," Report of a Conference on Defects in Crystalline Solids, The Phys. Soc., (London), 391 (1954) ;
"The Generation of Lattice Defects by Moving Dislocations," Phil. Mag. 46, 1194 (1955)

64. J. Weertman, "Theory of Steady-State Creep Based on Dislocation Climb," J. of Appl. Phys. 26, 1213 (1955)

65. R. W. Christy, "Theory of Creep Limited by Self-Diffusion," J. of Appl. Phys. 30, 1803 (1959)

66. O. D. Sherby, "Factors Affecting the High Temperature Strength of Polycrystalline Solids," Acta Met. 10, 135 (1962)

67. J. C. Fisher, "On the Strength of Solid Solution Alloys," Acta Met. 2, 9 (1954)

68. A. Cochardt, G. Schoeck and H. Wiedersich, "Interaction Between Dislocations and Interstitial Atoms in Body-Centered Cubic Metals," Acta Met. 3, 533 (1955)

69. B. A. Bilby, "On the Interactions of Dislocations and Solute Atoms," Proc. Phys. Soc., (London) A63, 191 (1950)

70. J. M. Cowley, "An Approximate Theory of Order in Alloys," Phys. Rev. 77, 669 (1950)

71. P. A. Flinn, "Electronic Theory of Local Order," Phys. Rev. 104, 350 (1956)

72. J. D. Mote, K. Tanaka and J. E. Dorn, "Effect of Temperature on Yielding in Single Crystals of the Hexagonal Ag-Al Intermetallic Phase," Trans. Met. Soc. AIME 221, 858 (1961).